Modeling Cliff Erosion in Salt Marshes: Spatially varying erodibility coefficient based on vegetation

(Picture by Dorreboom, (2022))

Rienk Pasma (2874172)

02-10-2024

Colophon

Title:

Modeling Cliff Erosion in Salt Marshes: Spatially varying erodibility coefficient based on vegetation

Author's details

Author: Rienk Pasma

Student number: 2874172

Study: Civil Engineering and Management (CEM)

Profile: River and Coastal Engineering

University: University of Twente

Committee:

Dr. ir B. Bosje (University of Twente)

Dr. ir. V. Kitsikoudis (University of Twente)

Ir. S. Dzimballa (University of Twente)

Dr. ir. I. Y. Georgiou (The Water Institute)

Ir. M. C. Bregman (The Water Institute)

Date: 2nd of October 2024

Place: Enschede

Version: Final version

Preface

This thesis presents research on enhancing a salt marsh cliff erosion model by incorporating the effects of vegetation on reducing cliff erodibility and adapting the model to the specific geographical context of Wierum, the Netherlands. Conducting this study has been challenging and rewarding, and I deeply appreciate the support and guidance I have received along the way.

I want to express my sincere gratitude to my supervisors, ir. S. Dzimballa, Dr. ir. V. Kitsikoudis, and Dr. ir. B. Bosje from the University of Twente, as well as Dr. ir. I.Y. Georgiou and ir. M.C. Bregman from The Water Institute, for their invaluable advice and constant encouragement throughout the research process.

My thanks also go to ir. P. Overes, Dr. ir. C. Esposito, and Deltares for their insightful answers to my questions. This thesis would not have been possible without the data and resources provided by the University of Twente and The Water Institute, for which I am sincerely grateful.

Finally, I hope that the findings of this research will contribute to a deeper understanding of salt marsh dynamics and support more effective coastal management and conservation efforts.

Rienk Pasma

Enschede, October 2, 2024

Summary

Salt marshes are vital coastal ecosystems that serve as natural buffers, protecting shorelines from erosion and flooding while providing critical habitats for wildlife and contributing to carbon sequestration. These ecosystems are characterized by halophytic vegetation, which is uniquely adapted to saline environments and plays a significant role in stabilizing sediments and attenuating wave energy. The dynamic interactions between sediment deposition and vegetation growth are central to the health and resilience of salt marshes, enabling them to maintain elevation relative to sea levels.

Salt marshes are increasingly threatened by rising sea levels, more frequent and intense storms, and human activities that accelerate erosion, particularly at their seaward edges. Understanding the dynamics of salt marsh erosion is crucial, as these areas play a vital role in coastal protection and habitat provision. These challenges highlight the need for accurate predictive models of cliff erosion. However, many existing models rely on simplified assumptions, such as a linear relationship between erosion rates and wave power, represented by an empirical coefficient for erodibility. This coefficient is however spatially uniform and does not fully capture the variability in erodibility introduced by different vegetation types, densities, and geotechnical parameters of the soil along the salt marsh, resulting in less accurate predictions. To address these gaps, this thesis investigates improving of a salt marsh cliff erosion model by incorporating the influence of vegetation on erosion and adapting the model to a different geographical location.

A model, originally developed for the Mississippi River Delta Plain (MRDP), was adapted to simulate salt marsh development in Wierum, the Netherlands. To adapt the model for a different geographical location, several adjustments were made, and additional processes were incorporated to account for site-specific variations. One key modification, prompted by the shift from a micro-tidal to a meso-tidal regime, was the exclusion of wave power when the cliff is flooded, as the higher tidal range increased the likelihood of marsh inundation. Additionally, the model was refined to use different datasets that reflect local conditions, deviating from those used in previous applications. These modifications underscore the uniqueness of each salt marsh system and highlight the implications of these differences for accurate salt marsh modeling. The cliff erosion model employed offline coupling with the Delft3D-FM model, which simulates hydrodynamic and morphodynamical processes. The study involved calibrating an erodibility coefficient and parameterizing vegetation effects on salt marsh cliffs. Validation was conducted using observed erosion rates from 27 cross-sections with varying vegetative cover, employing statistical metrics to assess model accuracy. The study iteratively parameterized five stem densities to maximize these statistical metrics. Key findings demonstrate that vegetation significantly reduces cliff erodibility, with reductions ranging from 27% to 68% depending on stem density.

The implications of this research are substantial for coastal management practices, offering a more accurate predictive tool for erosion rates and informing targeted conservation and restoration efforts. By improving the representation of vegetation effects in erosion models, this study contributes to a deeper understanding of the resilience of coastal ecosystems and supports the development of sustainable coastal defense strategies. Future research recommendations include refining erosion models by incorporating additional site-specific factors, conducting multiple case studies across different geographical locations, and improving model stability and accuracy. These enhancements will support more effective coastal management practices and contribute to a broader knowledge base regarding the resilience of coastal ecosystems, ensuring sustainable protection against coastal hazards.

List of figures

List of tables

Nomenclature

Acronyms

- **AHN:** Actueel Hoogtebestand Nederland
- **DCSM:** Dutch Continental Shelf Model
- **Delft3D-FM:** Delft3D Flexible Mesh
- **LIDAR:** Light Detection and Ranging
- **MAE:** Mean Absolute Error
- **MHW:** Mean High Water
- **MRDP:** Mississippi River Delta Plain
- **MSL:** Mean Sea Level
- **NAP:** Normaal Amsterdams Peil
- **NDVI:** Normalized Difference Vegetation Index
- **R-squared:** Coefficient of Determination
- **RMSE:** Root Mean Squared Error
- **SWAN:** Simulating WAves Nearshore

Symbols

- $\boldsymbol{a_{er}}$: Erodibility coefficient
- $\boldsymbol{b_{cell}}$: Width of cell
- $\boldsymbol{c_g}$: Wave group celerity
- $\boldsymbol{g}$: Gravitational force
- $\boldsymbol{h}$: Water depth
- $\boldsymbol{\Delta h}$: Elevation difference
- $\boldsymbol{H_w}$: Wave height
- $\boldsymbol{L_{ero}}$: Lateral erosion
- $\boldsymbol{V_{eroded}}$: Eroded volume
- $\boldsymbol{W_p}$: Wave power
- $\boldsymbol{\rho}$: Density of water

Units

- $\boldsymbol{J/m^2}$: Joules per square meter
- $\boldsymbol{kg/m^3}$: Kilograms per cubic meter
- $\boldsymbol{m}$: Meter
- $\boldsymbol{m^2}$: Square meter
- $\boldsymbol{m^3}$: Cubic meter
- $\boldsymbol{m/s^2}$: Meters per second squared
- $\boldsymbol{m/yr/(W/m)}$: Meters per year per watts per meter

Contents

1. Introduction

Salt marshes are dynamic coastal ecosystems situated at the boundary between land and sea, renowned for their ecological significance and their ability to serve as natural barriers against coastal hazards (Leonardi et al., 2018). These environments, characterized by halophytic (salt-tolerant) vegetation, play a crucial role in coastal defense, carbon sequestration, and biodiversity support. Covering an estimated 200,000 to 400,000 square kilometers of the global coastline, salt marshes act as vital buffers by absorbing wave energy, mitigating the impact of storms, and reducing erosion in coastal areas (Neumeier & Amos, 2006; Möller et al., 2014; Anderson & Smith, 2014). This protective function is largely due to the marshes' capacity to increase the roughness of the intertidal area, thereby reducing wave power and erosion rates (Micheli & Kirchner, 2002). Understanding and harnessing these protective functions are imperative for sustainable coastal management and climate resilience (Gedan et al., 2011).

Vegetation plays a crucial role in the functioning and resilience of salt marsh ecosystems. Different species, such as *Puccinellia Maritima*, thrive in salt marsh environments, contributing to the biodiversity and stability of these ecosystems (Esselink, 2017). Vegetation zones within salt marshes, including pioneer, low marsh, and high marsh areas, exhibit distinct characteristics and species compositions (Wanner et al., 2014). The spatial distribution of vegetation influences hydrodynamics, affecting current velocities and wave attenuation (Christiansen et al., 2000). During floods, vegetation within salt marshes attenuates waves and currents, due to the increase in roughness, which in turn influences the transport and deposition of sediments (Christiansen et al., 2000). Sedimentation processes contribute to the lateral extension and elevation of salt marshes, although they are limited by external factors, such as storms, and erosion (Christiansen et al., 2000). Channels formed within salt marshes play a vital role in draining water, sediment, and nutrients, influencing the expansion and dynamics of vegetated areas (Coco et al., 2013; FitzGerald & Hughes, 2021).

Despite their resilience, salt marshes face increasing threats from anthropogenic pressures, sea level rise, and intensified storm activity (Leonardi et al., 2018). Mechanisms such as marsh drowning, channel widening, and cliff erosion contribute to the loss of salt marsh extent, posing challenges for coastal protection efforts, by reducing the marsh's ability to buffer wave energy and protect against storm surges (Gedan et al., 2011). Cliff erosion involves the retreat of the marsh edge or scarp due to the persistent action of waves and tidal forces, leading to the collapse and landward retreat of the marsh edge (Gedan et al., 2011). The rate of this retreat can vary significantly, influenced by factors such as wave energy, sediment composition, and vegetative cover (Fagherazzi, et al., 2013). Despite the recognized importance of lateral salt marsh extent for flood protection, the dynamics of cliff erosion remain poorly understood, hampering effective conservation strategies (Neumeier & Amos, 2006; Finotello et al., 2020b)

The dynamic nature of salt marsh ecosystems is characterized by the cyclic behavior of lateral marsh extension over timescales of decades to centuries (Van der Wal et al., 2008). This cyclic behavior highlights alternating periods of marsh extension towards the sea during establishment phases of pioneering vegetation, characterized by low hydrodynamic activity, erosion, and sedimentation rates (Balke et al., 2014). However, under increasingly challenging conditions such as intensified wave action or higher water levels, the erosion of the mudflat can accelerate. This can result in increased cliff height, which in turn leads to greater instability and promotes further cliff erosion (FitzGerald & Hughes, 2021). Vegetation plays a crucial role in reducing erosion by increasing sediment resistance through its root system (Lo et al., 2017). The below-ground biomass of vegetation correlates negatively with erosion,

indicating that larger biomass of roots contributes to lower erosion rates (Lo et al., 2017). This multifaceted interaction between vegetation, sediment dynamics, and erosion processes underscores the complexity of salt marsh ecosystems and the need for a comprehensive understanding for coastal protection and conservation efforts.

1.1 Problem statement

Current models of salt marsh cliff erosion often simplify the complex relationship between erosion rates and wave power by using a constant empirical coefficient to represent the erodibility of the marsh edge (Marani et al., 2011; Leonardi et al., 2016). While practical, this approach does not adequately account for the variability introduced by vegetation and other site-specific conditions (e.g. cliff shape and edaphic factors), leading to potential inaccuracies in predicting erosion rates. Recent studies suggest that the erodibility coefficient is not fixed; it varies significantly depending on factors such as vegetation type and density (Houttuijn Bloemendaal et al., 2023). This variability is a critical gap in current modeling approaches, which often overlook the detailed influence of vegetation on erosion processes.

This thesis addresses these gaps by enhancing the modeling of salt marsh cliff erosion through the parameterization of vegetation effects. In this thesis, the parameterization of the vegetation effects is defined as a vegetation density factor. Parameterization is based on how much percent each vegetation density decreases the erodibility of the salt marsh edge. This is particularly through the role of root systems in stabilizing soil and reducing lateral erosion rates. By developing a better representation of the erodibility coefficient that varies spatially according to vegetation cover, this research aims to improve the predictive accuracy of cliff erosion models.

Furthermore, this study examines the implications of applying erosion models to a different geographical location. As erosion models are adapted from one region to another, from the Mississippi River Delta Plain (MRDP) in the United States of America, to Wierum in the Netherlands, adjustments are necessary to accommodate differences in data availability, tidal ranges, climatic conditions, and vegetation dynamics. Understanding and documenting these adjustments is crucial for maintaining the accuracy and relevance of the models across diverse settings.

The specific objectives of this research are to:

- **Document the effects of changing geographical locations:** The study will assess how geographical variations impact the modeling approach and parameter adjustments. This included changes in data availability, resolution, tidal ranges, climatic conditions, and other changes.
- **Enhance an existing cliff erosion model to integrate vegetation effects:** This research will refine an existing erosion model to incorporate the effects of vegetation on top of the cliff. The enhanced model will account for the influence of vegetative cover in reducing erosion rates, improving the model's ability to simulate the protective role of vegetation in coastal environments.
- **Parameterize the impact of different vegetation densities on cliff erosion:** Through salt marsh modeling, this research will quantify the effects of various vegetation densities on erosion resistance. The findings will be used to develop parameterized functions that accurately represent the varying degrees of protection provided by different vegetation densities.

- **Analyze site-specific conditions and vegetation densities:** This research will examine how site-specific factors, such as wave energy, and vegetation densities, influence erosion rates. The findings will help to tailor the enhanced model to different environmental conditions, improving its applicability across diverse salt marsh ecosystems.

These objectives are reached through answering the following research questions:

Main Research Question:

- *How can the integration of a spatially varying erodibility coefficient based on vegetation density improve the predictive accuracy of salt marsh cliff erosion models in terms of erosion rates and spatial patterns?*

This main research question guides the research, directing efforts toward refining, adjusting, and testing the hydrodynamic model for widespread application in smaller salt marsh systems worldwide.

Sub-Questions:

1. *What specific adjustments in boundary conditions, domain, and physical processes are required to adapt the hydrodynamic and cliff erosion models to the Wierum salt marsh?*
2. *How can vegetation density effects be parameterized and incorporated to create a spatially varying erodibility coefficient in the erosion model?*
3. *How does the spatial variability of the erodibility coefficient impact the model's predictive accuracy in simulating short term spatial cliff erosion rates?*

By incorporating the detailed influences of vegetation into erosion models, this research aims to provide a more comprehensive and accurate understanding of salt marsh dynamics, supporting the development of targeted conservation and management practices. This introduction sets the stage for the following chapters, which will explore the fundamental characteristics of salt marshes, the current understanding of cliff erosion dynamics, the specific research gaps addressed by this thesis, methods to improve cliff erosion modeling, the modeling results, and the discussion and conclusion.

1.2 Reading guide

This section outlines how the research questions will be addressed across different chapters of this thesis, with a brief description of the content of those chapters.

The first sub-question is answered in Chapter 3.3, which focuses on the key modifications made to the salt marsh cliff erosion model, originally developed by the Water Institute, as it was adapted from the MRDP to the Wierum region in the Netherlands. This chapter discusses changes in data availability, model resolution, and processes, including adjustments to salt marsh classification and cliff erosion mechanisms. Challenges related to refining the model for local conditions, such as grid resolution, vegetation variability, and bathymetric instability, are also explored.

The second sub-question is covered in Chapter 3.9, where the role of vegetation in stabilizing salt marsh cliffs is examined. The chapter focuses on how root systems contribute to sediment binding, with an emphasis on stem density parameterization to represent vegetation's impact on erosion. It also discusses adjustments to the erodibility coefficient to improve model accuracy.

The third sub-question is addressed in Chapter 4, which explain the parameterization of both vegetated and unvegetated cells in the model. These chapters provide details on how erodibility coefficients were adjusted based on stem densities and describe the iterative process of calibrating the model to align with observed erosion patterns. The impact of these adjustments on model performance is analyzed, noting areas where improvements were made and where discrepancies remained.

Finally, the main research question is answered in the Conclusion chapter, bringing together the findings from the sub-questions.

2. Theoretical framework

This theoretical framework chapter provides the foundational concepts guiding this study on salt marsh cliff erosion dynamics. This chapter examines existing ecological and geomorphological theories relevant to salt marsh ecosystems, explores the mechanisms driving cliff erosion processes, and evaluates current numerical modeling approaches. By combining these insights, this chapter aims to clarify the complex interactions between vegetation dynamics, sediment dynamics, and erosion processes in salt marsh environments. Ultimately, this theoretical framework provides a structured basis for investigating how vegetation influences erosion rates and for improving numerical models.

2.1 Salt marshes

Salt marshes are complex and dynamic coastal ecosystems that undergo continuous changes due to the interplay between biological, physical, and chemical processes (Fagherazzi, Mariotti, et al., 2013). This section delves deeper into the intricate processes governing salt marsh development, focusing on sediment dynamics, hydrodynamics, vegetation interactions, and the impacts of external factors such as sea level rise and climate change.

2.1.1 Sediment dynamics

Sediment dynamics in salt marshes are driven by the deposition and erosion processes that occur due to tidal actions and storm events (Belliard et al., 2016; Temmerman et al., 2013). Sediment deposition is crucial for marsh accretion, which is necessary for the marsh to keep pace with rising sea levels (Marion et al., 2009). The primary sources of sediments in salt marshes include tidal influxes and riverine inputs, which deposit both mineral and organic matter onto the marsh surface (Vernberg, 1993).

The distribution of sediment within a salt marsh is not uniform. Areas closer to tidal channels tend to receive more sediment due to higher water velocities, while regions further away experience less sedimentation (Friedrichs C. T. & Perry J. E., 2001). This gradient is influenced by the frequency and duration of tidal inundation, with lower elevation areas receiving more frequent and prolonged flooding, leading to higher sediment deposition rates (Belliard et al., 2016).

These tidal creeks typically start as small erosional features on the marsh surface, typically in non-vegetated areas (Temmerman et al., 2007). Over time, repeated tidal inundations and runoff events deepen and widen these channels, establishing a more permanent creek system (Temmerman et al., 2007).

2.1.2 Vegetation dynamics

Vegetation in salt marshes plays a critical role in sediment stabilization and accumulation. Plant roots bind the soil, reducing erosion and enhancing sediment retention (Peralta et al., 2008). Additionally, the above-ground biomass of marsh vegetation attenuates wave energy, which further protects the marsh surface from erosion and promotes sediment deposition (Anderson & Smith, 2014).

The type of vegetation present in a salt marsh can vary depending on salinity levels, tidal inundation frequency, and sediment composition (Wanner et al., 2014). For example, low marsh areas, which are frequently inundated, are typically dominated by species such as *Spartina Alterniflora* (Belliard et al., 2016). These species are called pioneering vegetation. These locations are naturally species-poor, meaning a few different kinds of species (Wanner et al., 2014). This type of vegetation is the first one to grow in the mudflat and can typically withstand more extreme conditions. They form the basis of the salt

marsh and reduce hydrodynamic activity. Under these calm conditions, other salt marsh species can grow, increasing the species richness. However, the significance of competition between different species increases, and the prevalence of competitive species can diminish the diversity of species (Wanner et al., 2014)

Higher marsh areas, which experience less frequent flooding, support species like *Spartina patens* and *Juncus gerardii* (Belliard et al., 2016). The salt marsh can be spatially divided into three zones in the cross-shore direction: the pioneer zone, the low marsh, and the high marsh (Figure 1). In this figure it is also visible that the more densely vegetated areas are higher up in the marsh, this is due to the calmer conditions (Wanner et al., 2014).

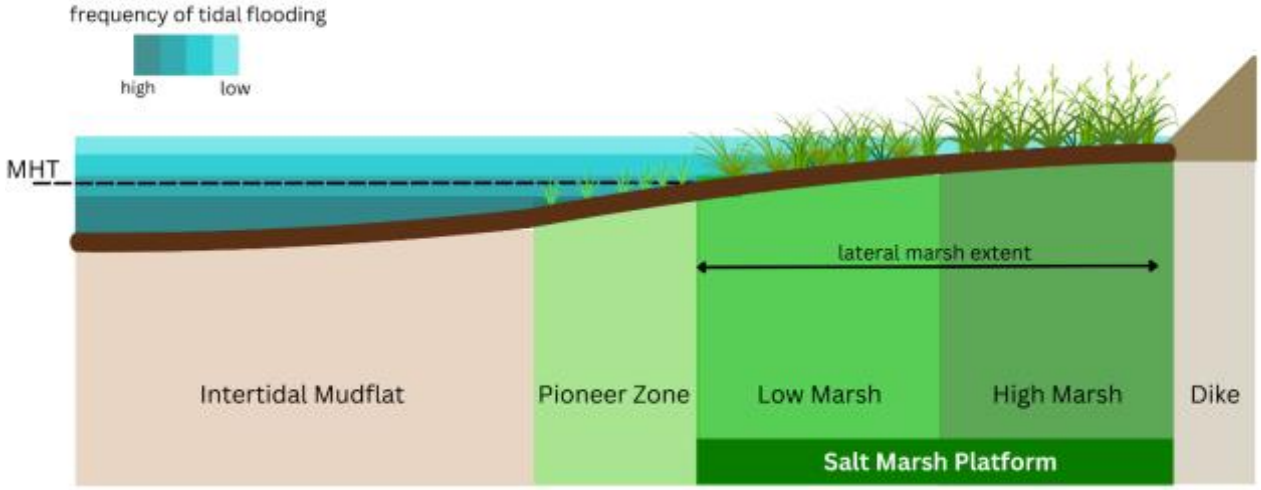

Figure 1 Cross section of a salt marsh, with its different areas (MHT = Mean High Tide) (Dzimballa, 2023).

2.1.3 Feedback mechanisms

The interaction between sediment and vegetation dynamics creates feedback mechanisms that are crucial for the stability and resilience of salt marshes. For instance, increased sediment deposition can enhance plant growth by providing essential nutrients and creating a more stable substrate for root establishment (Mudd et al., 2013). In turn, denser vegetation can trap more sediments and reduce erosion, creating a positive feedback loop that supports marsh elevation gain and resilience to sea level rise (Palmer et al., 2004).

Conversely, negative feedback can occur if sediment supply is insufficient or if vegetation is damaged by storms or human activities. In such cases, erosion may outpace sediment deposition, leading to marsh degradation and loss. This delicate balance between sediment supply, vegetation growth, and external stressors determines the long-term sustainability of salt marsh ecosystems (Belliard et al., 2016).

2.1.4 External forces on salt marshes

Salt marshes play a crucial role in attenuating storm surges and wave energy. The dense vegetation and complex geomorphology of salt marshes act as natural barriers, reducing the velocity and energy of incoming water (Leonardi et al., 2018). Studies have shown that salt marshes can reduce storm surge levels by 1.7 to 25 cm per kilometer, depending on the specific characteristics of the marsh and the storm (Wamsley et al., 2010) .

2.1.4.1 Wave energy dissipation

The effectiveness of salt marshes in dissipating wave energy is particularly significant during storms. The stems and roots of marsh vegetation absorb and dissipate wave energy, thereby reducing the impact on inland areas (Leonardi et al., 2018). The flexibility of the vegetation plays a key role; flexible stems are likely to bend and lay flat during intense storms, protecting the marsh surface from erosion by dissipating less energy, while stiffer plants might break and increase turbulence (Mullarney & Henderson, 2010).

2.1.4.2 Impact on salt marsh morphology

The external forces can have varied geomorphic impacts on salt marshes, influencing their long-term resilience. These impacts include incision, erosion, deposition, and deformation:

Incision: Storm-induced ponds form in lower terrain areas, which can enlarge and deepen over time. When these ponds are connected to tidal channels, it can lead to sediment loss when there is more erosion than sedimentation. This is because eroded sediment can be transported away through these channels. The increasing size of the ponds can lead to edge erosion due to wind waves generated within the ponds, and the redistributed sediment is then carried out of the salt marsh system (Fagherazzi et al., 2013).

Erosion: Currents and waves induce shear stresses on the vegetated surface of the marsh. This can cause denudation of marsh vegetation (root scalping) (Priestas et al., 2015). The depth of denudation influences the likelihood and speed of recovery in the affected areas. If the eroded regions stay above permanently submerged levels and the roots remain intact, recovery can happen in the following growing seasons. However, if these conditions are not met, the areas might turn into ponds or bare tidal flats (Leonardi et al., 2018).

The deepening of ponds or bare tidal mudflats increases wave energy at these locations, which promotes lateral erosion (Leonardi et al., 2018). Additionally, the removal of vegetation near the marsh edges can increase the lateral erosion of marsh banks (Fagherazzi et al., 2006).

Deposition: External forces can deposit sediments into the marshes, especially during storms where breaching and flooding of the salt marsh occur (Leonardi et al., 2018). The direction of sediment transport influences whether deposits are laid over marsh surfaces or moved seaward. Storms enhance tidal deposition through increased sediment concentrations and flow velocities. Large storms increase mineral matter supply from offshore via tidal creeks (Leonardi et al., 2018).

Deformation: Subsurface processes like soil compaction or swelling due to storm surges can cause substantial changes in marsh elevation. The increased weight on top of the salt marshes due to floodings compacts the soil (Leonardi et al., 2018).

2.1.4.3 Sediment budget

The sediment budget of a salt marsh is a critical factor in its resilience to external factors. Salt marshes rely on a balance of sediment input and erosion to maintain their elevation relative to sea level. Storms can disrupt this balance by either adding large amounts of sediment (which can be beneficial in the long term) or by eroding significant portions of the marsh surface (Ganju et al., 2013); (Rosencranz et al., 2016). The sources of sediment include external contributions from eroded neighboring coasts and riverine discharge, as well as internal resuspension from intertidal flats and marsh edges (Leonardi et al., 2018).

2.1.4.4 *Resilience to sea level rise*

External forces also impact the ability of salt marshes to keep pace with sea level rise. Severe storms can deposit significant sediment layers that contribute to vertical accretion, helping marshes maintain their elevation. However, continuous erosion from frequent storms can undermine this resilience, especially if sediment is permanently lost from the system rather than redistributed within the marsh complex (Leonardi et al., 2018).

2.2 Cliff erosion

Cliff erosion at the salt marsh edge is a process affected by multiple factors. This erosion phenomenon involves the gradual retreat of salt marsh edge, primarily influenced by natural forces. A key focus lies on the impact of waves, highlighting the intricate relationship between waves and the salt marsh edge.

The interaction between waves and the salt marsh edge is the main mechanism that drives erosion. Waves striking the sensitive marsh scarp initiate cliff erosion, leading to salt marsh retreat. Annual rates of salt marsh retreat vary globally, ranging from 0.1 meters to over 3 meters (Fagherazzi et al., 2013). The intensity of wave impact significantly correlates with the rate of cliff erosion, especially when water levels align with the elevation of the salt marsh. While storm surges contribute to cliff erosion, cyclical variations in water levels during tidal cycles suggest that storm surges alone may not be the main driver of this phenomenon (Fagherazzi et al., 2013). Other factors influencing salt marsh edge erodibility encompass both biotic and abiotic elements. These include the geotechnical properties of sediments, vegetation characteristics, marsh scarp elevation, and the presence of organisms like mussels or burrowing crabs (Leonardi et al., 2016).

The intensity of wind waves influences the shape of marsh boundaries, with wave intensity and spatial variability in marsh resistance playing key roles (Leonardi & Fagherazzi, 2015; Leonardi & Fagherazzi, 2014). Natural differences in soil resistance and ecological processes cause variability in erosional resistance. Low wave energy leads to unpredictable, jagged boundary profiles, while high wave energy results in consistent erosion and smoother profiles. Frequent intense storms further smooth marsh boundaries without significantly altering average erosion rates. Marshes with weak wave energy are most vulnerable to extreme event frequency variations (Leonardi & Fagherazzi, 2015; Leonardi & Fagherazzi, 2014).

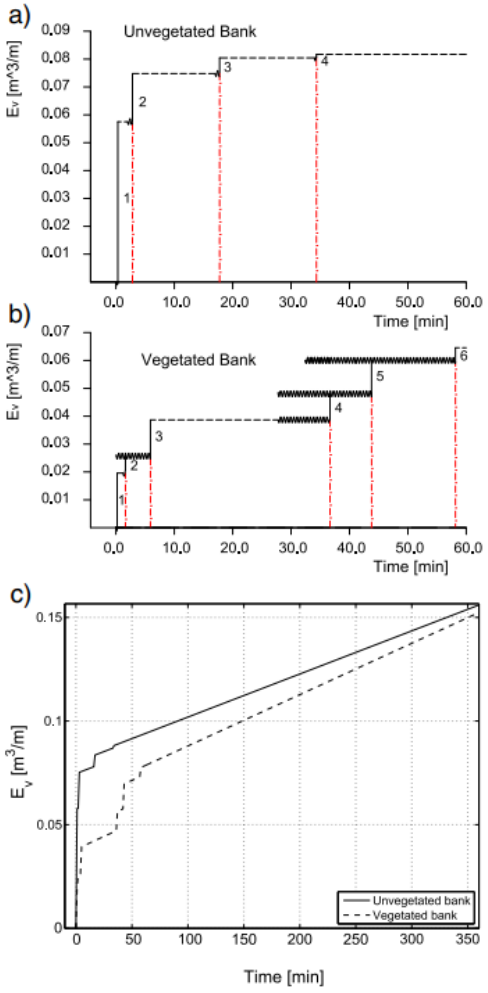

Figure 2 Volume lost due to cliff erosion for unvegetated (a) and vegetated (b) banks over time. c) shows the cliff erosion over a longer time frame. Graphs shows less cliff erosion when the bank is vegetated (E_v=Eroded volume in cubic meters per meter) (Francalanci et al., 2012).

The significance of wind waves in contributing to cliff erosion is underscored by Francalanci et al. (2012). Their flume laboratory experiments reveal that the forcing of wind waves plays a crucial role in cliff erosion. Vegetation,

particularly the presence of roots, proves instrumental in maintaining soil integrity and delaying mass failures, highlighting the role of vegetation in erosion resistance (Figure 2).

Furthermore, Francalanci et al. (2012) explore the failure mechanisms of the salt marsh edge (Figure 3). Tidal forcing in unvegetated scenarios creates tension cracks during tidal peaks, weakening the soil. With subsequent tidal lowering, water pressure within these tension cracks increases, triggering slide failures. The addition of wind waves increases pressure in tension cracks, expediting failure mechanisms. Vegetation, especially root systems, mitigates these processes, enhancing stability.

Vegetation's role is further supported by Fagherazzi et al. (2013), which emphasizes the role of both aboveground and belowground vegetation in cliff erosion. Aboveground elements, such as plants, mitigate flow velocities, trap sediment, and attenuate waves. Belowground roots and rhizomes stabilize sediment, providing an additional layer of erosion resistance (Lo et al., 2017).

According to Lo et al. (2017), vegetation on top of the salt marsh scarp can greatly decrease the erodibility of the salt marsh edge. The effectiveness, however, is influenced by the type of soil the salt marsh has. Lo et al. (2017) stated that cliff erosion decreased by 80% when vegetation was placed on top of sandy soils. While vegetation decreased cliff erosion by 17% on silty soils.

Furthermore, the effectiveness of marsh edge stability depends on the root system's binding capacity to sediment, influenced by factors like biomass, root length, diameter, and tensile strength. Despite these stabilizing factors, marsh edges remain vulnerable to undercutting, especially in conditions of excessive nutrients weakening creek banks, leading to slumping and lateral erosion (Fagherazzi et al., 2013). The effectiveness of the vegetation is also a seasonal variable. According to Du et al. (2019), roots die off when stem densities and height decrease, reducing the root system’s binding capacity to sediment.

The shape of cliffs also affects the processes of cliff erosion and wave impact. Different cliff geometries result in varied interactions with incoming waves, influencing both the intensity of erosion and the

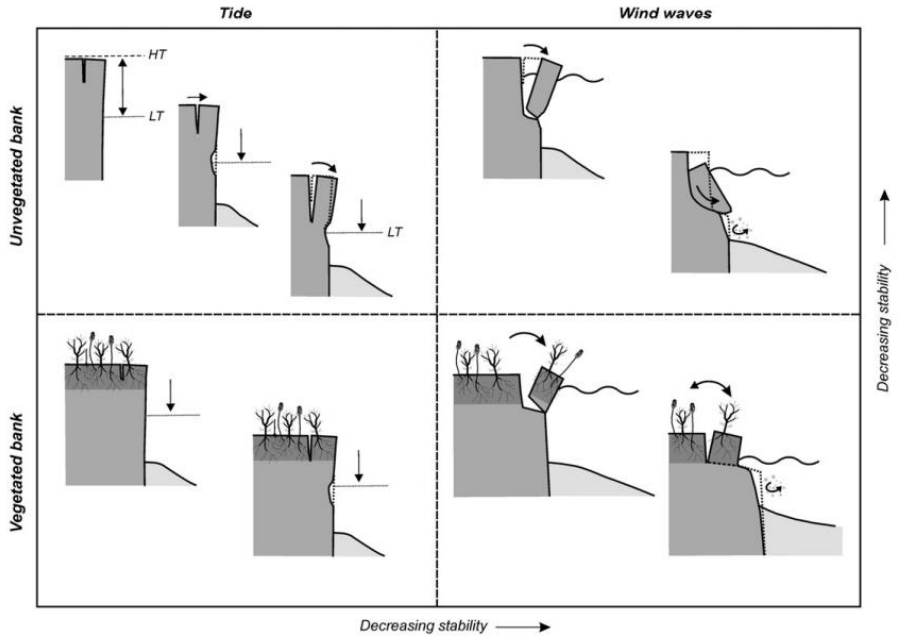

Figure 3 Different failure mechanisms of vegetated and unvegetated salt marsh cliffs due to tidal currents and wind waves (Francalanci et al., 2012).

pattern of wave reflection and dissipation. Tonelli et al. (2010) provides insights into how vertical, sloping, and terraced cliffs interact with wave forces and contribute to erosion (Figure 4).

Vertical cliffs reflect incoming waves almost entirely, meaning that the waves hit the cliff face and bounce back into the ocean rather than being absorbed or dissipated. This reflection leads to a doubling of wave height at the cliff base because the incoming and reflected waves combine their energies. This increased wave height intensifies the force exerted on the cliff, which accelerates the erosion process, particularly at the base of the cliff, leading to undercutting and collapse. The vertical structure often results in significant undercutting at the base, creating overhangs that eventually fall due to gravity and further wave action. This process contributes to the formation of an eroding scarp (Tonelli et al., 2010).

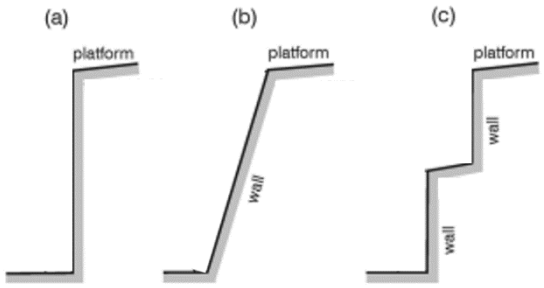

Figure 4 Different cliff shapes, a) vertical cliff, b) sloped cliff, c) terraced cliff (Tonelli et al., 2010).

Sloping cliffs, or ramped edges, dissipate wave energy more gradually. The sloping nature reduces the height of the reflected waves compared to vertical cliffs, resulting in a lowered erosive power of the waves and potentially reducing the rate of erosion. Although sloping cliffs still experience significant wave impact, the force is spread over a larger area, mitigating some of the direct erosive effects seen in vertical cliffs (Tonelli et al., 2010).

Terraced cliffs, consisting of a series of steps or terraces, provide a complex interaction with wave forces. The terraces can break and dissipate wave energy at multiple points, significantly reducing the overall force impacting any single section of the cliff. The highest platform of the terraced boundary typically lies above mean sea level, reducing direct wave impact on the upper sections of the cliff. The lower sections, such as the wave terrace, handle the majority of the wave energy, thus protecting the upper cliffs from severe erosion (Tonelli et al., 2010).

The shape of the cliff, therefore, determines how wave energy is distributed and dissipated, influencing the rate and pattern of erosion. Vertical cliffs face higher direct wave impact and rapid undercutting, sloping cliffs experience more gradual erosion due to energy dissipation, and terraced cliffs benefit from stepped energy absorption n, reducing the erosive force on the upper cliff sections. This understanding is crucial for managing and mitigating coastal erosion effectively (Tonelli et al., 2010).

According to Leonardi et al. (2016), observations in eight different salt marshes in the United States, Australia, and Italy show that salt marsh erosion occurs continuously, even at low wave energy conditions. Therefore, there is no critical threshold where erosion occurs. When wave energy does increase, no catastrophic erosion rates occur, highlighting salt marshes' resilience against extreme events. Leonardi et al. (2016) states that the highest contributor to erosion is moderately frequent weather conditions, whereas storms and hurricanes only contribute

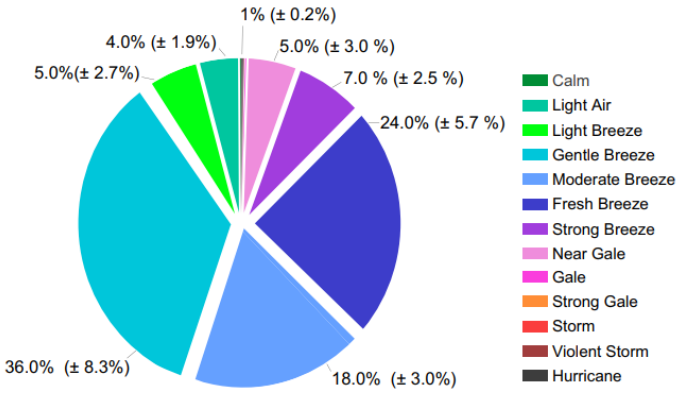

Figure 5 Pie chart of contributors to cliff erosion (Leonardi et al., 2016).

less than one percent to total yearly cliff erosion (Figure 5). Supported by these findings, a linear relation suggested by Marani et al. (2011) between cliff erosion and wave power has been made:

$$E_w = \alpha_w \cdot W \quad [1]$$

Herein is E_w, W and α_w the erosion rate, wave power and empirical erodibility coefficient respectively. The linear relation is in line with the observations, as there is no critical threshold for erosion to occur, and there is no exponential growth in erosion with increasing wave power (Leonardi et al., 2016).

Finotello et al. (2020) confirmed that there is indeed a linear relation between wave power and erosion rates, by simulating salt marsh edge erosion along the Venice Lagoon. In this paper, a model based on field data was created to investigate the relation between cliff erosion and wave power. This paper also states the importance of vegetation on the cliff, which influences the empirical erodibility coefficient. The coefficient is used as a constant in Leonardi et al. (2016), however Finotello et al. (2020) states that different kinds of vegetation within a salt marsh have different effects on the stability of the soil. This would rule out the existence of a constant erodibility coefficient. This theory is suggested by Houttuijn Bloemendaal et al. (2023), as they mention that the relation is site-specific.

In the paper by Houttuijn Bloemendaal et al. (2023), the linear relation between cliff erosion and wave power has been reevaluated. According to this paper, there is no clear universal relationship between erosion and wave power, linear or otherwise. It is important to consider the complexity of each salt marsh system individually, as different influences on the marsh retreat are present (Houttuijn Bloemendaal et al., 2023). Various influences shape the dynamics of coastal areas. These include the bioturbation activities of crabs, the resilience of local marshes against erosion, clamming, and other region-specific human activities. Differences in edge morphology play a role in determining exposure to local wave patterns, while the fluctuation in bulk density and bank height adds complexity to the coastal dynamics. In addition, variations in adjacent water depths affect factors such as wave energy dissipation, sediment transport, and tidal dynamics, which together influence erosion patterns and marsh stability. These hydrodynamic variations, combined with other influences like vegetation cover and bank height, shape the complex interplay of forces acting on the coastal ecosystem (Houttuijn Bloemendaal et al., 2023).

2.3 Regional and geographical variations

Salt marshes are dynamic ecosystems whose characteristics and behaviors vary significantly across different regions and geographical contexts. Understanding these regional variations is crucial for accurately modeling salt marsh dynamics and developing effective conservation strategies. This chapter examines the various factors that may differ from one location to another, such as climate, water movement, sediment composition, vegetation types, geographical features, human activities, and data availability, and how these differences can influence salt marsh ecosystems.

2.3.1 Climate

Climatic conditions, including temperature, precipitation, and storm frequency, significantly influence the development, stability, and erosion of salt marshes. In temperate areas like Western Europe, seasonal changes impact plant growth and sediment deposition (Fagherazzi et al., 2013). Conversely, subtropical regions such as the MRDP experience milder winters and more frequent hurricanes, resulting in distinct erosion and deposition patterns (Cahoon, 2006).

Research indicates that rising temperatures can boost plant productivity, thereby stabilizing sediments and encouraging marsh expansion (Coldren et al., 2016). However, increased temperatures can also lead to higher evaporation rates, elevating salinity levels and potentially stressing salt-tolerant plants (Pearey & Ustin, 1983). Moreover, areas with substantial precipitation and frequent storms exhibit dynamic sediment transport processes, which have a profound impact on marsh morphology (Cahoon, 2006; Fagherazzi, FitzGerald, et al., 2013).

2.3.2 Hydrodynamics

Hydrodynamics are spatially variable all over the world. Salt marshes can be influenced by micro- (mean tidal range smaller than two meters) meso-(mean tidal range between two and four meters) and-macro-(mean tidal range larger than four meters) tidal ranges and different wave heights (French, 2018). Smaller tidal ranges tend to have smaller velocity currents, resulting in smaller sediment transport. This is, however, very site-dependent, as microtidal can cause strong tidal currents within constricted inlets. In addition, flooding events caused by storms are often of greater importance in a micro-tidal setting. This is because storms can introduce sediment deposition where deposition during normal tidal conditions is limited (French, 2006). Higher tidal amplitudes generally introduce higher tidal currents within the salt marsh and tidal mudflat systems, increasing the suspended sediment concentration and thus, sediment transport (French, 2018).

Waves are dependent on multiple factors and thus can vary spatially. Wind waves are influenced by wave speed and direction, fetch, and morphology. Waves along the coast are generally higher and contribute more to sediment redistribution and erosion compared to lower waves within a sheltered estuarine setting (French, 2018).

Other aspects that are influenced by hydrodynamics such as salinity and suspended sediment concentrations also differ for each specific site. Salinity influences the sedimentation, as for certain sediment types a higher salinity means more sedimentation (Gorakhki & Bareither, 2015).

2.3.3 Soil composition

The soils of salt marshes vary spatially, in grain sizes and cohesiveness. The smaller the grain size of the sediment, the more cohesive it is. Cohesive soils, such as silt and clay, are more resilient against erosion compared to more coarse sediments, such as sand. The soil type and its availability thus impact the morphology of the salt marshes (Esselink, 2017).

2.3.4 Vegetation

Different types of halophytic vegetation can be found in salt marshes around the world. These species of vegetation have different characteristics, such as stem height, stem width, stem density, and flexibility. These characteristics influence the ability for soil stability, erosion resistance, and sediment retention. Therefore, it is crucial to select vegetation characteristics that accurately represent the species found within the study area for use in the model (Peralta et al., 2008).

2.3.5 Geographical features

Local geographical features, such as the presence of tidal creeks, proximity to rivers, and coastal topography, influence salt marsh dynamics. Tidal creeks play a vital role in draining water, sediment, and nutrients, affecting the expansion and dynamics of vegetated areas (Friedrichs C. T. & Perry J. E., 2001). The proximity to freshwater sources, such as rivers, can also impact salinity levels and sediment supply, influencing marsh growth and stability (Boorman, 2018).

2.3.6 Human activities

Human activities, including coastal development, land use changes, and resource extraction, vary across regions and significantly impact salt marsh ecosystems. Coastal development can lead to habitat loss and increased erosion, while land use changes, such as agriculture and urbanization, can alter sediment supply and water quality (Gedan et al., 2009).

Also, interventions intended for salt marsh restoration, like brushwood dams, can alter the hydrodynamic conditions. These brushwood dams successfully trap sediment and decrease the current velocities and wave action at the salt marshes (Vuik et al., 2019).

2.3.7 Data availability

Data availability and quality vary significantly across regions, influencing the accuracy and applicability of salt marsh models. Some regions have extensive monitoring programs and high-quality datasets, while others may lack comprehensive data coverage (Gedan et al., 2011). These disparities necessitate adjustments in modeling approaches to account for regional differences in data availability and environmental conditions.

By understanding and documenting these regional and geographical variations, this research aims to improve the accuracy and relevance of salt marsh erosion models, supporting targeted conservation and management efforts across diverse coastal settings.

2.4 Background in numerical models in salt marsh modeling

Previous studies have utilized various modeling approaches to simulate the intricate dynamics of salt marshes. This chapter summarizes methodologies for modeling these complex interactions by examining how different models simulate forcings, vegetation, and overall salt marsh development.

2.4.1 Simulating forcings

Forcings, such as waves, tides, and sediment transport, play a crucial role in shaping salt marshes. Different models incorporate these forcings to simulate the hydrodynamic environment and its impact on salt marsh boundaries.

Multiple studies have incorporated the Delft3D model to simulate hydrodynamical forcings. Willemsen et al. (2022) and Mariotti & Canestrelli (2017) both incorporated Delft3D, with the modules D-Flow, D-Waves, and D-Morphology. These extensions allowed for the simulation of two-dimensional unsteady shallow water equations, wave propagation, and cohesive sediment transport. These studies emphasized the importance of detailed hydrodynamic processes, such as tidal variations and wind-induced wave actions, in driving marsh morphodynamics.

On the contrary, Bendoni et al. (2014) utilize a different approach, incorporating wave thrust forcings against the marsh boundaries. For a regular wave train moving towards the scarp, the wave thrust can be evaluated based on the water depth, water displacement, and period of the waves. In the case of irregular wave series, wave thrust is determined theoretically using linear wave theory applied to each wave, identified from the zero-up crossing technique. Here, wave thrust is calculated without accounting for reflection effects. The zero-crossing wave height is defined as the difference between the highest crest and lowest trough between successive zero crossings.

2.4.2 Vegetation modeling

The modeling approaches by Mariotti and Canestrelli (2017) and Willemsen et al. (2022) highlight different methodologies for incorporating vegetation dynamics into salt marsh models.

Mariotti and Canestrelli (2017) used a simplified approach where vegetation growth was modeled between mean sea level and mean high water. They employed a parabolic function to represent the yearly peak of aboveground biomass, and the impact of vegetation on erodibility and drag force was modeled using different critical shear stresses and Chézy coefficients for vegetated and unvegetated cells. This approach provided a straightforward means of capturing vegetation effects but lacked dynamic growth and decay processes.

In contrast, Willemsen et al. (2022) integrated a dynamic vegetation growth module into the Delft3D-FM model. This module included processes like vegetation establishment, lateral expansion, clonal growth, mortality due to shear stress, and inundation stress. By incorporating these detailed processes, the model could simulate realistic vegetation dynamics over time.

2.4.3 Salt marsh cliff erosion modeling

There are different modeling approaches regarding salt marsh development. For example, marsh edge retreat due to wave impact in the model by Mariotti & Canestrelli (2017), is calculated based on empirical coefficients related to wave power, with erosion primarily occurring on unvegetated cells adjacent to vegetated marsh boundaries. To model marsh edge erosion numerically, a probabilistic approach is employed to determine whether a marsh boundary cell erodes during a time step, based on the wave-induced erosion rate at each edge. This method ensures that erosion rates align with observed field measurements, maintaining realism in long-term simulations.

In their paper, Mariotti & Canestrelli (2017) list two different approaches for marsh cliff erosion: a probabilistic approach (used in their study) and a deterministic approach. The probabilistic approach uses the erosion rate (Equation 1) and a randomly determined number to decide whether the marsh cell erodes or not. In contrast, the deterministic approach tracks the percentage of erosion that occurs in a grid cell, eroding the cell only when erosion reaches a certain threshold.

Both approaches have their advantages and drawbacks. The deterministic approach offers a more realistic representation of the erosion process by monitoring it over time. However, it has a limitation: if one marsh cell experiences 80% erosion, the neighboring cell, which has not yet undergone erosion, remains unaffected, even though in reality, erosion would likely propagate to adjacent areas. The probabilistic approach avoids this problem by introducing randomness into the erosion process.

Mariotti & Canestrelli (2017) chose the probabilistic approach for their study, but it is important to consider the benefits of both approaches when modeling salt marsh development.

In both approaches, eroded sediment from marsh edged is treated by considering a fraction that is quickly oxidized or uptaken, while the remainder is redistributed uniformly over adjacent unvegetated cells. This process accounts for the dynamic nature of sediment transport within the marsh system (Mariotti & Canestrelli (2017).

Due to Mariotti & Canestrelli (2017) and Willemsen et al. (2022) using both D-Morphology, erosion, and sedimentation also occurred at the surface of the salt marsh. Although using two different vegetation modules, both influenced the erosion and sedimentation on top of the marsh.

In the study by Bendoni et al. (2014), a simplified scheme was developed to model toppling failures of cohesive soil blocks within marsh banks. The approach involved a cross-sectional representation of the soil block in the x-z vertical plane, characterized by dimensions of length, depth, and height. This block was treated as a rigid body connected to an underlying layer via a damping system, simulating its viscoelastic behavior (Bendoni et al., 2014).

The modeling considered various forces acting on the block, including gravity, hydrostatic thrust from water inside and in front of cracks, and hydrodynamic thrust induced by wave impact. These forces were found to induce small clockwise rotations around an equilibrium configuration (Bendoni et al., 2014).

Failure mechanisms were assumed to initiate when tensile stresses along a predefined plane failure surface exceeded the material's tensile strength. This failure surface was idealized as a plane tilted at a slight angle relative to the horizontal (Bendoni et al., 2014).

Numerical simulations were conducted using a fourth-order Runge-Kutta method to solve the differential equations governing the block's rotational motion. This computational approach allowed for the dynamic representation of toppling failure processes induced by wave interactions on marsh banks, incorporating both static and dynamic forces influencing the cohesive soil block (Bendoni et al., 2014).

3. Methods

This chapter outlines the methodologies employed to address the research questions of this study. It begins with an overview of the study area, where the case study is conducted. The subsequent sections detail the models used, along with any modifications made for this research. Sections 3.4 to 3.6 focus on the configuration and inputs of the hydrodynamic model, while Sections 3.7 to 3.9 discuss the methods for incorporating vegetation density, calibrating the salt marsh model, and integrating the spatially varying erodibility coefficient. The structure of this chapter reflects the workflow undertaken during this thesis, guiding the reader through the study's sequential methodological steps.

3.1 Study area

This study will use a case study of the salt marshes located in Wierum, the Netherlands. This area is specifically chosen for this research, as abundant data and information are available for this location.

Wierum is located in the northern part of the Netherlands, in the province of Friesland (Figure 6b). Positioned along the Wadden Sea, this area is characterized by a dynamic coastal landscape that includes extensive tidal flats and salt marshes with cliffs.

The hydrodynamic conditions in Wierum are dominated by a semi-diurnal tidal regime, exhibiting an average tidal range of approximately 2.5 meters. Seasonal variations in wave activity are notable, with

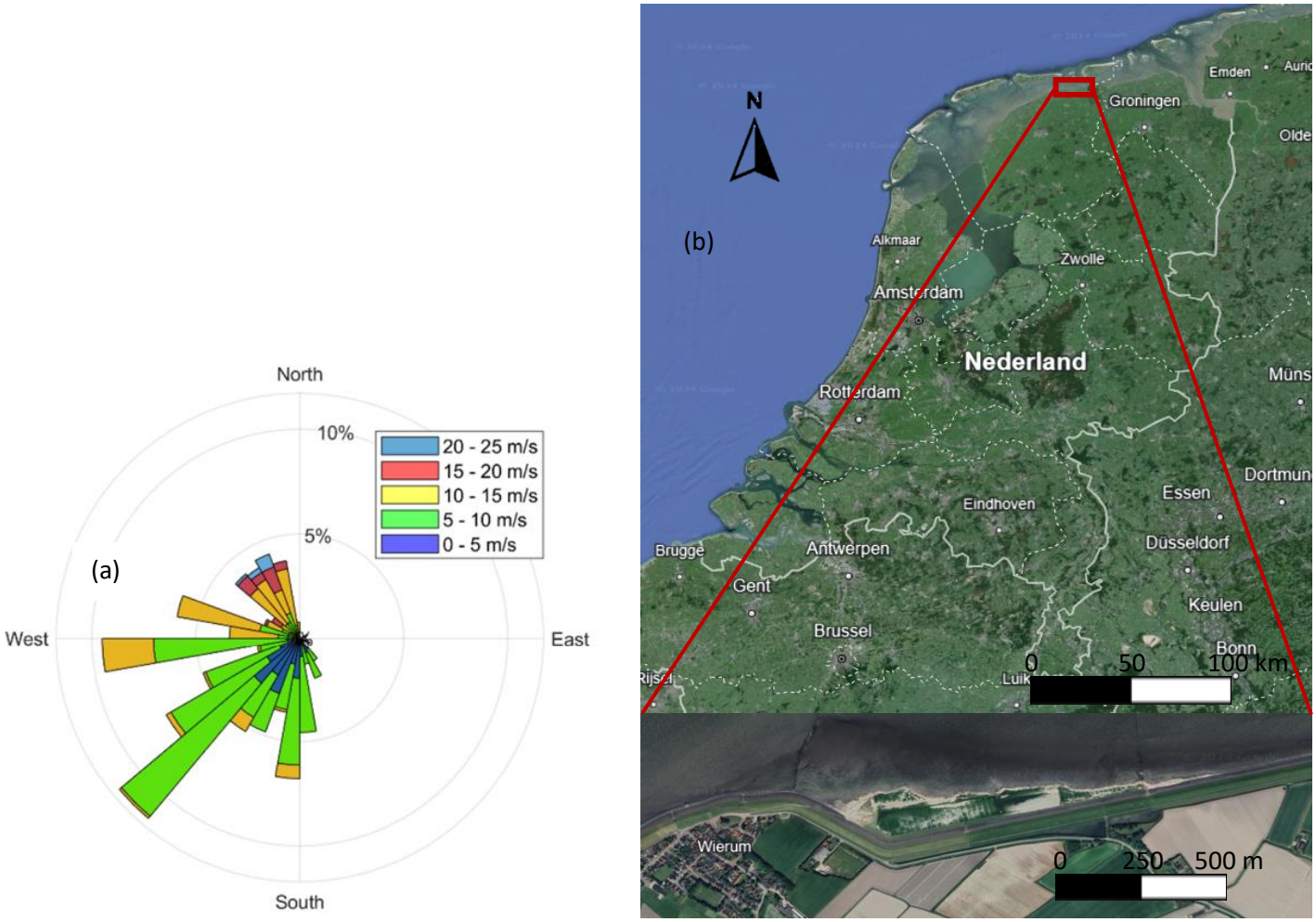

Figure 6 Wind rose at Wierum (Siemes et al., 2020). (b) Location of the salt marsh at Wierum, the Netherlands.

more significant impacts observed during the autumn and winter months due to increased storm frequency and intensity. Wave heights in this region vary from 0.05 to 1.1 meters (Rijkswaterstaat, 2024). The predominant wind direction is from the southwest, although stronger winds are typically from the northwest (Figure 6a) (Siemes et al., 2020). The time frame of this case study is from 05-02-2023 to 25-01-2024. During this period, a storm occurred on December 21-22, 2023, with winds reaching force nine on the Beaufort scale.

The cliffs along the salt marsh exhibit considerable variability in both height and shape. These variations in elevation and morphology can influence the rate of lateral retreat, which averages 1.91 meters per year for this salt marsh (Siemes et al., 2020). This average lateral retreat was observed over six years, from spring 2008 to spring 2014. The interplay between these hydrodynamic forces and the spatial heterogeneity of the cliffs creates a compelling setting to investigate the contributions of wave action to cliff erosion and the potential mitigating effects of vegetation.

Vegetation within Wierum's salt marshes primarily consists of the halophytic species *Puccinellia maritima* (Marin-Diaz et al., 2023). The soil characteristics at the salt marshes of Wierum vary spatially. According to Basismonitoring Wadden (2024), sediment on the intertidal mudflat showed small variations in the sand/mud ratio, being mainly composed of sand (80% ±10%). Moving closer to the coast, the sediment becomes less sandy. Median grain sizes at the intertidal mudflat were found to be different for various regions within the study area, ranging from 0.07 to 0.12 mm. Sediment data on the salt marshes, retrieved via Cone penetration tests, revealed a friction number of 3, translating to the classification of coarse clay (Wetterskip Fryslân, 2019).

3.2 Model framework

The framework of the model used in this paper was created by the Water Institute, located in Baton Rouge. This model has previously been used in their project called "Partnership for Our Working Coast." In that project, the modeling framework consisted of four different components: the Morphology Model, the Hydrodynamics Model, the Coastal Wetland Carbon Model, and the Storm Impacts Model (Georgiou et al., 2022). However, not all four models are used in this study.

Delft3D Flexible Mesh (Delft3D-FM) has been used for the Morphology and Hydrodynamics models. The Coastal Wetland Carbon Model and the Storm Impact Model are executed within MATLAB. The Storm Impact Model, which was used to select storms to test the effectiveness of certain projects, is not necessary for this study and has therefore been neglected.

The Morphology Model within Delft3D-FM has also been excluded. Initially, this model was used, but due to instabilities within the Delft3D-FM runs, it was decided to remove it. Despite the Morphology Model's function of adjusting bed elevation along the salt marsh edge, it was determined to have a negligible impact on cliff erosion. To justify its exclusion, a comparison was made between the model results with and without the Morphology component. The comparison revealed minimal erosion and sedimentation along the mudflat adjacent to the salt marsh edge between 05-02-2023 and 25-01-2024, supporting the decision to omit the Morphology Model from further consideration.

The hydrodynamic model and Coastal Wetland Carbon Model were used in this study, with certain settings neglected within the Coastal Wetland Carbon Model. This model includes both a salt marsh edge erosion module and a carbon module. The carbon module, which calculates carbon storage on the salt marsh, is not needed in this study and is therefore neglected.

The two models used in this study are connected via offline coupling. This means that the total simulation duration is divided into multiple model domains. The Delft3D-FM model runs the first model domain, and after it is finished, the salt marsh module uses its results to update the bathymetry. The bathymetry is updated in a restart file along with the hydrodynamics of the last time step of the Delft3D-FM model. This restart file is used for the next simulation period within Delft3D-FM. This process continues until the total simulation duration is finished. It is important to keep the coupling as frequent as possible because eroded cliffs only get updated in the next hydrodynamic model domain. Without frequent coupling, newly formed cliffs are not exposed to wave impact until the next Delft3D-FM run. To avoid this problem, the coupling time is kept short, occurring every two months within the simulation. For December and January, the coupling time is shortened due to Storm Pia, which occurred on December 21st. During this storm, cliff erosion can occur at a large rate, justifying the shorter coupling time. Thus, two coupling times were ultimately employed: two months for normal conditions and one month for storm conditions.

3.2.1 Hydrodynamic and morphodynamic model

Delft3D Flexible Mesh (Delft3D-FM) is a numerical modeling suite designed for simulating hydrodynamics and morphodynamics in various aquatic environments. It uses a flexible mesh grid, allowing for adaptive grid refinement to capture local variations in the terrain. For this study, it is used for its flow and wave modules. In this chapter, the processes involved in these modules will shortly be described (Deltares, 2019).

The hydrodynamic component, D-Flow, simulates the dynamics of two-dimensional unsteady flow and transport influenced by tidal forces. D-Flow utilizes the unsteady shallow water equations in two dimensions, employing a set of equations and factors that encompass the conservation of mass and momentum, continuity equation, horizontal momentum equations, horizontal velocities, hydrostatic pressure assumption, and momentum diffusion. The module models flow velocities, water levels, and associated variables across the domain (Deltares, 2019).

Chézy values for vegetations based on bed roughness, are computed using the Trachytopes model in D-Flow. There are different classes of trachytopes; area classes, line classes, and point classes. In this model, the area classes are used (Deltares, 2019). For this classification, the Baptist model is used (Equation 2 & 3) (submerged vegetation and non-submerged vegetation respectively) (Baptist, 2005).

$$C = \frac{1}{\sqrt{\frac{1}{C_b^2} + \frac{C_D n h_v}{2g}}} + \frac{\sqrt{g}}{\kappa} \ln\left(\frac{h}{h_v}\right) \quad [2]$$

$$C = \frac{1}{\sqrt{\frac{1}{C_b^2} + \frac{C_D n h_y}{2g}}} \quad [3]$$

Herein is C the Chézy roughness parameter, C_b roughness of the bed, C_D the drag coefficient, n the vegetation density ($n = m \cdot D$ with D the stem diameter and m the stem density), h_v the vegetation

height, g the gravitational acceleration, κ the Von Kármán constant, and h the water depth (Baptist, 2005).

Wind waves are modeled using D-Waves coupling with SWAN. The SWAN model uses processes and variables such as wind strength, white capping, bed friction, and depth-induced breaking to simulate the waves inside the model. The evolution of the wave spectrum is described by the spectral action balance (Deltares, 2015). The model performs computations involving wave propagation, wind-induced wave generation, non-linear interactions between waves, and the dissipation of waves.

For further information about used equations and methods used in Delft3D-FM, it is recommended to read to Delft3D-FM manual (Deltares, 2019; Deltares, 2015).

3.2.2 Cliff erosion modeling

After the first Delft3D-FM domain is finished, the salt marsh module reads the output data and calculates the wave power at each grid cell for each time step using the following equation (Georgiou et al., 2022):

$$W_p = \left(\frac{1}{8}\rho g\right) c_g H_w^2 \quad [4]$$

$$With:$$

$$W_p = Wave\ power\ [J/m2]$$

$$\rho = Density\ of\ water = 1000\ kg/m^3$$

$$g = Gravitational\ force\ =\ 9.81\ m/s^2$$

$$c_g = Wave\ group\ celerity\ \left[\frac{m}{s}\right] = \sqrt{(g \cdot h)}$$

$$h = Water\ depth\ [m]$$

$$H_w = Wave\ height\ [m]$$

After calculating the wave power for each grid cell, the marsh is defined using vegetation coverage input. For each grid cell that has vegetation on it, it is defined as a marsh cell. It is therefore assumed that no pioneering vegetation is on the mudflat below the salt marsh cliff, and thus no seaward expansion of the marsh is possible. Identifying the salt marsh is crucial as erosion can only occur at the salt marsh edge cells, defined as the border between open water cells and salt marsh cells (Georgiou et al., 2022).

The next function calculates the evolution of the salt marsh cliff. It uses the linear relation between wave power and lateral retreat of the salt marsh edge described by Marani et al. (2011). This equation uses the wave power (W_p) and an empirical erodibility coefficient (α_w) to calculate the lateral retreat (E_w) (Equation 1).

Because the relationship between lateral retreat and wave power is linear, the wave power during each time step is summed and used in Equation 5. Since cliffs can erode from multiple directions, the area of the salt marsh is compared to the original area of the grid cell. If the marsh area decreases to a certain threshold, the marsh cell is considered eroded. If this occurs, the cell is set to an open water cell, and the elevation is lowered to the average of the surrounding open water cells. For stability purposes, the water level at this cell is also set to the average of the surrounding open-water cells (Georgiou et al., 2022).

Using the erodibility constant, the cliff retreat can be calculated for each time step. The eroded volume is calculated using the lateral retreat distance, height difference, and cell width (Georgiou et al., 2022):

$$V_{eroded} = a_{ero} \cdot W_p \cdot b_{cell} \cdot \Delta h = L_{ero} \cdot b_{cell} \cdot \Delta h \quad [5]$$

$$With:$$

$$a_{er} = erodibility\ coeffiecient$$

$$L_{ero} = a_{ero} \cdot P_{wave}$$

$$b_{cell} = width\ of\ cell$$

$$\Delta h = elevation\ difference$$

Not all eroded volume is redistributed along the bare mudflat. The eroded soil may contain organic material, which degrades and disappears in the water. Therefore, only a fraction of the total volume is added to the bare mudflat (Georgiou et al., 2022). Due to the neglection of the morphology module in Delft3D-FM, the redistribution of sediment has been set to zero and thus turned off.

To track lateral erosion between model domains, ghost cells are introduced. A ghost cell keeps track of the amount of cliff erosion within a cell that has not yet been fully eroded. The ghost cells are updated after all processes (erosion, waves, and sediment redistribution) have taken place and are used in the next module domain. Figure 7 shows a representation of this process (Georgiou et al., 2022).

After calculating the salt marsh processes, the new bed level is saved in the restart file for the subsequent model domain. The trachytopes area file is also updated, removing vegetation where cliff erosion has occurred.

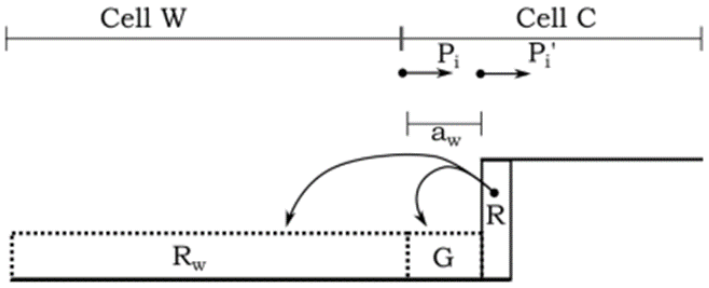

Figure 7 Visualization of the cliff erosion modeling (Rw= redistributed sediment to adjacent cell from eroding cell) (aw= Width of the ghost cell on the West side of Cell C. This is the distance by which the marsh has eroded back from the boundary between Cells W and C. Ghost cells along other edges will be indicated by the subscripts $W, S,$ and E) (G= Volume of eroded material in cell C. This is the sum of all ghost cells) (R= Volume of marsh eroded due to incoming wave energy) (Pi= Wave power component entering cell) (Pi' = Wave power component entering cell, transformed across width of ghost cell) (Georgiou et al., 2022).

3.3 Adjustments to the salt marsh model

The main changes in the salt marsh model due to the effects of changing geographical location are the data availability and what purpose the model is used for. For example, the Water Institute model was used to simulate marsh interaction over the whole MRDP. Therefore, certain additions were made to make it run more optimally. An example of this is the usage of two separate grids for hydrodynamics and morphology and coarse grid cells in previous use of the model.

The changes in the marsh module can be divided into two categories: type of input data (e.g. resolution, layout, neglecting functions) and different processes (e.g. tidal range and wave impact). The change in input data mainly consists of procedural differences, such as the use of different grids for hydrodynamics and morphodynamics and neglecting certain functions. These are relatively easy to change and did not show any difficulties.

There are also more difficult adjustments, the coding of the relation between salt marsh identification and vegetation location was harder to change. This change was needed due to the different grid sizes. Initially, the salt marsh was identified by using the vegetation map. In the unedited version of the model, each grid cell with vegetation was classified as salt marsh. When a finer grid was used in this study, the representation of vegetation became more detailed. However, it became apparent that not all parts of the salt marsh cliffs in Wierum contain vegetation. As a result, the original method was insufficient for accurately defining the salt marsh area because it did not account for the variability in vegetation coverage. Therefore, a different method was needed to define the salt marsh accurately.

To minimize model changes, the method was adjusted rather than deleted. Using scarp height, elevation, and grid size, a polygon was drawn around the salt marsh edge and extended inland. Grid cells within this polygon were then assigned to the salt marsh, ensuring an accurate representation of all cells, regardless of vegetation presence.

Additionally, the salt marsh module only erodes cells that are assigned as an edge. They are salt marsh cells that are bordered by open water cells. This method was reasonable for previous use of the model due to the coarse grid cells. Due to the coarse grid cells, the salt marsh cliff is clearly defined. When reducing the grid sizes and using actual bathymetry data, it is harder to define clear line of salt marsh cliffs. Due to the interpolation of the bathymetry file onto the hydrodynamic grid, multiple edges can be found behind the most seaward marsh cell. Therefore, the adjustment has been made that all salt marsh cells can experience cliff erosion, as long as it has a sufficient scarp height of 12 centimeters. This height was selected because it represents the cliff conditions in the model relative to real-life observations the best.

Since the grid cells have a resolution of 3x3 meters, elevation changes only occur when the lateral retreat is larger than the width of the grid cells. In this instance, smaller lateral retreats are not visible in the results. Therefore, for visualization, an additional function has been added that shifts the coordinates of the face of the grid cell southward. With this addition, the lateral retreat of every cliff cell is visible in the cross-sections, even when it is smaller than the grid cell itself.

By changing the geographical location, certain processes needed to be added or adjusted. Due to the micro-tidal components of the bay of Louisiana, the salt marshes rarely flood. This is not the case at Wierum. During the simulation, the salt marshes are flooded multiple times during high tide. When the

cliff is fully submerged, it is assumed that the waves have little impact on the cliff (Fagherazzi, Mariotti, et al., 2013). Therefore, when the cliff is fully submerged, the wave power will not lead to cliff erosion.

The first runs of the Delft3D-FM model encountered many instability errors. No clear reason for the instabilities was found. Adjusting parameters, like minimal depth for wave action and sedimentation/erosion, made the model more stable, but it still crashed at certain points in the hydrodynamic model. Eventually, it was found that different time domains had instabilities within the bathymetry file. Multiple smoothed versions of the bathymetry file were made. For certain domains, one bathymetry file worked, but for others, it did not. No single bathymetry file worked for all domains. Therefore, a combination of different bathymetry files, found by trial and error, was used. This meant that the cliff erosion per salt marsh module loop needed to be stored and added to the next bathymetry file so that erosion progress was not deleted.

This method only updates the bathymetry due to cliff erosion, ignoring changes in morphology due to Delft3D-FM. To verify if this is a reasonable choice, the observed erosion/sedimentation on the bare mudflat was examined with cross-sections. From these cross-sections, it is visible that at most cross-sections, the elevation of the mudflat barely changes. However, erosion of up to 20 centimeters has been observed at several cross-sections. The neglection of the morphology module is a limitation of this study (Appendix B).

3.4 Delft3D-FM setup

The Delft3D-FM model relies on actual bathymetry data and calibrated models. Bathymetry data is obtained from AHN5 (AHN, 2023; Haarbrink, 2023) and Vaklodingen Rijkswaterstaat. Data from AHN5 is utilized for determining the heights of the salt marsh and upper mudflats. The resolution of AHN5 is 0.5 x 0.5 meters, with a maximum standard deviation of three centimeters and a maximum systematic error of five centimeters (AHN, 2023; Haarbrink, 2023). The AHN5 measurements for Wierum were conducted on 5 February 2023 (AHN, 2023). The AHN5 data extends to the mudflat approximately 200 meters away from the salt marsh edge. However, additional data is required due to this limitation. The dataset from Vaklodingen Rijkswaterstaat extends further into the sea but has a lower resolution of 20 x 20 meters (Rijkswaterstaat, 2017). No information is available regarding the accuracy of these measurements. The measurements for Vaklodingen Rijkswaterstaat were taken on the 30th of December 2017, which does not align with the AHN5 measurement dates. However, it is anticipated that the discrepancy in measurement times will not significantly impact the model results. Loading both datasets into the Quickin function of Delft3D reveals a smooth transition of elevations between measurements (Figure 8).

To ensure the model runs without errors, specific adjustments were made based on the bathymetry. The bathymetry was set to a constant value at the open boundary conditions of -0.7 meters +NAP. This ensures that the grid cells surrounding the open boundaries remain submerged, enhancing stability in the model. Additionally, the elevation of the salt marsh further inland was increased. Initial model runs resulted in the flooding of the salt marsh, with water pooling in the lower areas. While this phenomenon

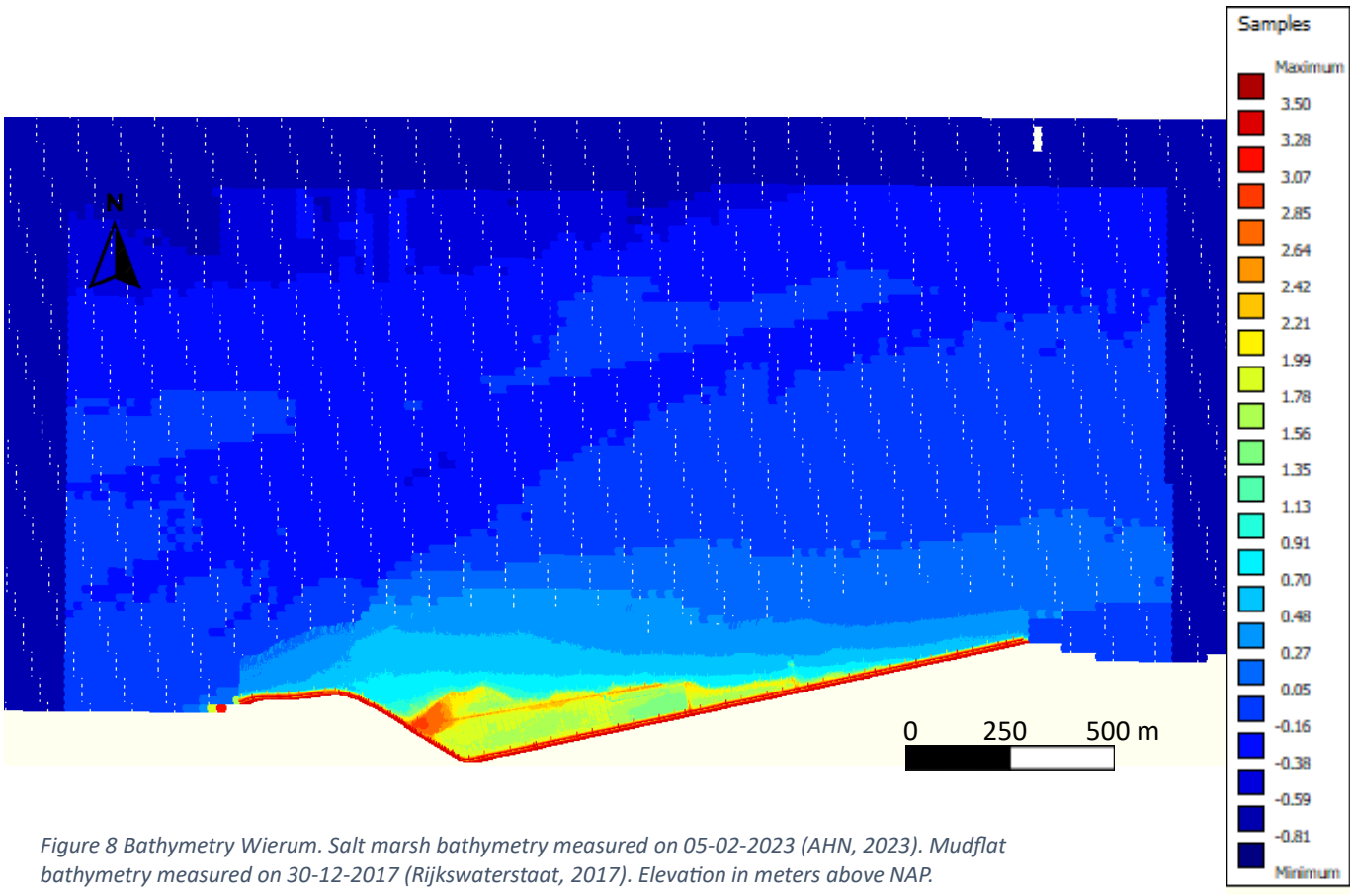

Figure 8 Bathymetry Wierum. Salt marsh bathymetry measured on 05-02-2023 (AHN, 2023). Mudflat bathymetry measured on 30-12-2017 (Rijkswaterstaat, 2017). Elevation in meters above NAP.

occurs, the model does not account for absorption in the soil and evaporation of water. This caused the model to become unstable. Increasing the bathymetry at these points resulted in a more stable model.

These adjustments are not expected to alter the results of the model. The deeper cells along the open boundaries do not affect the flow conditions closer to the salt marsh, which is the focus of this study. In addition, the increased bed levels will not alter the results because these lower points are situated relatively far away from the salt marsh edge. The lateral retreat will not be affected by this adjustment.

3.5 GRID

Because of the comparative nature of this study with real-life data, it is favorable to use fine grids. However, this results in higher computational times. It is therefore chosen to use different grid sizes depending on the location in the study area. Along the boundaries of the model, coarse grids are placed, with a size of approximately 115 x 100 meters. Five grid refinements are applied moving towards the marsh. The finest grids are around ten meters of the salt marsh edge, in both seaward and landward directions, with a size of approximately 3 x 3 meters (Figure 9). Any finer grid cells would not only increase the number of grid cells but also decrease the computational time steps, and therefore increase the computational time significantly (Deltares, 2019).

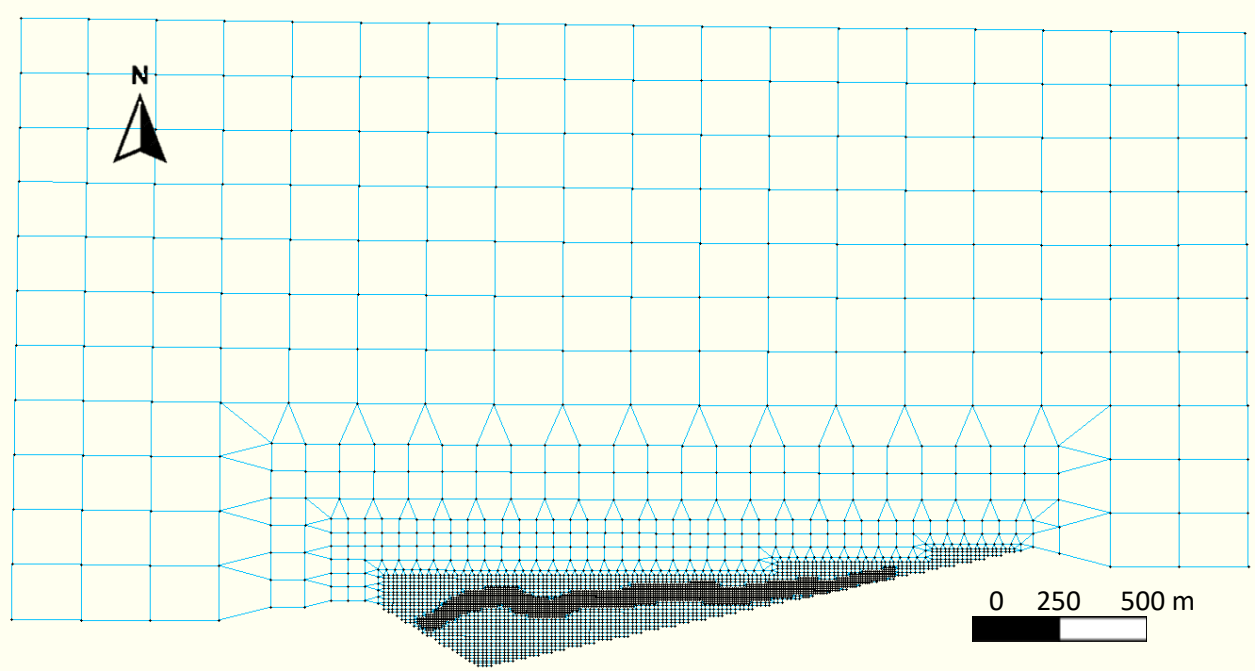

Figure 9 Hydrodynamic grid of Delft3D-FM. Cell resolution becomes finer when moving closer to the salt marsh cliff.

3.6 Hydrodynamic input

The hydrodynamic forcings are simulated using open boundary conditions. These hydrodynamic forcings are the tidal amplitude and wave conditions. The northern open boundary is located 1.5 kilometers seaward, and the west and east boundaries are distanced 1.8 kilometers from each other, with the salt marsh in the middle. A closed boundary is automatically created where grid cells do not border anything, so not another grid cell or an open boundary. This closed boundary does not have any forcings and aligns with the levee.

The boundary conditions are calculated using two different schematizations of Delft3D-FM and SWAN, specifically the Dutch Continental Shelf Model (DCSM) and SWAN-Kuststrook, respectively. Both schematizations are provided by Rijkswaterstaat and managed by Deltares. These models have been calibrated and checked for accuracy (Deltares, 2022; Deltares, 2023).

3.6.1 Dutch Continental Shelf Model

The DCSM models flow characteristics of the whole North Sea and are influenced by multiple tidal components. Several factors affect the results of this model, such as air pressure at mean sea level, wind speeds in northern and eastern directions, Charnock coefficients, and atmospheric pressure. These factors are gathered using the ERA5 model, which has a spatial resolution of 0.25° x 0.25°, approximately 28 x 28 kilometers depending on longitude and latitude. Observation points are placed at the location of the open boundaries in the Wierum model to derive water levels and velocities from the outputs.

For verification, DCSM results were compared to observation points in Holwerd and Lauwersoog for normal and storm conditions, respectively. The correlation coefficients were calculated for both observation points. Initially, the whole time series was compared to observation data, revealing that the tidal components of the DCSM moved slightly faster than in real life, causing the observed water levels to lag and resulting in low correlation. However, when the tested time was shortened to two months, the correlation coefficients increased to 0.99 and 0.98 for Lauwersoog and Holwerd, respectively. It is expected that the faster tidal component does not significantly affect the results, as the actual water levels are still accurately represented, though slightly earlier in the time series.

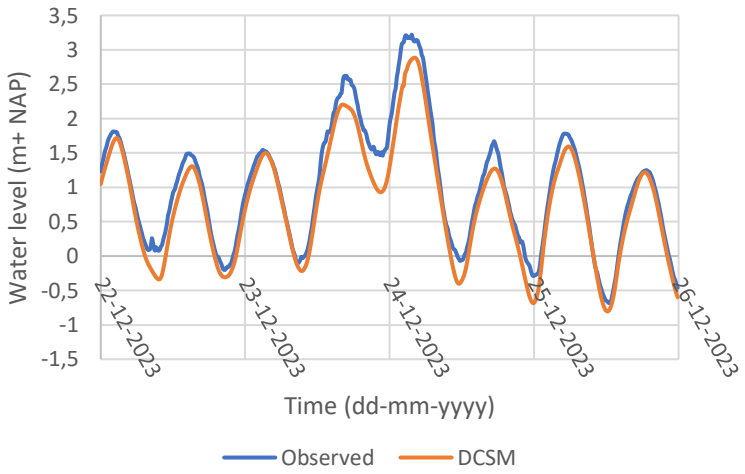

Figure 10 Verification water levels DCSM Storm 'PIA'. Observation have been done in Lauwersoog and the simulation for the water level is done by the DCSM.

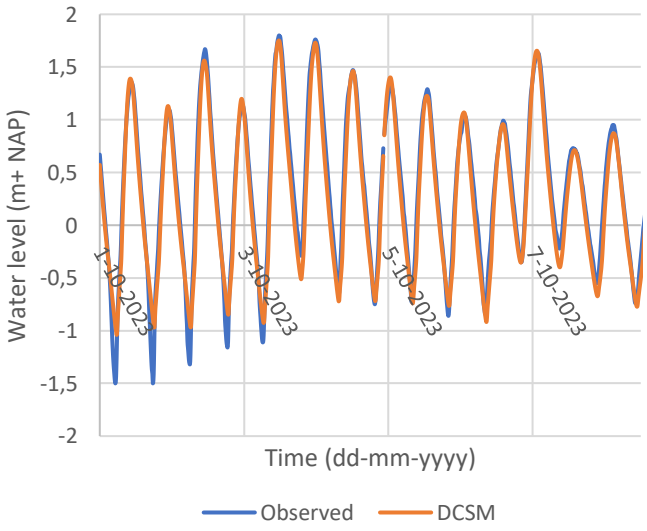

Figure 11 Verification water levels DCSM 'Normal' conditions. Observation have been done in Holwerd and the simulation for the water level is done by the DCSM.

3.6.1.1 DCSM verification

To further verify the DCSM results, the Mean Absolute Error (MAE), Root Mean Squared Error (RMSE), and Coefficient of Determination (R-squared) are calculated (Table 1). For a description of these methods see

Appendix A. For the MAE and RMSE, lower values indicate a better fit, while higher values indicate a worse fit. For R-squared, higher values indicate a better fit. The low values of MAE and RMSE and the high values of R-squared demonstrate that the simulated water levels align well with the observed values.

Table 1 Statistical metrics for the verification of the DCSM outputs of the storm and normal conditions in Lauwersoog and Holwerd respectively.

	Lauwersoog	**Holwerd**
Correlation (-)	0.99	0.98
MAE (m)	0.09	0.10
RMSE (m)	0.10	0.17
R-Squared (%)	98	95

When testing water levels based on actual events, it is important to account for the lag time. During normal conditions, the DCSM mimics the observed data accurately (Figure 11). For storm conditions, such as storm Pia on 23-24 December 2023, the model underestimates the water level at higher peaks. However, these differences are not expected to significantly affect the results, as storms are infrequent during the simulation period (Figure 10). During normal conditions, observed water levels are sometimes significantly lower than modeled results, likely due to the bathymetry used in the DCSM. When cells fall dry, the water level at that point can no longer decrease. The water levels for the storm are measured in Holwerd, and for normal conditions in Lauwersoog. Overall, the DCSM results are reliable for this research.

3.6.2 SWAN-Kuststrook Model

Wave data is collected from the SWAN-Kuststrook model results, which are accessible through the Rijkswaterstaat web extension Matroos. This data includes hourly measurements of wave height, direction, and period. In the SWAN-Kuststrook model, an observation point is located at the mudflats of Wierum. This observation point, called Wierumerwad 3, is about 250 meters away from the salt marsh, and thus cannot be representable for the open boundary conditions, which are 1.5 kilometers away from the salt marsh. It was possible to request additional data from Rijkswaterstaat for locations that do not

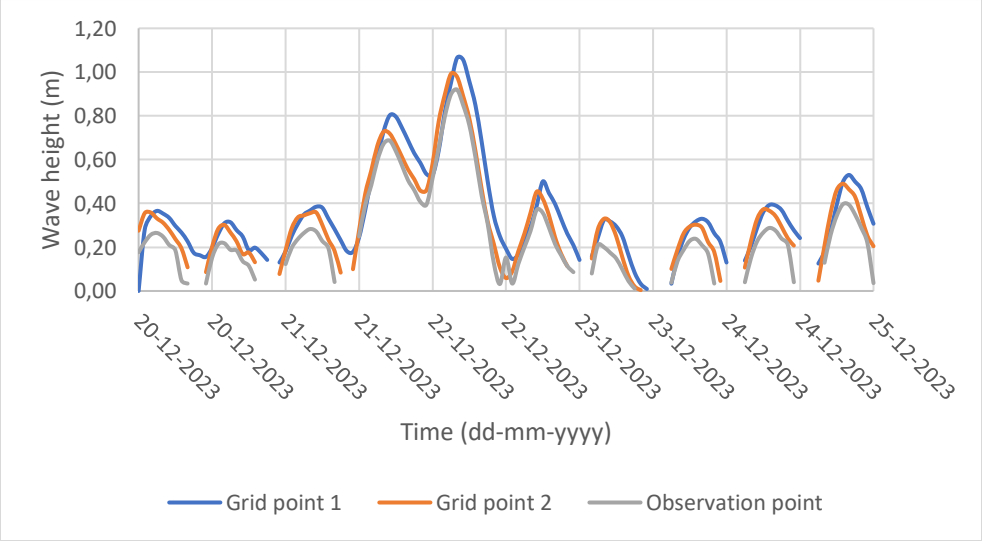

Figure 12 Wave heights of observation point according to Matroos, and two points in the grid representing the boundary conditions located near the salt marshes in Wierum.

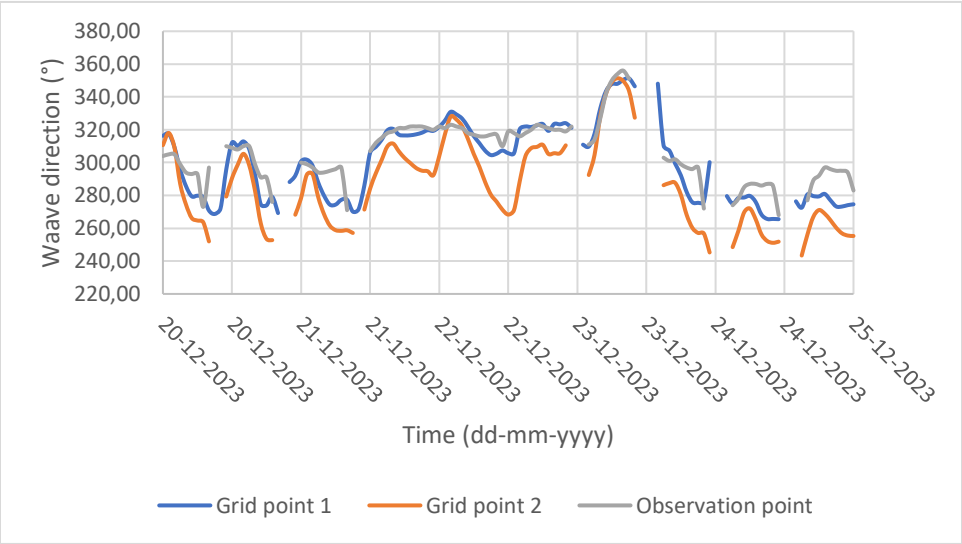

Figure 13 Wave direction of observation point according to Matroos, and two points in the grid representing the boundary conditions located near the salt marshes in Wierum.

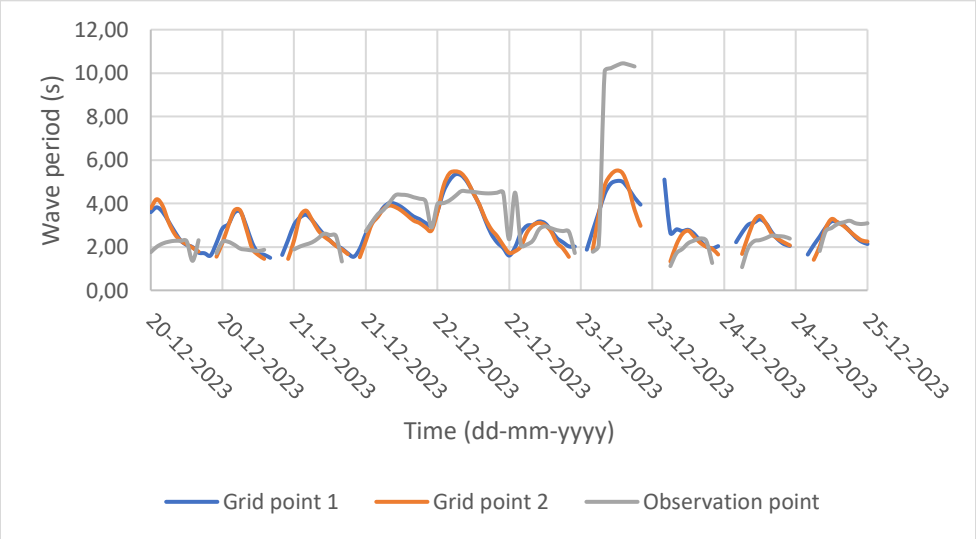

Figure 14 Wave period of observation point according to Matroos, and two points in the grid representing the boundary conditions located near the salt marshes in Wierum.

have an observation point. However, this can be requested only for a week of data. Two additional data sets have been retrieved at two different locations on the open boundary conditions. Differences between both locations were analyzed, revealing that wave heights at the boundary conditions are consistently about fifteen centimeters higher than at the original observation point (Figure 12). Wave direction showed maximum deviations of 25 degrees (Figure 13). The wave period roughly aligned between the two time series, however, no constant deviation or clear pattern was found. Therefore, it was assumed that the period at the observation point is equal to that at the boundary conditions (Figure 14). The wave period is not crucial for this study, as the amount of cliff erosion is based on wave power against the scarp, which is not influenced by the wave period (Equation 4). At last, for the wave spreading direction, no data is stored for the non-observation point. It is therefore assumed that this would be the same as at the observation point.

3.6.2.1 SWAN-Kuststrook Verification

To ensure the selected wave data corresponds accurately to the input required at the open boundaries, an observation point is positioned at a similar distance and depth as Wierumerwad 3. Initial model runs experienced crashes due to varying spreading directions, so the average series value of 28 degrees was used. The influence of this variable was assessed, showing minimal impact on wave height and direction. The average deviation for wave height was two centimeters, and for wave direction, three degrees, both having a negligible influence on the output (Figures 15 and 16). The statistical metrics indicate that the input data sufficiently mimics the simulated wave data from SWAN-Kuststrook (Table 2).

Table 2 Statistical metrics for the verification of the SWAN-Kuststrook outputs at the boundary conditions compared to the observation point.

	Wave height	**Wave direction**
Correlation (-)	0.92	0.97
MAE (m)	0.04 m	5.3°
RMSE (m)	0.06 m	10.7°
R-Squared (%)	0.83	0.94

Validation of the SWAN-Kuststrook model is conducted by Deltares, calculating the Statistical Confidence Interval (SCI), Relative Bias (relBias), and Root Mean Square Error (RMSE) for a location in deep and shallow water (Tabel 3) for the wave height (Hm0), wave period (Tm-1.0), and low-frequency wave height (HE10). These statistical metrics suggest that the SWAN-Kuststrook model provides reasonably accurate predictions, with minor biases and acceptable error margins across both deep and shallow water locations.

Table 3 Statistical metrics for the verification of the SWAN-Kuststrook output compared to observations (Deltares, 2023b).

	Hm0			**Tm-1.0**			**HE10**		
	SCI	relBias	RMSE	SCI	relBias	RMSE	SCI	relBias	RMSE
Deep	0.15	0.05	0.29	0.12	-0.03	0.79	0.39	-0.08	0.23
shallow	0.2	-0.04	0.27	0.12	-0.03	0.72	0.52	-0.07	0.19

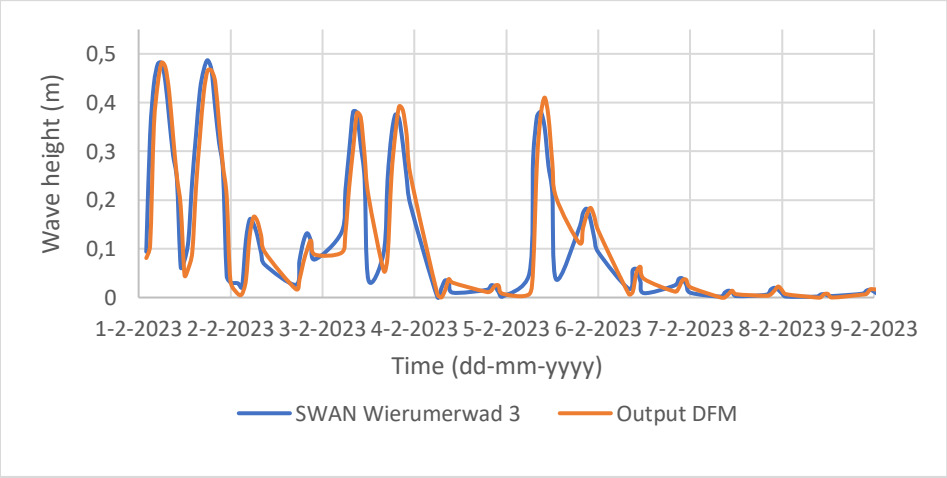

Figure 15 Wave height comparison between simulated series from Matroos at Wierumerwad 3 and the output of Delft3D-FM with adjusted wave characteristics at the same point.

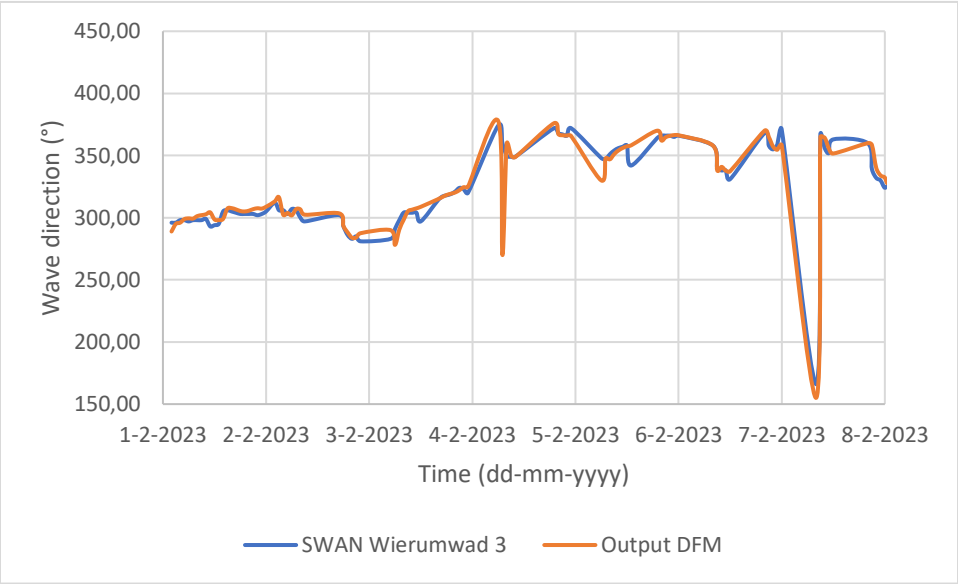

Figure 16 Wave direction comparison between simulated series from Matroos at Wierumerwad 3 and the output of Delft3D-FM with adjusted wave characteristics at the same point.

3.7 Vegetation

The dominant vegetation species at the salt marsh in Wierum is the *Puccinellia Maritima*. *Puccinellia Maritima* is a grass species and reaches its maximum extent typically in stabilized lower marshes (Marin-Diaz et al., 2023). However, this species can be found along the whole salt marsh (Langlois et al., 2001). For simplicity's sake, only this vegetation type is incorporated into this study.

The model framework does not have a vegetation growth module. However, the vegetation coverage map in previous runs did get updated. In this file, the type of vegetation and its coverage is listed. Each vegetation type is based on its living conditions, such as inundation and salinity. Each vegetation species has different characteristics, such as stem density and vegetation height. These parameters were placed and updated in the Trachytopes module in Delft3D. Although only one vegetation species is present in the study area, the coverage area, and thus the trachytopes module will be updated. This is based on seasonal change.

Vegetation density across the salt marsh varies seasonally and is assessed using the Normalized Difference Vegetation Index (NDVI). NDVI is a measure of vegetation greenness and vitality, calculated using the red (R) and near-infrared (NIR) spectral bands:

$$NVDI = \frac{NIR - R}{NIR + R} \quad [6]$$

The NDVI values are computed using data from the NSO-SatellietdataPortaal and processed in QGIS, providing values with a resolution of 0.3x0.3 meters. In the study area, NDVI values range from 0 to approximately 0.8.

According to Marin-Diaz et al. (2023), the stem density of *Puccinellia Maritima* varies significantly between seasons. In that study, stem densities and vegetation heights for *Puccinellia Maritima* have been measured in winter and summer:

Winter:

- Average stem density: 1550 stems per square meter
- Maximum stem density: 5000 stems per square meter
- Vegetation height: 8 to 18 centimeters

Summer:

- Average stem density: 3000 stems per square meter
- Maximum stem density: 9400 stems per square meter
- Vegetation height: 8 to 18 centimeters

The highest NDVI values correspond to the peak stem densities observed:

- Winter: Highest NDVI around 0.6, correlating with 3000 stems per square meter.
- Summer: Highest NDVI around 0.8, correlating with 9400 stems per square meter.

Table 4 Relationship between NDVI values and stem density in the winter, showing increasing vegetation density with higher NDVI measurements.

NDVI Value (-)	Stem density (stems/m^2)
$NDVI \leq 0$	0
$0 < NDVI \leq 0.2$	500
$0.2 < NDVI \leq 0.3$	1000
$0.3 < NDVI \leq 0.4$	1500
$0.4 < NDVI \leq 0.5$	2000
$0.5 < NDVI \leq 0.6$	2500
$0.6 \leq NDVI$	3000

Table 5 Relationship between NDVI values and stem density in the summer, showing increasing vegetation density with higher NDVI measurements.

NDVI Value (-)	Stem density (stems/m^2)
$NDVI \leq 0$	0
$0 < NDVI \leq 0.2$	1340
$0.2 < NDVI \leq 0.3$	2680
$0.3 < NDVI \leq 0.4$	4020
$0.4 < NDVI \leq 0.5$	5360
$0.5 < NDVI \leq 0.6$	6700
$0.6 < NDVI \leq 0.75$	8040
$0.8 \leq NDVI$	9400

To model the seasonal variation in vegetation density, a linear relationship between NDVI and stem density has been established. The conversion scales for winter and summer NDVI values are presented in Tables 4 and 5 respectively. These scales ensure that the average NDVI values for both seasons align with the average stem densities reported by Marin-Diaz et al. (2023). The conversion of the NDVI to stem densities can be found in Figures 17 and 18. Comparing these figures, it is evident that vegetation is more present in the summer than in the winter. In Figure 17, it is visible that vegetation is present on the mudflat. This is likely because it was low tide during the measurement. The NDVI values found here could be organic or other material. It is assumed that there is no vegetation on the mudflat.

The fine-grid stem densities derived from NDVI measurements have been interpolated onto the hydrodynamic grid. Due to limitations in the Trachytopes module, stem densities are rounded to values specified in Tables 4 and 5. This integration allows the model to simulate realistic vegetation patterns and their influence on hydrodynamic processes in the salt marsh ecosystem at Wierum.

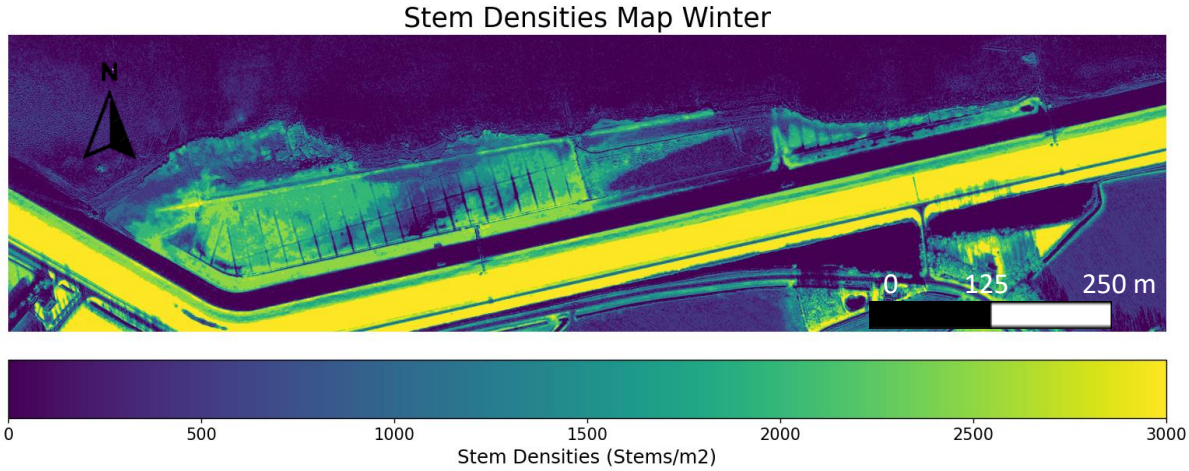

Figure 17 Spatial distribution of stem densities across the salt marsh in Wierum in the winter.

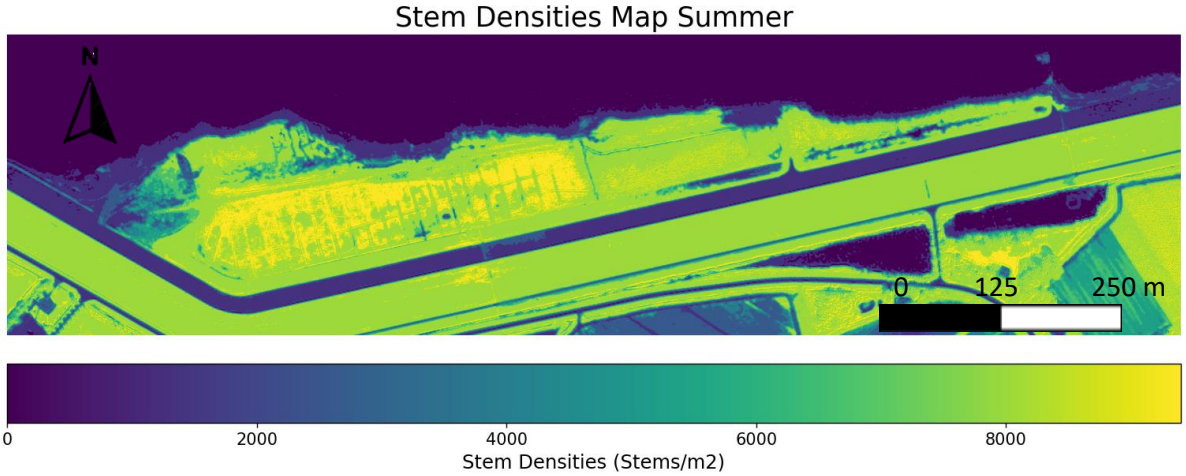

Figure 18 Spatial distribution of stem densities across the salt marsh in Wierum in the summer.

3.8 Calibration of the model

Before implementing the parameterization of vegetation on top of the cliff to the model, the erodibility coefficient needs to be calibrated first. With the adjustments to the original salt marsh module, it was applied to calibrate the erodibility coefficient in the initial set of runs. To achieve this, the observed average lateral retreat between 05-02-2023 and 25-01-2024 from drone measurements needed to be calculated. The elevation data from 05-02-2023 is from AHN5 and is also used as the bathymetry file for the simulations. The drone data from 25-01-2024 is from the PhD of Dzimballa, (2023). This elevation data set is of a higher resolution of 0.3x0.3 meters. In QGIS, elevation maps for both dates were plotted. Using an elevation tool, 27 cross-sections were created along the salt marsh edge at equal intervals of 35 meters (Figure 19). The lateral retreat for each cross-section was manually calculated using two different methods. The first method was applied to cross-sections with clearly defined cliffs (Figure 20), while the second method was used for cross-sections where cliffs were less visible, measuring average cliff erosion across the entire cross-section (Figure 21). The observed average lateral retreat was determined by averaging these measurements. Given that drone measurements provide finer detail than the hydrodynamic grid, normalization of the observed lateral retreat was chosen. This involved averaging the

retreat on a cross-section, as depicted in Figure 19, and two adjacent cross-sections within a 5-meter distance. Using this method, the average lateral retreat along the entire salt marsh edge was found to be 2.05 meters over a period of 354 days.

The measurements indicate significant variation in lateral retreat along the coast. The smallest lateral retreat, approximately 0.86 meters, was observed at cross-section 7, while the largest retreat, 3.9 meters, occurred at cross-section 2. The most substantial lateral retreats were concentrated at the west and east ends of the salt marsh (Figure 19). Notably, the west end consistently exhibited high lateral retreats, whereas the east end showed more fluctuation.

The average simulated lateral retreat was calculated using a similar approach. Since the Delft3D-FM model employs grid cells, and these grid cells are all the same size along the salt marsh cliff, the lateral retreat is already averaged for each specific section. Therefore, multiple cross-sections were not required for these measurements.

The erodibility coefficient will be adjusted iteratively to achieve a match between the average lateral retreat in the model results and the observed data. Due to the interpolated elevation data on the hydrodynamic grid, the salt marsh edge is not uniformly defined across all cross-sections. Multiple edges are visible, each influenced by cliff erosion. The largest retreat observed in these cross-sections is taken into consideration to calculate the lateral retreat (Figure 22). In cases where an entire cliff cell erodes, the distance from the eroded cliff cell to the next simulated cliff cell is considered the lateral retreat (Figure 23). Completely eroded cells are identifiable in the cross-sections by their lower elevation compared to the original cliff interpolated by Delft3D-FM.

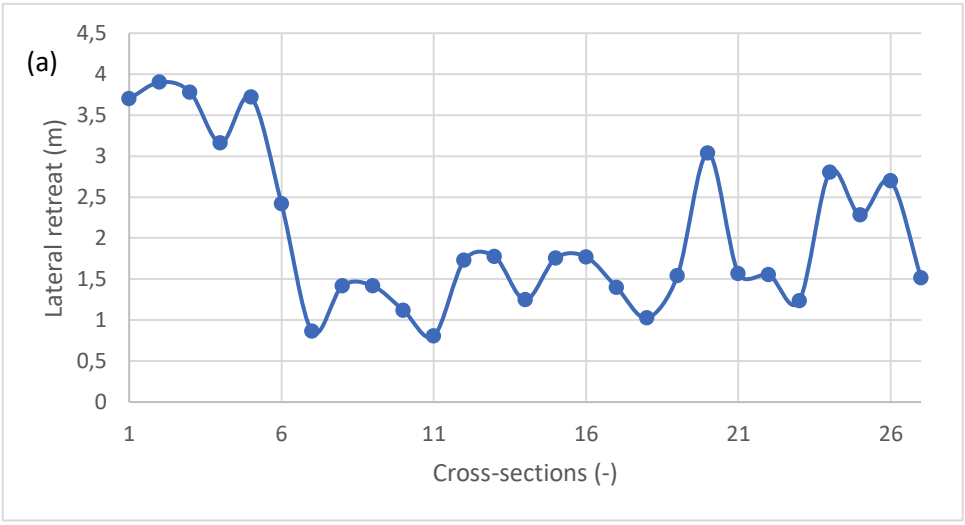

Figure 19 (a) Observed lateral retreat for each cross-section. (b) Location of each cross-section. The width of the salt marsh of figure a and b aligns with each other. The numbering of cross-sections can be found in figure a.

First method measuring observed lateral

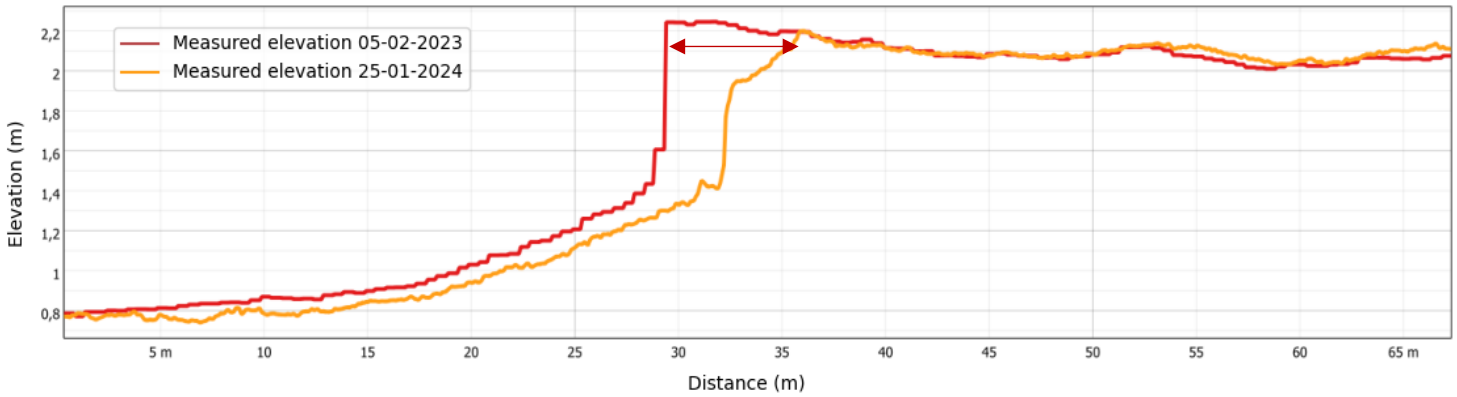

Figure 21 First method to measure the observed lateral retreat. Shows a clear distinction how much the cliff has retreated landwards.

Second method measuring observed lateral retreat

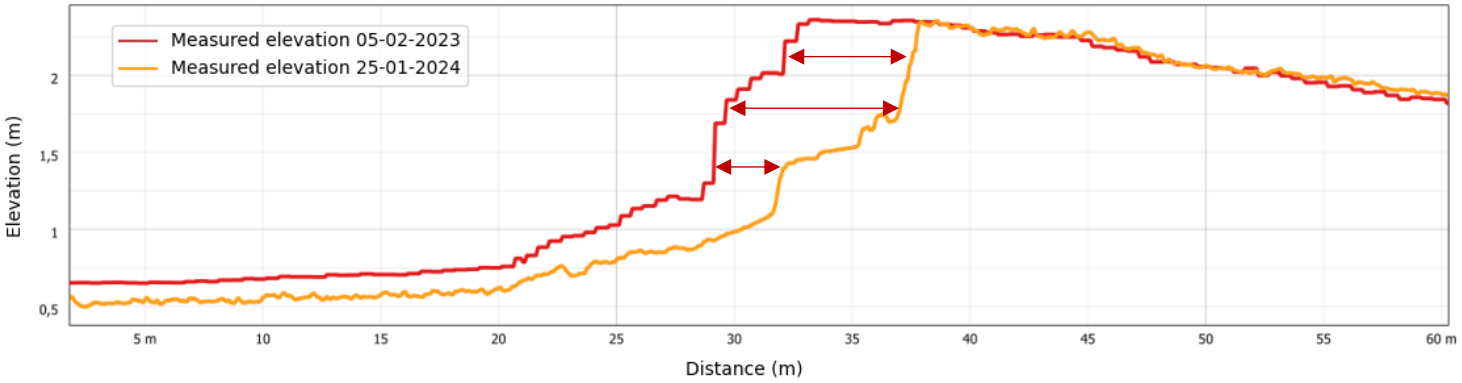

Figure 22 Second method to measure the observed lateral retreat. No clear distinction of how much the cliff has retreated landwards. An average will be calculated based on multiple measurements in this cross-section.

First method measuring simulated lateral retreat

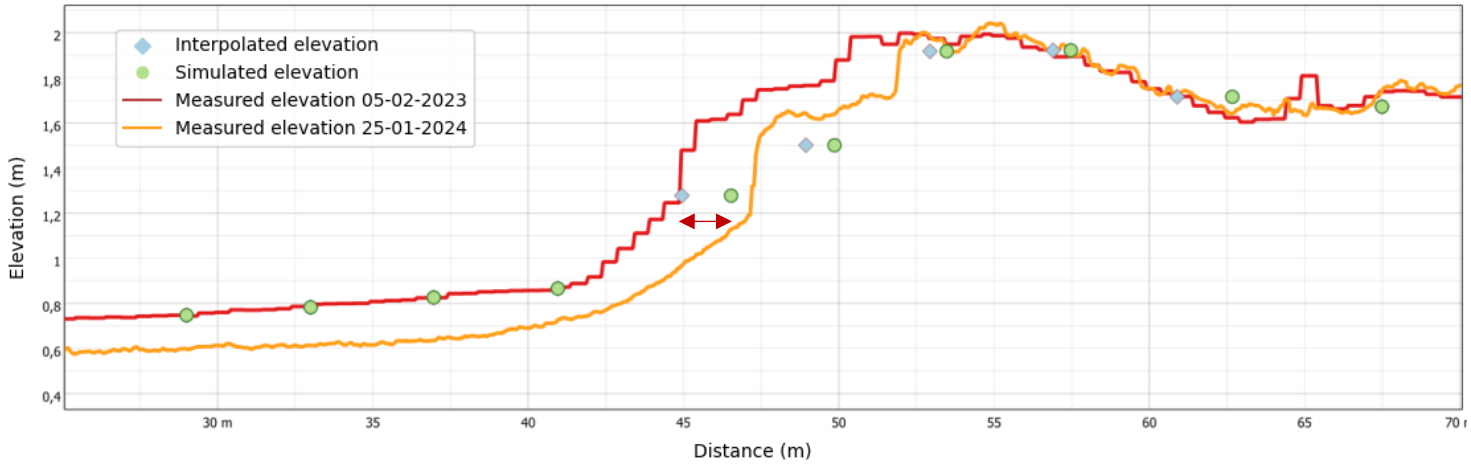

Figure 20 First method to measure the simulated lateral retreat. No cells are completely eroded. The largest lateral retreat in the cross-section will be representative of the lateral retreat.

Second method measuring simulated lateral retreat

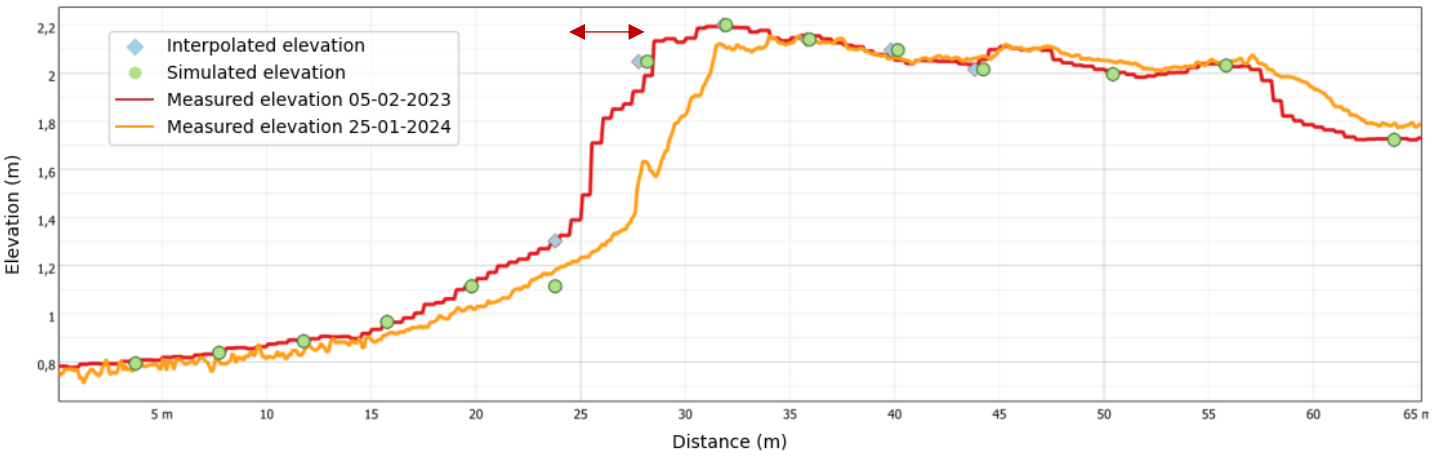

Figure 23 Second method to measure the simulated lateral retreat. When a cell is completely eroded the distance from the original cell to the next is measured and representative of the latera retreat in this cross-section

3.9 Addition of a spatially varying erodibility coefficient

In this thesis, the calibrated uniform erodibility coefficient will be divided with a parameter based on vegetation density. By doing this, the erodibility coefficient will become spatially varying. As stated previously, the effectiveness of marsh edge stability due to vegetation depends on the root system's binding capacity to sediment, influenced by factors like biomass, root length, diameter, and tensile strength (Fagherazzi et al., 2013).

Since detailed data on these parameters are not widely available, a more simplified approach is used. Specifically, root length and root density are inferred based on stem height and stem density. It is assumed that stem height correlates directly with root length and stem density correlates directly with root density. Initially, both root characteristics are assigned an equal weight in influencing the reduction of the erodibility of the salt marsh cliff. However, this balance can be adjusted during the fine-tuning process to better reflect observed conditions.

After the calibration of the erodibility coefficient, the effectiveness of the vegetation on top of the cliff to reduce cliff erosion will be fine-tuned. The results of the model will be assessed through statistical comparison with field observations. Various statistical methods will be employed to evaluate the accuracy and predictive performance of the model. The following key statistical metrics will be used: Correlation Coefficient (R), Mean Absolute Error (MAE), Root Mean Squared Error (RMSE), and Coefficient of Determination (R-squared) (see Appendix A for a more detailed description).

These statistical methods collectively offer a comprehensive evaluation of the model's accuracy, capturing different aspects of the predictive performance. The chosen metrics will provide valuable insights into the model's ability to replicate the observed data, assisting in the assessment and refinement of the model for robust predictions.

The parameterization of the effectiveness of the vegetation on top of the cliff will be adjusted until the best-fitted lateral retreat rate is found. The first step of this process is to find the increase in erodibility where there is no vegetation present, which increases the erosion along these points. When this value is

found, the parameterization of the next density will start, until all densities are parameterized. The parameterization will be done by comparing the increase in Correlation Coefficient and the Coefficient of Determination, and the decrease in Mean Absolute Error and Root Mean Squared Error, until the maximum and minimum respectively are found.

On top of the cliffs, only 5 different densities are found, no vegetation, 500 stems/m^2, 1000 stems/ m^2, 1340 stems/ m^2, and 2680 stems/ m^2. Therefore, it is only possible to parameterize these five stem densities. After these densities have been parameterized, one last check is performed to maximize the accuracy of the results. If the parameterization reduces or increases the average lateral retreat rate too much as it is not more representative of real life, the erodibility coefficient can be adjusted to increase the accuracy of the results again. See Table 6 for an example of the parameterizations that could be used. The parameterization in Table 6 is based on a percentage of reduction due to vegetation found by Lo et al. (2017). For each grid cell, the uniform calibrated erodibility coefficient is divided by this parameter based on vegetation density, creating a spatially varying erodibility coefficient.

Table 6 Example of the parameterization of vegetation on top of the cliff that the erodibility coefficient will be divided with. Higher values equals higher erodibility reduction. Current parameter values based on findings of Lo et al. (2017).

Stem density (stems/m^2)	**0**	**500**	**1000**	**1340**	**2680**
Reduction parameter due to vegetation	0.95	1.0	1.5	1.1	1.15

4. Results

This chapter presents the results of the model simulations conducted in this thesis. It includes the calibration of the initial uniform erodibility coefficient, the parameterization of vegetation on the salt marsh cliff, and the final outcomes after incorporating the spatially varying erodibility coefficient into the model.

4.1 Calibration erodibility coefficient

After iteratively adjusting the erodibility coefficient, a coefficient of 0.73 m/yr/(W/m) was found to produce a simulated average lateral retreat closely matching the observed average lateral retreat. The model's average lateral retreat is 2.07 meters within the time frame from January 5, 2023, to January 25, 2024, resulting in a negligible difference of two centimeters compared to the observed average lateral retreat of 2.05 meters (Figure 24).

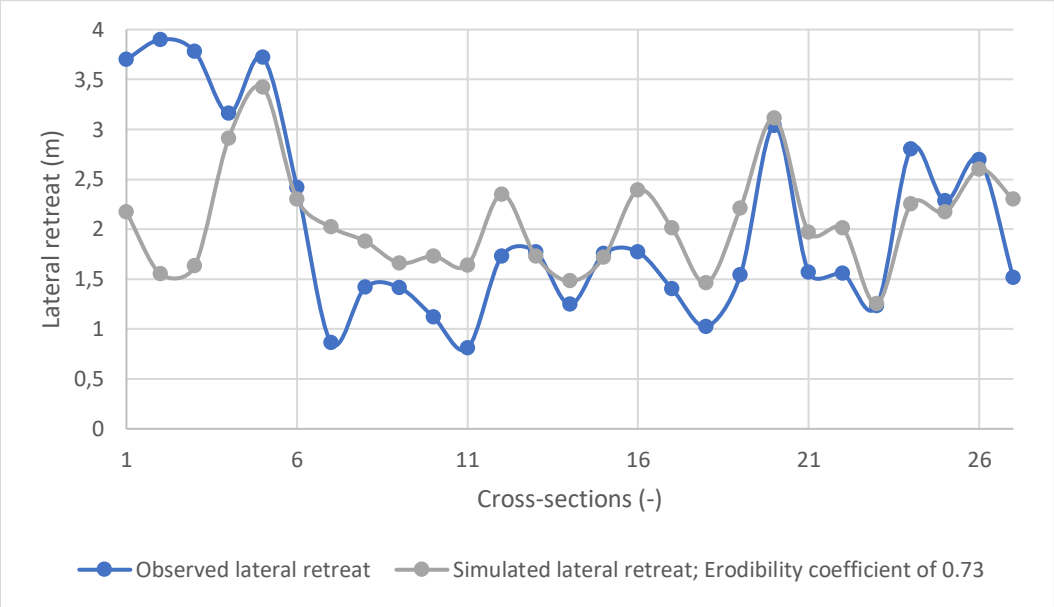

Figure 24 Observed and simulated lateral retreat found in the cross-sections. Simulated lateral retreat is modeled using an erodibility coefficient of 0.73. Showing large deviations in cross-sections 1-3.

It was found that the model did not accurately simulate the large erosion rates in the western part of the salt marsh, with differences of more than two meters observed (cross-sections 1 to 3) (Figure 24). Incorporating these cross-sections into the calibration of the vegetation parameterization would result in a biased representation. The differences between the simulated and observed values were so large that, according to the statistical metrics, increasing the erodibility coefficient continued to improve accuracy. However, this trend persisted to the point where the average simulated lateral retreat no longer represented the average measured retreat. This is because the differences in these three cross-sections are the highest found in the results. Therefore, these cross-sections are considered outliers and will not be included in the calibration of the erodibility coefficient. These cross-sections are the first three, excluding approximately 100 meters of salt marsh from this study (Figure 19).

Excluding the outliers, the average observed lateral retreat was found to be 1.83 meters. The best-fitted erodibility coefficient also decreased to 0.65 m/yr/(W/m) (Figure 25). In this instance, the simulated

average lateral retreat was 1.77 meters, a five-centimeter difference. The statistical metrics can be found in Table 7.

The correlation coefficient of 0.77 indicates a strong positive linear relationship between the simulated and measured lateral retreat. This means that, overall, when the observed retreat increases, so does the simulated data. The MAE value indicates that the model's predictions are off by 0.43 meters from the actual values, leaving room for improvement. The RMSE value indicates that, on average, the model's predictions deviate from the measurements by approximately 0.52 meters, with larger errors being more significant. Lastly, the R^2 value shows that the model explains 54% of the variance in the actual data, which means there is room for improvement, but the model has captured a reasonable amount of the underlying pattern.

Overall, the metrics suggest that the model performs well, but there is still room for improvement in reducing prediction errors and better capturing the variance in the data.

Table 7 Statistical metrics of erodibility coefficient of 0.65 m/yr/(W/m).

Statistical metric	**Erodibility coefficient: 0.65 m/yr/(W/m)**
Correlation Coefficient (-)	0.77
Mean Absolute Error (m)	0.43
Root Mean Squared Error (m)	0.52
Coefficient of Determination (%)	54

Figure 25 compares observed and simulated lateral erosion across 24 cross-sections (4 to 27) showing that the model generally follows the observed data trends, indicating a reasonable alignment between predicted and actual erosion patterns. However, while many cross-sections, such as 5, 6, 8, 9, 10, 13, 14, 15, 21, 22, 23, 25, and 26, exhibit close matches with differences typically less than 0.5 meters, there are notable discrepancies at specific points. Significant deviations are observed at cross-sections 7, 12, 16, 19, and 27, where the model tends to overpredict erosion, and at cross-sections 4, 11, 18, and 24, where the model underpredicts the erosion.

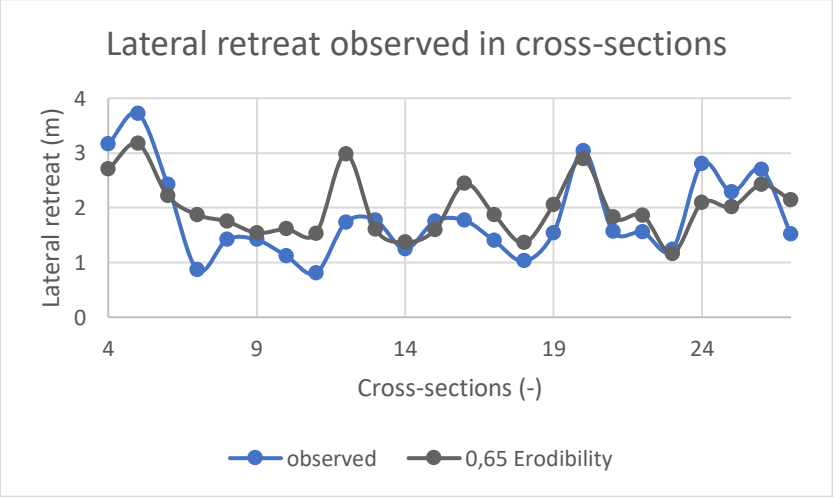

Figure 25 Lateral retreat of observed and initially simulated lateral retreat without outliers from cross-sections 1-3. Showing better aligning results.

4.2 Parameterization of the vegetation on top of the cliff

The parameterization of the vegetation on top of the cliff started with the increase of erosion where no vegetation was present. In most cases, especially in the winter, no vegetation was present on top of the cliff. This means that this parameter would have the most effect on the lateral retreat in the whole area of the salt marsh. In order to see which vegetation densities apply for each cliff, Table 8 is made. In this table, it is also stated if there needs to be more, or less erosion to grow closer to the actual measurements.

Table 8 Overview of vegetation on the cliffs for each cross-section. The over-and-under estimation can be found under model bias. + indicates that more erosion is needed, while – indicates that less erosion is needed according to observations. Two times a double minus is given which indicate that the erosion needs to be significantly decreased.

Cross-section	Density winter (stems/m2)	Density summer (stems/m2)	Model bias (+/-)
4	0	0	+
5	0	0	+
6	0	0	+
7	0	0	--
8	0	0	-
9	0	0	
10	500	1340	-
11	500	1340	-
12	1000	1340	--
13	0	1340	-
14	0	1340	+
15	0	0	-
16	0	0	-
17	500	1340	-
18	0	1340	-
19	0	0	-
20	0	0	-
21	500	1340	-
22	0	1340	-
23	0	2680	
24	0	1340	+
25	0	1340	+
26	0	0	+
27	0	1340	-

Table 8 presents the relationship between vegetation presence and the erodibility coefficient. The data show that not all cross-sections align with the stem densities observed at the cliffs. For example, in unvegetated cliffs, the number of required increases and decreases in lateral retreat is equal, indicating no clear trend regarding the adjustments needed to the erodibility coefficient. In contrast, the cliffs with vegetation exhibit a more consistent alignment with the necessary adjustments for cliff erosion. Specifically, the non-vegetated grids show a nearly equal distribution between cliffs requiring more erosion and those requiring less.

The erodibility coefficient found in Chapter 4.1 was used to parameterize the effect of vegetation. The parameter used in this thesis for the vegetation on top of the cliff will be used to divide the erodibility coefficient, making the erodibility coefficient spatially varying. For the unvegetated cells, a 15% increase in the erodibility coefficient initially appeared to improve the statistical metrics the most. However, this adjustment significantly increased the average lateral retreat to 1.97 meters. To address this, a lower erodibility coefficient of 0.61 was chosen, balancing lower erodibility with better statistical metrics (Table 9). The optimal increase for non-vegetated cells was determined to be 8%.

Adding non-vegetated cells to the dataset resulted in slight but noticeable improvements in several statistical measures, enhancing overall accuracy:

- Correlation Coefficient: Increased by 0.03.
- Mean Absolute Error (MAE): Decreased by 0.02 meters.
- Root Mean Squared Error (RMSE): Decreased by 0.01 meters.
- Coefficient of Determination (R^2): Increased by 1%.

Table 9 Statistical metrics of the uniform erodibility coefficient of 0.68 and 0.61 m/yr/(W/m).

Statistical metric	Erodibility coefficient of 0.68 m/yr/(W/m)	Erodibility coefficient of 0.61 m/yr/(W/m)
Correlation Coefficient (-)	0.77	0.77
Mean Absolute Error (m)	0.43	0.42
Root Mean Squared Error (m)	0.52	0.49
Coefficient of Determination (-)	54	58

Although these improvements were minimal, they collectively enhanced statistical accuracy. This modest impact is expected, as Table 8 shows an even distribution of cliffs requiring more and less erosion among non-vegetated cells.

The parameterization for unvegetated cells has notably enhanced model accuracy across various cross-sections. Specifically, cross-sections 4, 6, 8, 9, 14, 15, 16, 20, 24, 25, and 26 exhibit reduced discrepancies, indicating better alignment with observed values (Figure 26). This highlights the effectiveness of the parameterization in improving the model's ability to predict lateral erosion.

Despite these improvements, some discrepancies remain, particularly at cross-sections 12, 13, and 17, where the parameterization had minimal impact on accuracy. Additionally, the parameterization makes predictions worse in some areas. Notably, cross-sections 7, 8, 14, 16, 18, 19, 22, and 27 see increased discrepancies compared to the initial simulation. These cross-sections show that the parameterization approach, while generally beneficial, can sometimes misalign with observed data, leading to less accurate predictions.

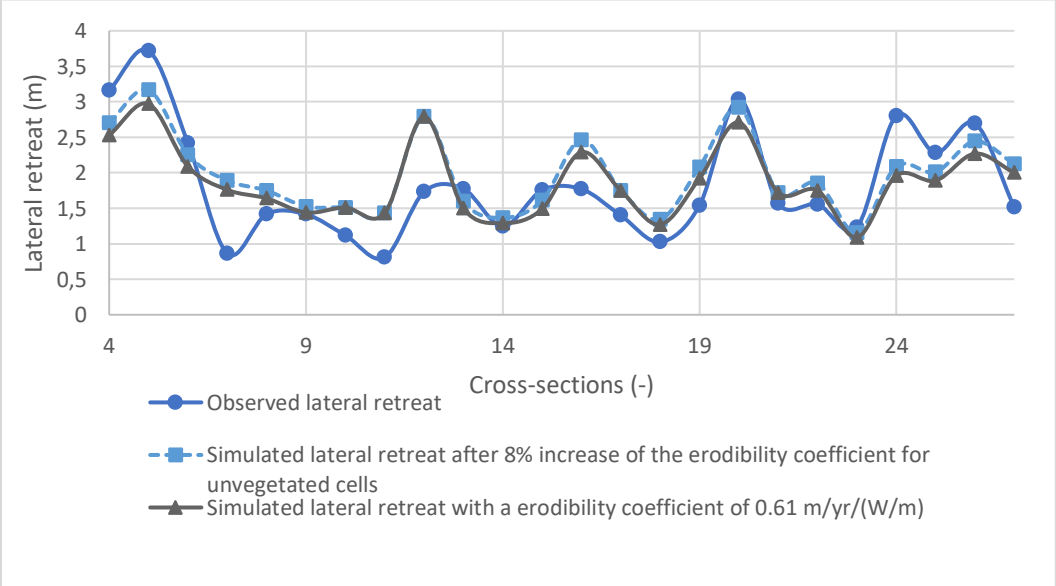

Figure 26 Lateral retreat of observed and simulated lateral retreat before and after the parameterization of unvegetated cells. Simulated lateral retreat before the parameterization is noted with the erodibility coefficient. Simulated lateral retreat after the parameterization is noted with the increase in erodibility coefficient.

Next, the parameterization of a stem density of 500 stems/m² was conducted at four locations. Table 8 shows that four out of four cliffs needed less erosion. This indicates a need to decrease erodibility at these locations. Through iterative steps, a 19% decrease in the erodibility coefficient was determined to be the best fit. This adjustment further increased accuracy:

- Correlation Coefficient: Increased by 0.01.
- Mean Absolute Error (MAE): Decreased by 0.03 meters.
- Root Mean Squared Error (RMSE): Remained unchanged.
- Coefficient of Determination (R^2): Increased by 4%.

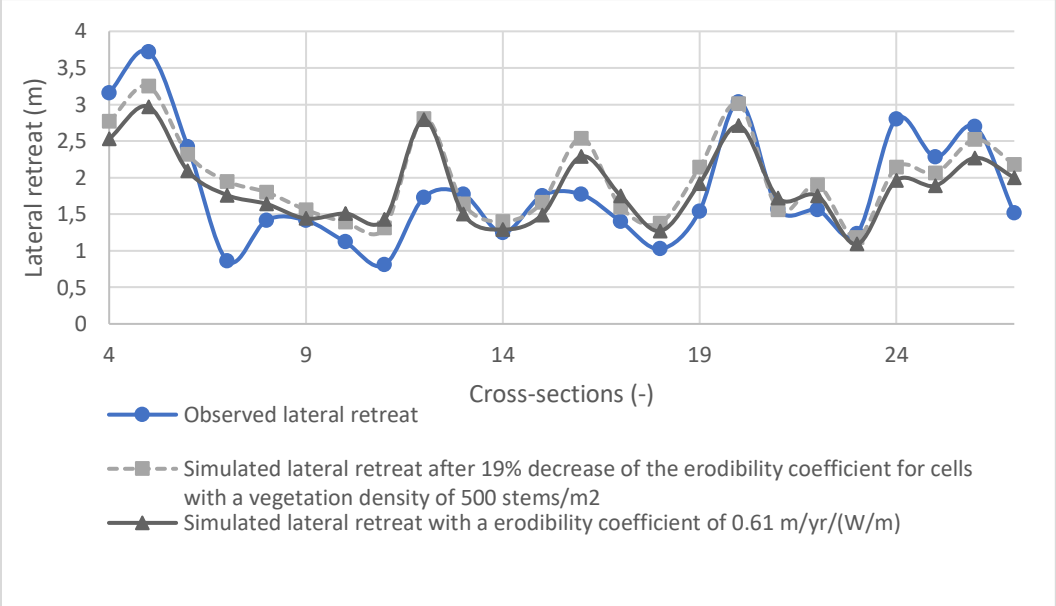

Figure 27 Lateral retreat of observed and simulated lateral retreat before and after the parameterization of stem density with 500 stems/m². Simulated lateral retreat before the parameterization is noted with the erodibility coefficient. Simulated lateral retreat after the parameterization is noted with the decrease in erodibility coefficient.

The introduction of a stem density of 500 stems/m2 has significantly boosted model accuracy across multiple cross-sections. Cross-sections 10, 11, 17, and 21 demonstrate reduced discrepancies, indicating improved alignment with observed values (Figure 27). This underscores the effectiveness of this parameterization in enhancing the model's predictive capabilities for lateral erosion. Because at all cross-sections where a stem density of 500 stems/m2 is located the lateral erosion needed to decrease, no increase in discrepancies is found compared to the previous parameterization. Thus, this parameterization has no decreases in accuracy at all cross-sections.

Because the stem density of 1340 stems/m² was more prevalent on the cliffs than the other remaining two, this density was parameterized next. Table 8 shows that most cliff cells with this stem density required less erosion. Consequently, this adjustment affected a larger number of cliffs. It was therefore expected to have a larger statistical impact. The best-fitted decrease in erodibility of this density was found to be 60%. This adjustment produced the following improvement in the dataset's accuracy:

- Correlation Coefficient: Increased by 0.01.
- Mean Absolute Error (MAE): Decreased by 0.03 meters.

- Root Mean Squared Error (RMSE): Decreased by 0.03 meters.
- Coefficient of Determination (R^2): Increased by 2%.

The parameterization of stem density of 1340 stems/m^2 has considerably enhanced model accuracy across numerous cross-sections. Cross-sections 10, 11, 12, 14, 17, 18, 22, and 27 show reduced discrepancies, demonstrating improved alignment with observed values (Figure 28).

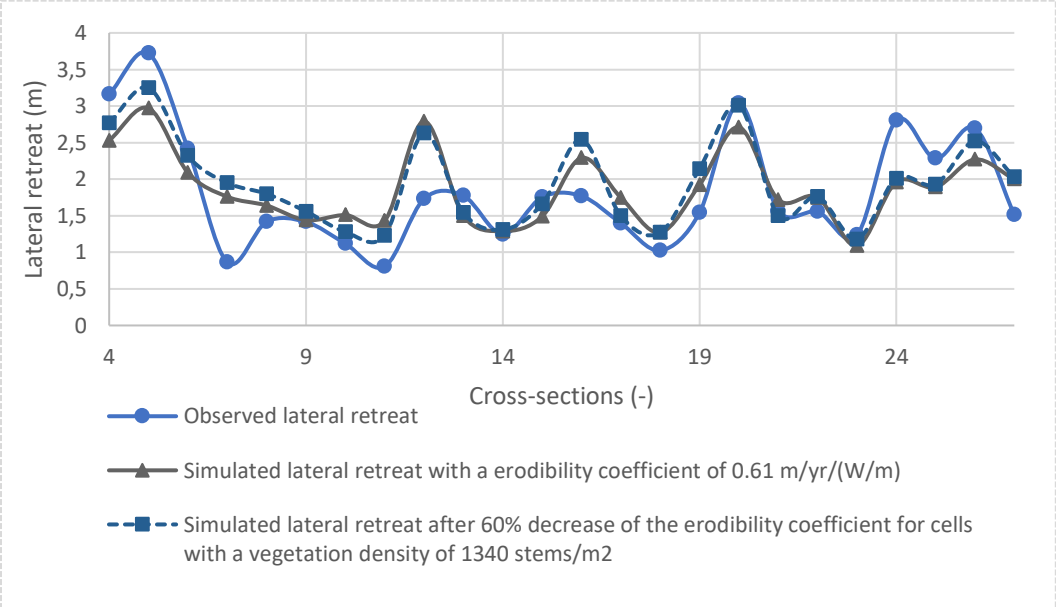

Figure 28 Lateral retreat of observed and simulated lateral retreat before and after the parameterization of stem density with 1340 stems/m^2. Simulated lateral retreat before the parameterization is noted with the erodibility coefficient. Simulated lateral retreat after the parameterization is noted with the decrease in erodibility coefficient.

Despite these improvements, the parameterization has led to worsened predictions in specific areas. Notably, cross-sections 13, 21, and 25 exhibit increased discrepancies compared to the initial simulation. These findings illustrate that while the parameterization generally benefits accuracy, it can occasionally misalign with observed data, resulting in less accurate predictions.

Both stem densities of 1000 and 2680 stems/m^2 only appeared once on the cliffs, at cross-sections 12 and 23, respectively. The erodibility at cross-section 12 needed to be as high as possible, while at cross-section 23, it needed to be as low as possible, capped at 60% due to the parameterization of the 1340 stems/m^2. Implementing the 60% decrease for the cell with 1000 stems/m^2 appeared to be spot on, as the newly modeled value was only three centimeters larger than the observed one. This adjustment significantly increased accuracy:

- Correlation Coefficient: Increased by 0.03.
- Mean Absolute Error (MAE): Decreased by 0.04 meters.
- Root Mean Squared Error (RMSE): Decreased by 0.04 meters.
- Coefficient of Determination (R^2): Increased by 6%.

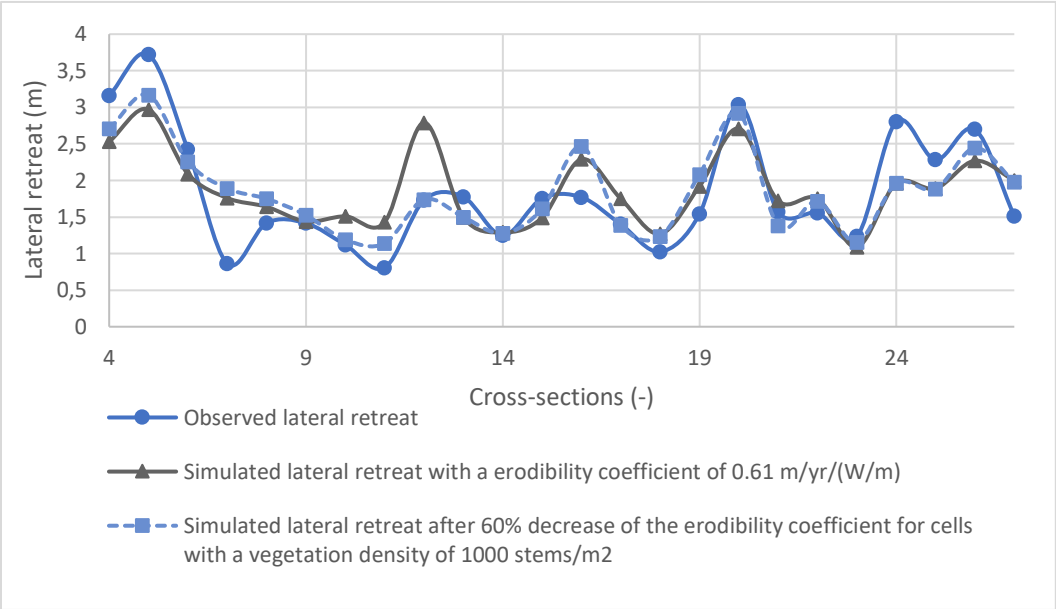

Figure 29 Lateral retreat of observed and simulated lateral retreat before and after the parameterization of stem density with 1000 stems/m^2. Simulated lateral retreat before the parameterization is noted with the erodibility coefficient. Simulated lateral retreat after the parameterization is noted with the decrease in erodibility coefficient.

As noted previously, a stem density of 1000 stems/m2 was only present in one instance, at cross-section 12. The parameterization of this stem density almost entirely resolved the discrepancy at cross-section 12, as evident in Figure 29.

The last parameterization of the stem densities was for the density of 2680 stems/m². This parameterization needed to be as low as possible, which was a 60% reduction of the erodibility coefficient. This is because the initial simulated lateral retreat was already close to the observed value. Having the initial value deviate too much would result in a decrease in accuracy. The effects of this parameterization decreased the statistical metrics slightly:

- Correlation Coefficient: No change.
- Mean Absolute Error (MAE): Increased by 0.02 meters.
- Root Mean Squared Error (RMSE): No change.
- Coefficient of Determination (R^2): No change.

The effect of the parameterization of 2680 stems/m2 is barely visible in the graph (Figure 30). The lateral retreat only decreased by 15 centimeters. Proving the very low significance of the parameterization.

In total, the Correlation Coefficient, Mean Absolute Error, Root Mean Error, and Coefficient of Determination reached statistical values of 0.85, 0.32 meters, 0.41 meters, and 71% respectively (Table 10). This means that all statistical metrics have improved (Table 11). For the parameterization used to adjust the uniform erodibility coefficient of the unvegetated cells, the following stem densities and corresponding erodibility values were applied: unvegetated resulted in a value of 0.92, 500 stems/m² in 1.19, and 1000, 1340, and 2860 stems/m² all produced a value of 1.6.

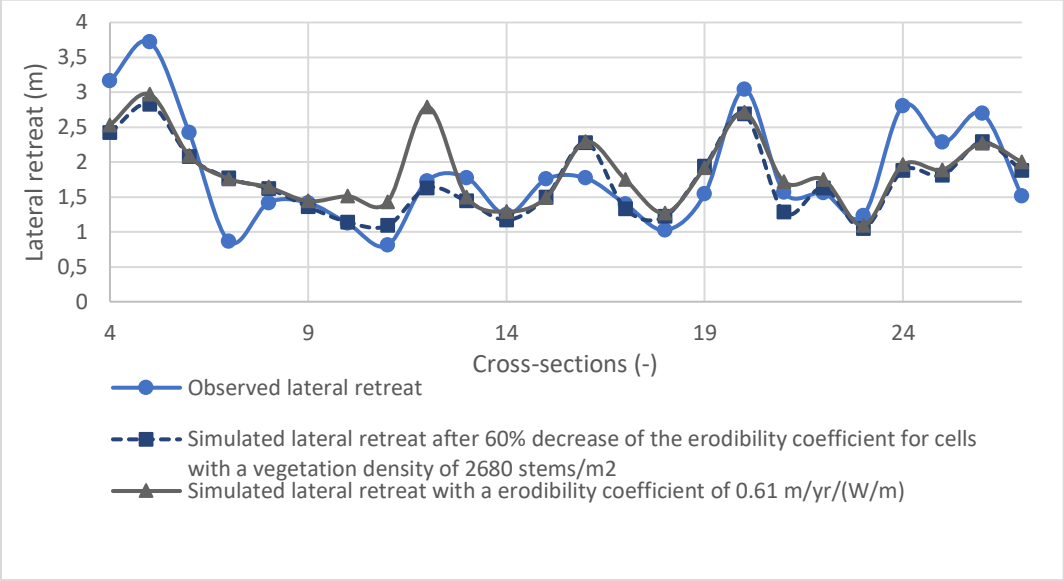

Figure 30 Lateral retreat of observed and simulated lateral retreat after the parameterization of all stem densities. Simulated lateral retreat before the parameterization is noted with the erodibility coefficient. Simulated lateral retreat after the parameterization is noted with the decrease in erodibility coefficient.

Table 10 Overview of statistical metrics before and after each parameterization.

Statistical metric	Erodibility coefficient of 0.61 m/yr/(W/m)	Parameterization value of 0.92 based on no vegetation	Parameterization value of 1.19 based on stem density of 500 stems/m²	Parameterization value of 1.60 based on stem density of 1340 stems/m²	Parameterization value of 1.60 based on stem density of 1000 stems/m²	Parameterization value of 1.60 based on stem density of 2680 stems/m²
Correlation Coefficient (-)	0.77	0.80	0.81	0.82	0.85	0.85
Mean Absolute Error (m)	0.42	0.40	0.37	0.34	0.30	0.32
Root Mean Squared Error (m)	0.49	0.48	0.48	0.45	0.41	0.41
Coefficient of Determination (%)	58	59	63	65	71	71

Table 11 Overview of changes in statistical metric after each parameterization.

Statistical metric	Parameterization value of 0.92 based on no vegetation	Parameterization value of 1.19 based on stem density of 500 stems/m²	Parameterization value of 1.60 based on stem density of 1340 stems/m²	Parameterization value of 1.60 based on stem density of 1000 stems/m²	Parameterization value of 1.60 based on stem density of 2680 stems/m²	Total
Correlation Coefficient (-)	+0.03	+0.01	+0.01	+0.03	0	+0.08
Mean Absolute Error (m)	-0.02	-0.03	-0.03	-0.04	+0.02	-0.10
Root Mean Squared Error (m)	-0.01	0	-0.03	-0.04	0	-0.08
Coefficient of Determination (%)	1	4	2	6	0	+13

4.3 Final simulated lateral retreat and erodibility coefficient

The final simulated average lateral retreat was found to be 1.89 meters within the simulation time. This equals a lateral retreat of 1.92 meters per year. The simulated lateral retreat is about 0.05 centimeters higher than the observed values, which indicates a slight overestimation of the model.

To further assess the model's performance, the lateral retreat was plotted in a top view of the salt marsh (Figure 32), while the observed elevation difference is shown in Figure 31. Although these figures display different variables—lateral retreat per grid cell in Figure 32 and elevation differences in Figure 31—they can still be compared. Figure 32 shows that the redness indicates the amount of lateral retreat in each grid cell, with thicker red lines along the cliff edges corresponding to greater retreat. Figure 31 presents elevation differences, where redder areas represent higher differences in elevation. Comparing both figures reveals that the model underestimated lateral retreat on the west side of the salt marsh. In this region, Figure 31 shows the thickest red line, indicating significant retreat, while Figure 32 suggests less erosion than expected. The area should be black according to Figure 31, corresponding to a lateral retreat greater than 3.5 meters, but the model does not reflect this.

Overall, the model accurately simulates areas of smaller to moderate retreat, as shown by the alignment between both figures along most of the cliff edges. However, the larger lateral retreat, especially in the western region of the salt marsh and around 300 meters west of its easternmost part, is underestimated by the model.

Figure 31 Observed elevation differences between 05-02-2023 and 25-01-2024. Redness indicates how much elevation decreased.

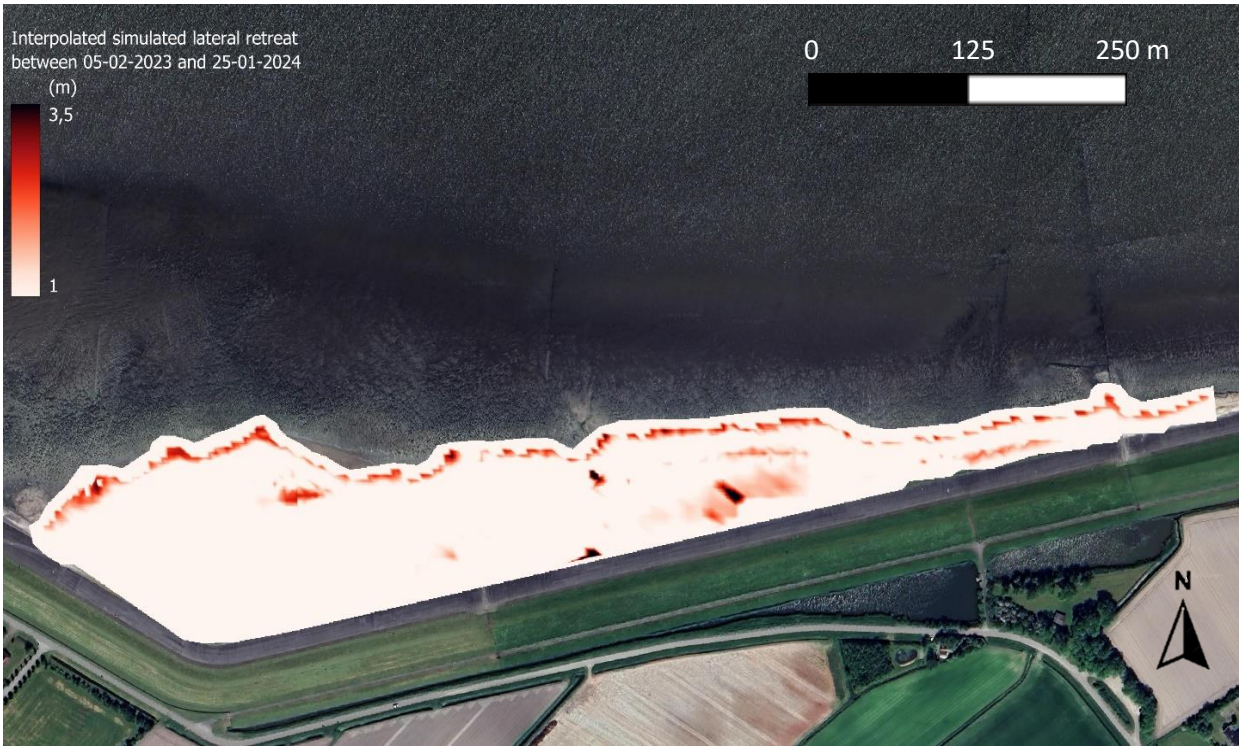

Figure 32 Interpolates simulated lateral retreat between 05-02-2023 and 25-01-2024. Redness indicate how much lateral retreat is present in that area.

Furthermore, the extent of lateral erosion per time frame was also analyzed. Figures 33 and 34 show the cumulative lateral retreat and the lateral retreat that occurred during each respective simulation respectively. The time frame of these simulations is 05-02-2023 to 01-04-2023 for simulation 1, 01-04-2023 to 01-06-2023 for simulation 2, 01-06-2023 to 01-08-2023 for simulation 3, 01-08-2023 to 01-10-2023 for simulation 4, 01-10-2023 to 01-12-2023 for simulation 5, 01-12-2023 to 28-04-2023 for simulation 6, 28-12-2023 to 25-01-2024 for simulation 7. From Figures 33 and 34, it is visible that the highest contribution to the total lateral retreat occurred in the final simulation, whereas simulation four exhibited the least erosion.

The average lateral retreat for each time frame and the cumulative lateral retreat are presented in Table 12. Notably, the magnitude of retreat varied across the simulations, with some time frames displaying more significant erosion than others. These differences are clearly illustrated in the time series presented in Figures 33 and 34.

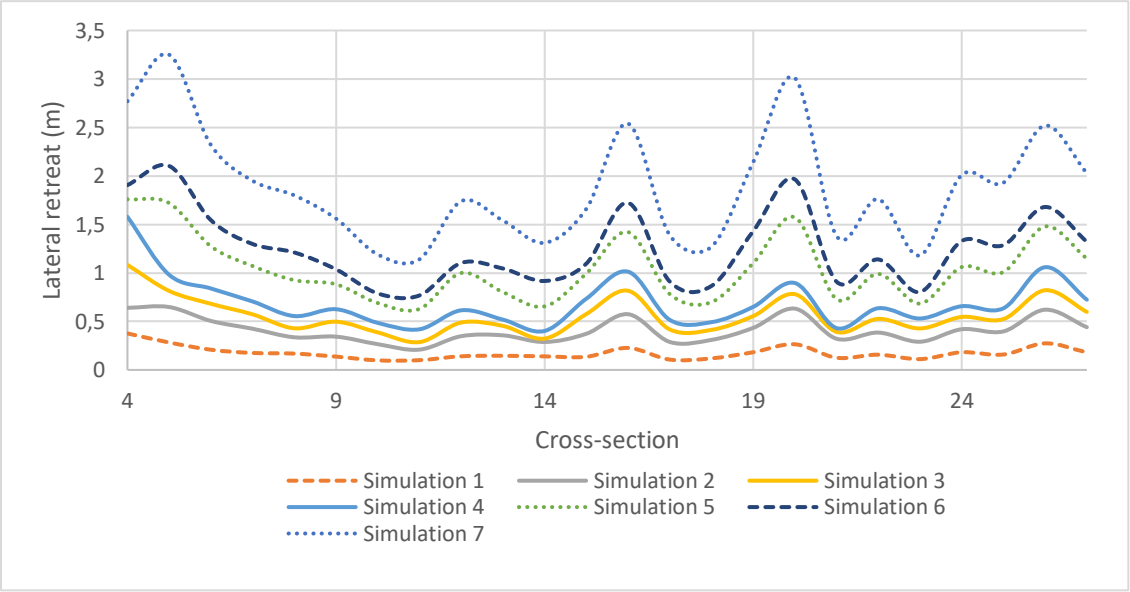

Figure 33 Cumulative lateral retreat after each simulation at each cross-section.

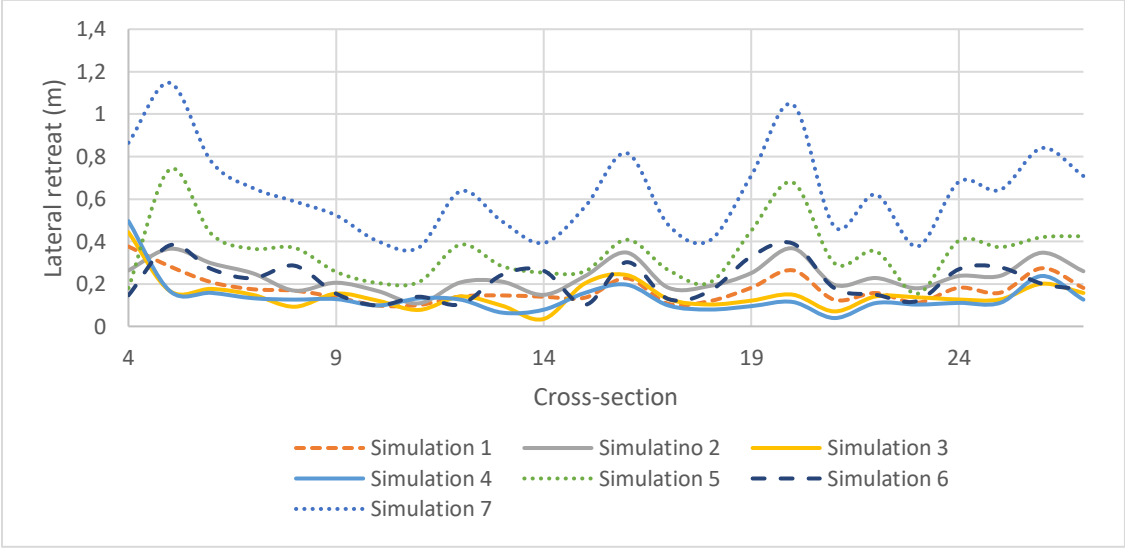

Figure 34 Lateral retreat per simulation at each cross-section.

Table 12 Average and cumulative lateral retreat per simulation

Simulation	Average lateral retreat occurred in this time frame	Cumulative lateral retreat after this time frame
1	0.18	0.18
2	0.24	0.41
3	0.15	0.56
4	0.14	0.70
5	0.35	1.05
6	0.21	1.27
7	0.64	1.91

The spatially varying erodibility coefficient for the winter and summer can be found in Figures 35 and 36 respectively. For the winter, three different erodibility coefficients can be found along the salt marsh, 0.38, 0.52, and 0.66 m/yr/(W/m). For the summer only two different coefficients can be found, 0.38 and 0.66 m/yr/(W/m). In these figures, all stem densities that are not parameterized, so above 1000 stems/m^2, are set on the lowest erodibility coefficient, thus 0.38 m/yr/(W/m). It is visible that in the winter, the erodibility coefficient varies more than in summer. In the summer, a clear border between 0.38 and 0.66 can be found along the salt marsh edge. In the winter, this is less the case. Different erodibility coefficients can be found along the salt marsh.

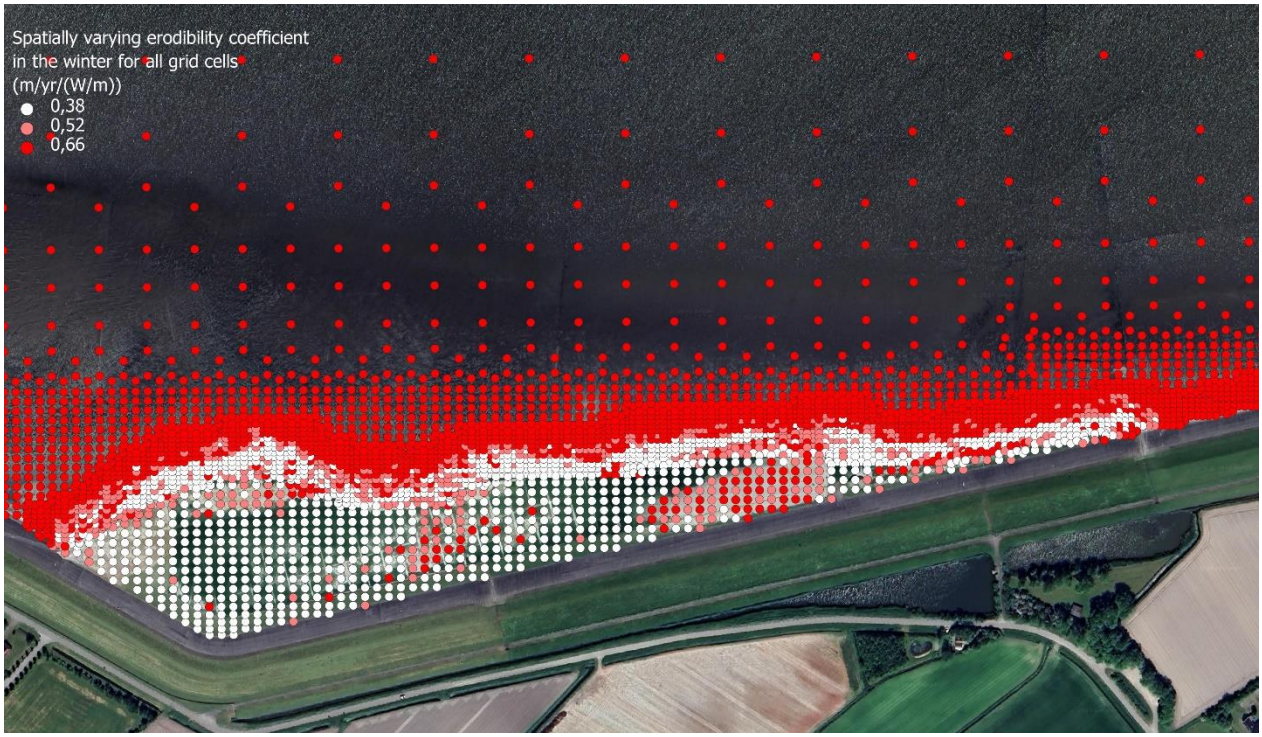

Figure 35 Spatially varying erodibility coefficient in the winter.

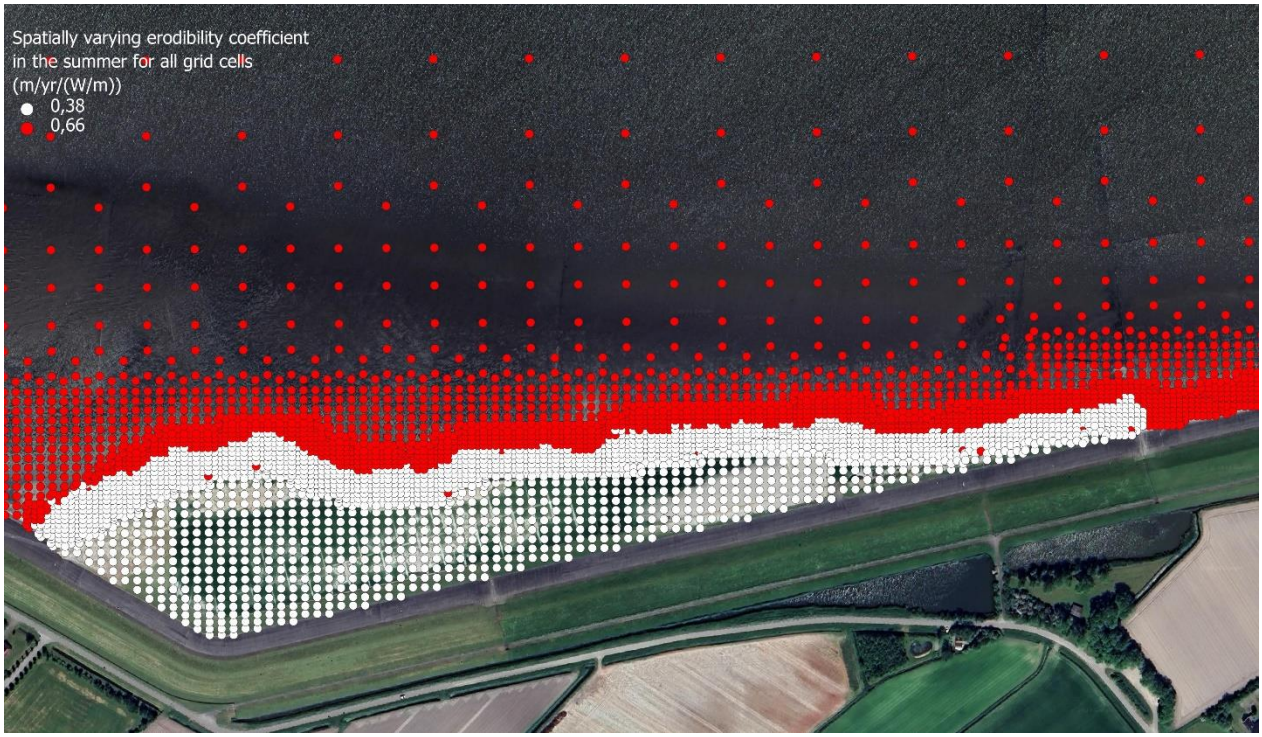

Figure 36 Spatially varying erodibility coefficient in the summer.

5. Discussion

5.1 Summary of key findings

Current methods of salt marsh cliff erosion modeling often rely on a simplified linear relationship between wave power and cliff erosion, as established by Marani et al. (2011). This approach uses a spatially uniform erodibility coefficient, which does not accurately reflect real-world conditions (Leonardi & Fagherazzi, 2015). In response, this study incorporates a parameterization that yields a spatially variable erodibility coefficient based on vegetation densities. Utilizing the modeling framework developed by Georgiou et al. (2022), which includes a hydrodynamic model and a salt marsh module, this study adapts the model previously used in the MRDP to the Wierum area in the Netherlands. This adaptation involves examining the implications of changing geographical locations.

Significant adjustments were made to refine the salt marsh module, including streamlining output files and excluding irrelevant functions. The main findings indicate that data availability and resolution are key factors driving modeling choices in the salt marsh module. Additionally, specific processes were added to account for different hydrodynamic conditions observed in the new geographical location, such as neglecting the effect of wave power against the cliff when it is fully submerged.

The research successfully calibrated the erodibility coefficient and parameterized the effect of vegetation on the salt marsh cliff through iterative adjustments, closely matching observed lateral retreat rates. The erodibility coefficient was validated against the average observed lateral retreat measured in 27 cross-sections. Incorporating the parameterization of vegetation increased the model's accuracy, as demonstrated by various statistical metrics. Vegetation was found to decrease the erodibility of the cliffs by 27% to 68%, determined by identifying the best statistical metrics.

5.2 Interpretations & implications

5.2.1 Changes in the model

The impact of changing geographical location mostly depends on the differences in data and the study's goal. Certain functions can be neglected with coarser grids and thus less accurate simulations. An example of this is the multiple-layered edge. With coarser grids, the edges are clearly defined, while with finer grids, multiple edges can be formed due to interpolation of the bathymetry data. Neglecting these edges would result in unrealistic erosion patterns.

The use of finer grid cells near the salt marsh edge can introduce more processes. Although not incorporated into this study, Tonelli et al. (2010) states that different cliff formations react differently to wave impact. By using smaller grid cells these cliff formations can be located within the model. So not only does using finer grid cells increase accuracy, but also introduces new processes that would increase accuracy even further. This statement is also supported by Néelz & Pender (2007). In this paper, it is demonstrated how high-resolution grids in urban flood modeling can capture small-scale topographic features and flow variations around structures. This included the addition of detailed surface and subsurface hydrodynamic processes, improving the representation of water movement and interaction in complex urban environments.

Other than changes in the input data into Delft3D-FM, no new processes or adjustments were needed in this model. Differences in hydrodynamic activity that would impact different hydrodynamical aspects (e.g. sediment transport, current velocities), are all already incorporated into Delft3D-FM. So, for example, the change from micro-tidal to macro-tidal only influenced the coding of the salt marsh

module. Based on Fagherazzi, Mariotti, et al. (2013), the wave power on the edge of the salt marsh cliff cell gets neglected while the cliff is submerged. In Figure 37 it is visible the reduction of wave power after this addition is quite significant. This statement is supported by Tonelli et al. (2010). This paper states that the wave thrust against the scarp increases with the water level until the cliff is fully submerged. When the cliff is submerged, the wave thrust decreases significantly until it does not affect the cliff erosion.

5.2.2 Outliers in the simulated lateral retreat

Initial results showed large differences in the three most western cross-sections (cross-sections 1 till 3) with the observed erosion. These differences were so large, that it affected the calibration too much. Therefore, it was chosen to mark these cross-sections as outliers, excluding them from the results. The reasons for these significant differences have been analyzed. Previous studies indicate that waves play a crucial role in dictating erosion patterns along the salt marsh edge (Finotello et al., 2020a). By examining the results, it is evident that the cumulative wave power responsible for erosion did not show significant increases at the outliers (cross-sections 1-3). Additionally, the potential impact of subtracting wave power when the salt marsh edge is submerged was considered (Figure 38). This factor also proved insignificant; in fact, the subtracted wave power is lower in this area compared to the rest. Therefore, it can be stated that either the model failed to accurately simulate the hydrodynamic forcing at these locations, or that in reality, other factors such as wind or human activity contributed to the substantial cliff erosion.

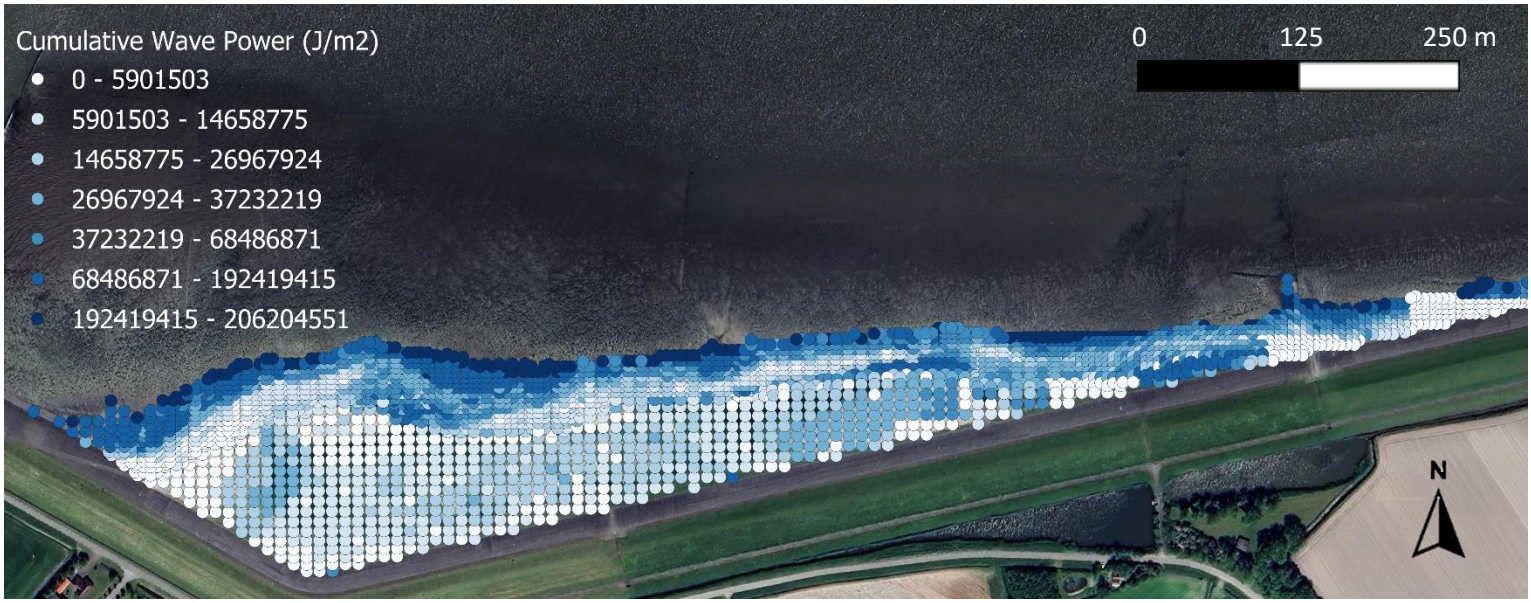

Figure 37 Total wave power over whole salt marsh between 05-02-2023 and 25-01-2024.

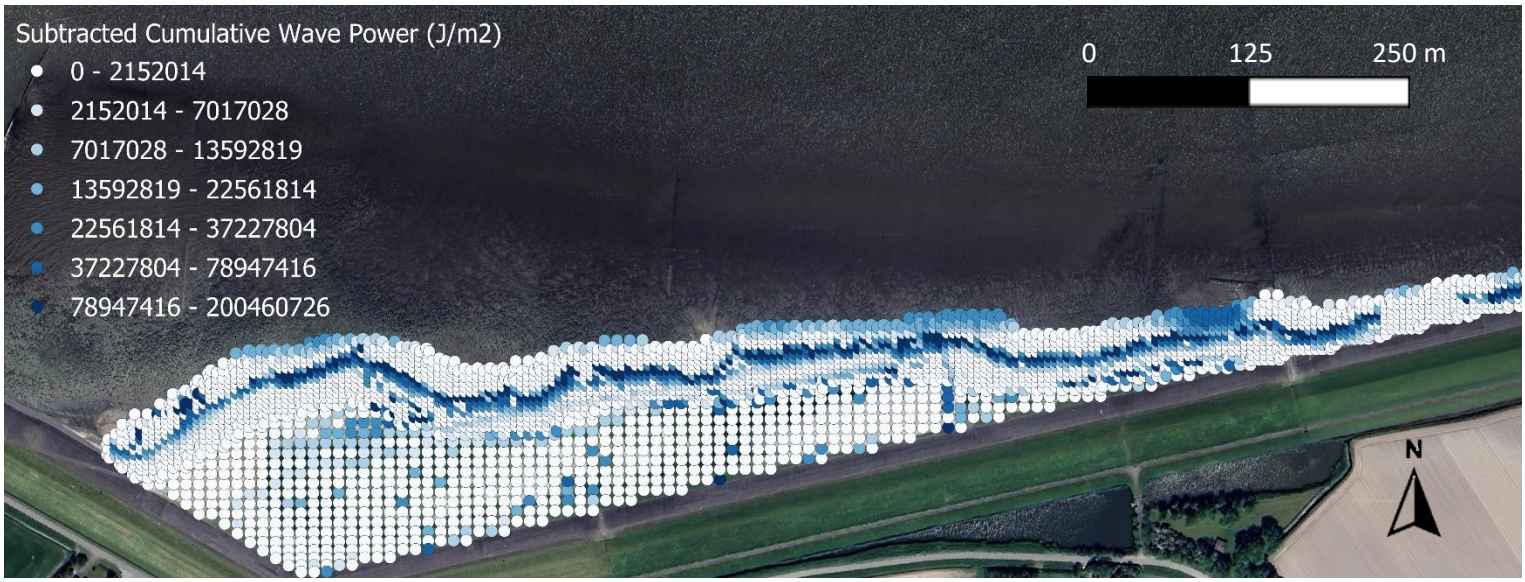

Figure 38 Total neglected wave power due to inundation of the cliffs from 05-02-2023 to 25-01-2024.

5.2.3 Comparing the observed lateral retreat

From the observed data, large amounts of lateral retreat are found, exceeding one meter at most points, averaging 1.84 meters within the time frame (1.87 meters/year). Siemes et al. (2020) has done similar measurements at the same salt marsh. According to Siemes et al. (2020), this average lateral retreat should be lower. In the paper by Siemes et al. (2020), the average lateral retreat was measured between spring 2008 and spring 2014. In this paper, cliff erosion rates along the salt marsh width averaged 1.1 $m^3/m/year$. Most of this erosion was caused by cliff erosion. Additionally, the average lateral retreat was found to be 0.9 meters/year. Both erosion rates in this study are found to be more than double the erosion rates according to Siemes et al. (2020). The difference in erosion rates could be due to the way the observed lateral retreat is calculated. In the paper by Siemes et al. (2020), it is not clearly stated how the average lateral retreat is calculated.

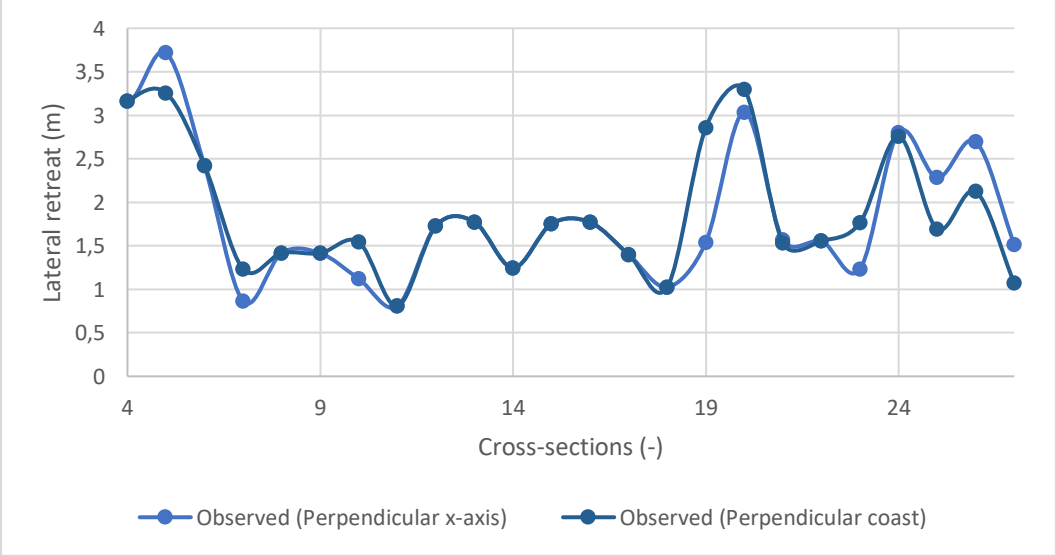

Figure 39 Comparison of observed lateral retreat perpendicular to the x-axis and to the coast.

Initially, because of the grid cells, cross-sections were made perpendicular to the x-axis. However, in real life, the cliff erosion would move perpendicular to the cliff. It is possible that different outcomes can result from this. Therefore, the measurements were done again but then with cross-sections perpendicular to the cliff. In Figure 39 it is visible that the difference in orientation of the cross-section did not change erosion rates significantly. Using the cross-section perpendicular to the cliff, increased the average lateral retreat by 2 centimeters.

The difference can also be caused by the two different sources for the bathymetry that are used. The bathymetry set used as input in Deltf3D-FM comes from AHN (2023), while the drone data that is used to verify the results is from Sarah Dzimballa (2023). The AHN5 data set is measured with planes, while the data set of Sarah Dzimballa (2023) are made with a drone. In the two types of bathymetry measurements, differences can occur which can explain the differences in erosion rate, such as different resolution and vertical accuracy. The AHN5 data has a resolution of 0.5x0.5 meters, while the drone data has a resolution of 0.3x0.3 meters. Because of these differences, an additional set of drone measurements was used to verify the AHN data. The additional drone footage comes from the same study and has the same methods as the one used for the verification of the results. This data set was not used previously as this data was not yet available at the time when the simulations were run. These drone measurements were taken on 24-11-2022, a bit before the AHN measurements. It is therefore expected that more erosion has occurred between 24-11-2022 and 25-01-2024, than 05-02-2023 and 25-01-2024.

The data indicate a total eroded volume of 2379 m^3, with the average lateral retreat remaining the same for the period of 24-11-2022 to 25-01-2024. The total eroded volume is lower compared to the AHN data, which shows 2434 m^3. This difference is mainly due to the eroded bare mudflat present in the AHN data. The cliff appears to have experienced minimal erosion between the 24-11-2022 and 05-02-2023 measurements. When the time frame increases while the lateral retreat barely increases, the average annual lateral retreat decreases to 1.42 meters/year, which aligns more closely with the findings of Siemes et al. (2020). From these findings, it is evident that either more wave action was present between 05-02-2023 and 25-01-2024, or the cliffs were more erodible. However, in Figure 40 it is visible that the erosion rates between 24-11-2022 and 05-02-2023 would be similar to erosion rates found in August and September. Analyzing the results, this period would on average contribute only about 14 centimeters towards to total lateral retreat found during the simulations. It is however important to note that water levels during the winter are normally higher than in the summer. This increases the amount of time the salt marsh is inundated, and less cliff erosion occurs.

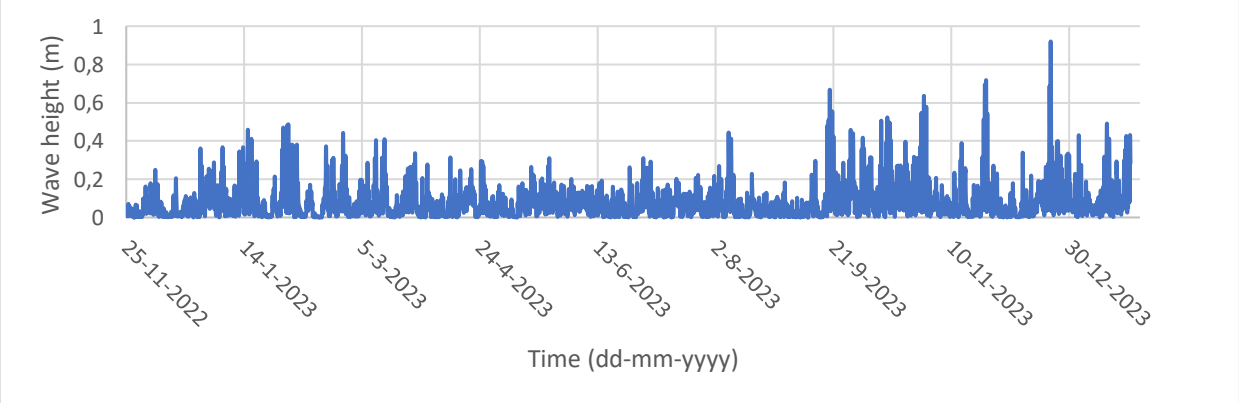

Figure 40 Wave heights from 24-11-2022 to 25-01-2024.

5.2.4 Found erodibility coefficient

The iterative process identified an erodibility coefficient of 0.61 m/yr/(W/m) as optimal with an average simulated lateral retreat of 1.88, closely matching the observed average lateral retreat of 1.83 meters. This indicates a good alignment between the model's predictions and actual measurements. However, certain cross-sections showed significant discrepancies, particularly in the western part of the salt marsh, suggesting model limitations in capturing high erosion rates. These outliers were excluded from calibration, indicating potential inaccuracies in hydrodynamic forcing or unaccounted factors like wind or human activity, such as trampling of the cliffs. The erodibility coefficient found during the calibration of the salt marsh module is on the higher side. Previous studies used lower erodibility coefficients, normally close to 0.3 m/yr/(W/m) (Mariotti & Canestrelli, 2017; Georgiou et al., 2022; Valentine & Mariotti, 2019). This is mostly likely the cause of the different time frames used in the models. The time frame in this study is quite small, about a year, while the time frame in the other studies are 3000 years, 30 years, and 140 years for Mariotti & Canestrelli (2017), Georgiou et al. (2022), and Valentine & Mariotti (2019) respectively. The rather small time frame used in this study makes the found erodibility coefficient a bit less reliable. Using larger time frames could lower the erodibility coefficient to similar values as found by Mariotti & Canestrelli (2017), Georgiou et al. (2022), and Valentine & Mariotti (2019). Other reasons for this large erodibility coefficient could be due to different vegetation and sediment properties.

Comparing the vegetation in Wierum with the vegetation found in the Louisiana salt marshes, differences in the characteristics of the vegetation are found. *Spartina Patens* and *Spartina Alterniflora* are mainly found in the salt marshes of Louisiana, while *Puccinellia Maritima* is mainly found in the salt marshes in Wierum (Georgiou et al., 2022) (Marin-Diaz et al., 2023). There are clear differences between the vegetation species. The vegetation found in Louisiana has a larger biomass above and beneath the ground. Larger biomass beneath the ground can increase the cohesiveness of the soil. According to Windham (2001) and Darby & Turner (2008), above and below ground biomasses averaged 500 g/m^2 and 900 g/m^2 respectively for *Spartina Patens* and 1500 and 1200 g/m2 respectively for *Spartina Alterniflora*. The biomass of the *Puccinellia Maritima* however was found to be way lower, with an average above and below-ground biomass of 244 g/m^2 and 364 g/m^2 respectively (Hussey & Long, 1982). These large differences can be the reason for the big difference in the erodibility coefficient found in this study versus the one used in Mariotti & Canestrelli (2017) and Georgiou et al. (2022).

5.2.5 Top view of the simulated lateral retreat

Looking at the top view created based on the simulated lateral retreat in Figure 32, there are red points visible on top of the salt marsh. This is because of the inundation of the salt marsh and the identification of cliffs. The model identifies a cliff when the elevation differences of grid cells are larger than 12 centimeters. This causes the model to apply cliff erosion on the marsh itself. During high tide, the salt marsh can inundate, and waves reach these so-called cliffs. This results in the cliff erosion simulated by the model on top of the marsh. The grid cells with lateral retreat are also plotted on top of the observed elevation differences in Figure 41. From this, it is visible that the largest lateral retreat is mostly found to be in front of the cliff. This is again due to the rather small cliff height requirement. Making the requirement higher would perhaps result in a better representation of the actual salt marsh cliff.

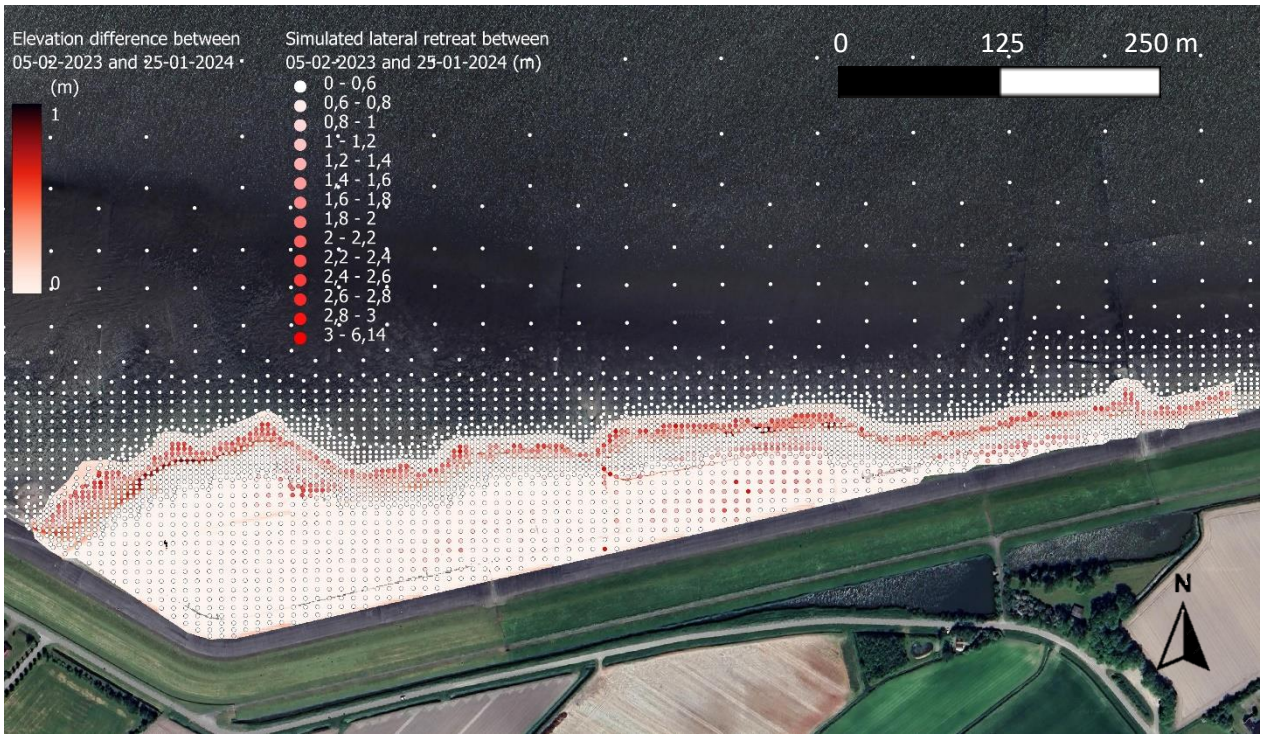

Figure 41 Observed elevation difference and simulated lateral retreat between 05-02-2023 and 25-01-2024.

5.2.6 Statistical metrics and simulation results

The correlation coefficient with the calibrated erodibility coefficient, without the parameterization of vegetation, is equal to 0.77. This suggests a strong positive linear relationship between simulated and measured retreats. The MAE of 0.43 meters and RMSE of 0.52 meters indicate moderate prediction errors, while an R^2 value of 0.54 shows that the model explains just over half of the variance in the data. This implies the model captures significant patterns but leaves room for improvement.

The parameterization of vegetation on top of the cliff improved the statistical metrics. The parameterization started with non-vegetated cells, resulting in an 8% increase in the erodibility coefficient, which marginally improved statistical accuracy. Successive parameterizations for different stem densities (500, 1000, 1340, and 2680 stems/m²) generally improved model accuracy, with each step enhancing correlation coefficients and reducing errors (Table 11). It is however important to note that these findings are site-specific. Different types of vegetation and soil characteristics can cause different results. The results found are specially for this specific location only. Other vegetation species can have a different effect on the erodibility of the marsh. *Puccinellia Maritima* has relatively smaller and less dense root systems than other halophytic vegetation. Salt marshes with vegetation with larger roots can decrease the erodibility even more than the parameterization found in this study.

Each of these statistical improvements signifies different aspects of model enhancement. The increase in the correlation coefficient shows better alignment with the observed trends, indicating improved consistency between predicted and actual data. The decrease in MAE points to smaller average errors, making the model's predictions more reliable for practical applications. The reduction in RMSE highlights a decrease in the impact of larger errors, making the model more robust against outliers or significant deviations. Finally, the increase in R^2 demonstrates that the model now accounts for a greater proportion

of the variability in observed data, providing a more comprehensive understanding of the underlying erosion dynamics.

The implications of these findings are significant for model accuracy and reliability. Improved calibration and vegetation parameterization enhance the model's predictive capabilities, making it more reliable for managing and mitigating erosion in salt marshes. These advancements can inform better coastal management practices, particularly in areas where vegetation plays a critical role in erosion control. Additionally, the results underscore the importance of incorporating vegetation dynamics into erosion models, allowing coastal managers to design interventions that either promote vegetation growth or consider vegetation density when planning erosion control measures. This is visible in the results as cliff erosion aligns better with the parameterization. Using this model on a larger scale, it can effectively detect weak points in salt marshes with higher certainty, and push for an increase in measurements at these locations.

However, since the cliff erosion was simulated over approximately one year, it is difficult to determine whether this specific time frame is sufficient. Extending the simulation period could provide a more robust evaluation of whether the parameterizations and calibrations are accurate.

5.3 Limitation

5.3.1 Model limitations

With the use of finer grids in salt marsh modeling, cliffs are not always clearly defined, and cliff heights are not always represented well enough. This is visible in Figure 42, while in the used bathymetry file, the cliff is clearly defined, and the cliff interpolated into the hydrodynamic grid is spread out over multiple grid cells. This however does not affect the results, as different methods are used in Chapter 3.7 to define the simulated lateral retreated. Also, the cliff height does not affect the erodibility of the cliff in the model. However, according to Van Eerdt (1985), cliff heights do affect the stability of the cliffs and thus also the erodibility. If this will get incorporated into the model it is important to validate that all cliffs are represented accordingly within the interpolated grid.

The morphological development of the mudflat influences the waves and thus the lateral retreat. Neglecting the morphology module of Deflt3D-FM impacts the results. Over the whole upper mudflat, it is visible that erosion occurs ranging from 0 to 20 centimeters between 5 February 2023 and 25 January 2024. According to the methods used within D-Waves, increased depth reduces energy dissipation due to bottom friction and depth-induced wave-breaking (Deltares, 2024). The increased depth would therefore increase the wave power affecting lateral retreat. Additionally, due to the lower mudflat, the cliffs would be impacted by waves more frequently, as the mudflat is more frequently underwater. It is expected that the addition of the D-Morphology module would increase the total lateral retreat rate.

5.3.2 Parameterization of the vegetation

The parameterization of stem densities of 1000 and 2680 stems/m^2 could be less accurate than the other parameterizations. This is because both stem densities are present only one time on the cliffs. If more cliffs had these densities, parameterization could be more certain.

The results of this study indicate that vegetation can reduce erosion rates by up to 68% percent. According to Lo et al. (2017), this reduction of this statement is rather high. Lo et al. (2017) states that vegetation roots can reduce edge erosion up to 17% and 80% for silty and sandy soils respectively. Since the salt marshes at Wierum contain mainly silty soils (more than 63% silt content (Basismonitoring Wadden, 2024)), there is a big difference in findings. The big difference in the study by Lo et al. (2017) is that it was done with laboratory experiments, where the only difference in cliff stability was the vegetation roots. During the elevation measurements used in this study, however, the observed erosion

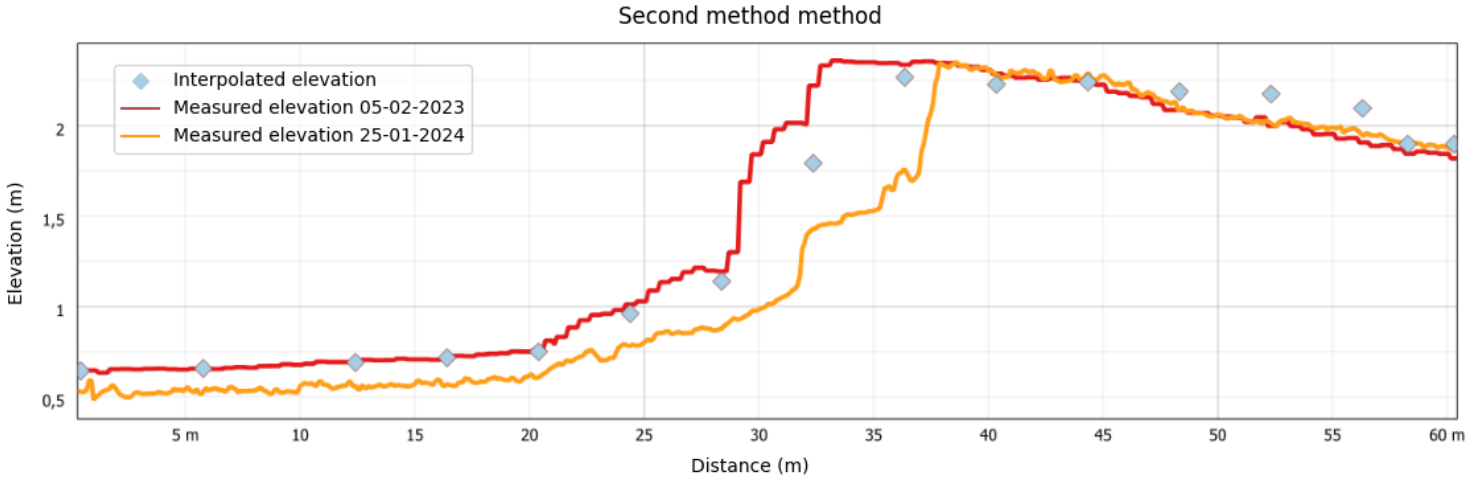

Figure 42 Cross section where elevation is not correctly interpolated into the hydrodynamic grid.

rates are influenced by all processes contributing to the lateral retreat. Vegetation on top of the cliff not only can increase stability, but also be an indicator of the cliffs' stability. Evans et al. (2022) states that vegetation distribution correlates with variability of the geotechnical parameters of the soil.

This paper highlights that spatial vegetation data can provide valuable insight into the spatial variability of the geotechnical parameters of the soil. Vegetation coverage is influenced by edaphic factors, examples of these are bulk density, moisture content, sedimentology, and soil redox potential (Huckle et al., 2000; Cui et al., 2011; De Battisti et al., 2020). Each of these factors influences the stability of the salt marsh edge (Feagin et al., 2009). From this it can be stated that the decrease in erodibility is not caused solely by the vegetation on top of the cliff, but a combination of different factors. The exact effect of only the vegetation on top of the cliff can therefore not be exactly determined in this study but is lower than the found parameterizations. The actual effect of vegetation on the cliff can therefore in reality be closer to the findings of Lo et al. (2017).

5.3.3 Cliff shapes

The results still have some deviations from the observed lateral retreat. This can be due to inaccuracies in hydrodynamic activity, other external forcings, or cliff shapes. As mentioned in the theoretical background, cliff shapes have an impact on the wave thrust against the cliff. Tonelli et al. (2010) conducted research about three different cliffs, vertical, sloped, and terraced cliffs. From this paper, it is evident that each cliff reacts differently to the wave thrust. To see if this would affect the results, the cliff at each cross-section is identified (Table 13). Comparing the identified cliffs with the simulated and observed lateral retreats, it is evident that small trends are visible. About 67% of sloped cliffs would need less erosion, while about 71% of the vertical cliffs need more erosion. All the terraced cliffs need less erosion; however, this sample size is rather small. These results support the findings of Tonelli et al. (2010). Tonelli et al. (2010) state that wave power is less attenuated by vertical cliffs compared to the other two cliff shapes, which causes more erosion with vertical cliffs.

Table 13 Overview of the type of cliffs for each cross-section. The over-and-under estimation can be found under model bias. + indicates that more erosion is needed, while – indicates that less erosion is needed according to observations. Two times a double minus is given which indicate that the erosion needs to be significantly decreased.

Cross-section	Type of cliff	Model bias (+/-)
1	Sloped cliff	-
2	Sloped cliff	+
3	Vertical cliff	+
4	Vertical cliff	+
5	Vertical cliff	+
6	Sloped cliff	+
7	Sloped cliff	--
8	Sloped cliff	-
9	Sloped cliff	
10	Sloped cliff	-
11	Sloped cliff	-
12	Sloped cliff	--
13	Sloped cliff	-
14	Vertical cliff	+
15	Terraced cliff	-
16	Sloped cliff	-
17	Sloped cliff	-
18	Sloped cliff	-
19	Terraced cliff	-
20	Vertical cliff	-
21	Vertical cliff	-
22	Sloped cliff	-
23	Sloped cliff	
24	Sloped cliff	+
25	Vertical cliff	+
26	Sloped cliff	+
27	Sloped cliff	-

6. Conclusion

The goal of this study is to improve the predictive accuracy of salt marsh cliff erosion models by integrating detailed vegetation parameterization and examining the modifications needed for a hydrodynamic model to be applicable to a different geographical location. The central research question addressed is:

How can the integration of a spatially varying erodibility coefficient based on vegetation density improve the predictive accuracy of salt marsh cliff erosion models in terms of erosion rates and spatial patterns?

The main research question is answered by answering the following sub questions.

1. *What specific adjustments in boundary conditions, domain, and physical processes are required to adapt the hydrodynamic and cliff erosion models to the Wierum salt marsh?*

The study shows that adapting salt marsh cliff erosion models to a different geographical location requires changes in both input data and process representation. Different settings demand specific adjustments, such as varying grid resolution and data inputs. For example, the Water Institute model for the MRDP used separate grids for hydrodynamics and morphology, with coarser grid cells to improve performance, emphasizing the need for location-specific data.

In Wierum, the tidal range and wave impact required process adjustments, such as neglecting wave power during full submersion, unlike in micro-tidal Louisiana marshes. These findings highlight the importance of customizing erosion models to the unique physical and environmental conditions of each location.

2. *How can vegetation density effects be parameterized and incorporated to create a spatially varying erodibility coefficient in the erosion model?*

Developing an advanced erosion model with vegetation effects involves integrating vegetation dynamics into the simulations. The model is first calibrated using an erodibility coefficient, adjusted to match observed lateral retreat rates. This process fine-tunes the model to reflect field data without directly using vegetation variables at first, resulting in an optimal uniform erodibility coefficient.

Once established, the model is refined by adding vegetation parameters to stabilize cliffs and bind sediment, impacting erosion rates at marsh edges and slopes. The accuracy of these vegetation effects is measured using statistical metrics (Correlation Coefficient, MAE, RMSE, and R-squared), ensuring the model accurately reflects the influence of vegetation on erosion. For each stem density, the best-fit change in erodibility was determined based on these metrics.

3. *How does the spatial variability of the erodibility coefficient impact the model's predictive accuracy in simulating short term spatial cliff erosion rates?*

Based on the study's findings, vegetation density was observed to reduce the erodibility of salt marsh cliffs by up to 68%. Higher stem densities corresponded with decreased lateral retreat rates, indicating a relationship between vegetation and erosion mitigation. The implementation of the parameterization of the vegetation improved the statistical metrics by 0.08, 0.1 meters, 0.08 meters, and 13% for the correlation coefficient, MAE, RMSE, and R-squared respectively.

However, it's important to note that while vegetation plays a crucial role, it may not be the sole contributor to this found decrease in erodibility. Vegetation can also serve more as an indicator of cliff stability. Thus, while vegetation density directly influences erodibility, its presence and density can also offer valuable insights into the overall stability and resilience of the salt marsh cliff for specific locations that are influenced by other factors (e.g. moisture content and bulk density). These findings reflect the complex interplay of ecological and geomorphological factors influencing erosion dynamics.

This research fills a critical gap in understanding the non-uniform erodibility of salt marsh cliffs. By integrating detailed vegetation effects and emphasizing regional customization, the study shows that vegetation parameterization increases model accuracy. These findings challenge the traditional use of a uniform erodibility coefficient, providing insights for both theoretical research and practical coastal management.

In conclusion, this thesis has successfully addressed the central research question by demonstrating how the predictive modeling of salt marsh cliff erosion can be improved through the integration of detailed vegetation parameterization and regional adjustments. The findings underscore the importance of considering local conditions and the calibration of the erodibility coefficient in erosion models. By advancing the understanding of the complex interactions between vegetation, hydrodynamic forces, and geographical variability, this research contributes to the development of more effective strategies for managing and conserving salt marshes worldwide.

7. Recommendations

Based on the findings and limitations, several recommendations can be made for future research and coastal management. Improving model stability and accuracy is essential, particularly by addressing instabilities caused by the Delft3D-FM modeling software. Resolving these issues would allow for dynamic updating of bathymetry and an accurate representation of morphological development. Ensuring consistency and accuracy in bathymetry measurements through thorough verification using multiple sources is also crucial.

Additionally, the use of even finer grids can be employed to more accurately define the cliffs within the interpolated bathymetry and identify different types of cliff formations. This can introduce the findings of Tonelli et al. (2010) into the model. The discussion reveals that incorporating these findings would most probably increase model accuracy, as clear patterns emerge in the lateral retreat observed at each cross-section based on cliff shape.

Vegetation is not the only factor influencing cliff erodibility. The stability of cliffs is affected by various factors, many of which are related to soil characteristics, such as shear strength. However, data on these soil properties are often limited, with fine-resolution measurements being particularly challenging and frequently unavailable. However, there are still several additions that can be made to improve the model. For instance, it can be researched how much erosion occurs at different heights where waves impact the salt marsh cliff. According to Tonelli et al. (2010), if the wave thrust is beneath the root mat, it significantly increases the amount of wave-induced erosion. Additionally, waves that impact the cliff at lower elevations increase the momentum caused by the eroded sediment under the scarp. Conversely, there is more cohesiveness between the eroding cliff and the salt marsh behind it. Thus, the height of the wave that impacts the cliff can influence the lateral retreat, and incorporating this can increase the accuracy of the model. This would be easy to implement, as the model keeps track of cliff heights. The cliff height should then be linked to a factor that increases or decreases the erodibility coefficient.

Improving field observations beyond numerical models will greatly benefit model accuracy. The inclusion of high-resolution data on soil composition, particularly on factors like soil shear strength, bulk density, and moisture content, could refine the erodibility coefficients used in the model. Continuous measurements of tidal ranges, storm surge effects, and extreme events should also be prioritized to better capture the dynamics that current models may not fully integrate, instead of using a simulated data set like in this study. Improved observation techniques, such as bathymetric surveys and real-time monitoring of hydrodynamic conditions, would support a more reliable and complete dataset, which will improve future model performance.

To better refine the parameterization of vegetation effects, detailed seasonal vegetation data is essential. For example, measuring root structure, root density, and tensile strength across different vegetation species will allow for a more accurate incorporation of vegetation’s stabilizing effects on cliffs. Incorporating techniques like NDVI more frequently to track seasonal variations in vegetation cover could be a valuable tool for more accurately reflecting vegetation’s temporal changes and its influence on erosion.

For further research on this specific topic, multiple case studies can be conducted. The findings from these case studies can further support the findings of this study on the extent of vegetation's effect on the erodibility of cliffs. By incorporating different vegetation types, densities, soil characteristics, and

hydrodynamic activity, a broader perspective can be achieved regarding the effect of vegetation. These case studies may also extend the timeframe of the simulations to capture longer periods, which would increase the certainty of the erodibility coefficient. As in this research, the erodibility coefficient is rather high compared to similar studies.

Further recommendations based solely on the findings of this research include validating the model over extended periods to assess the vegetation parameterization's accuracy across different temporal scales, particularly during extreme weather events. Additionally, obtaining high-resolution soil data and incorporating these characteristics into the model could increase the accuracy in predictions of erosion further. Exploring how geographical location changes influence the parameterization of hydrodynamic and geomorphological processes would also enhance the model's adaptability. Conducting systematic studies on the impact of wave characteristics at various heights on cliff erosion could reveal new insights into wave-cliff interactions.

Based on the findings of this study, vegetation significantly influences the erodibility of salt marsh cliffs. It is therefore recommended that future models include a detailed parameterization of vegetation effects. This involves considering both above-ground and below-ground vegetation dynamics, particularly stem density and root structure. For instance, in Wierum, the halophytic species *Puccinellia maritima* proved to reduce cliff erodibility by up to 68% depending on stem density. In different environments, other species may have varying impacts, and thus, future models should tailor vegetation parameters to local conditions, including soil composition, hydrodynamic forces, and vegetation characteristics.

The inclusion of site-specific data, such as local vegetation species, soil types, and hydrodynamic conditions, can substantially enhance model accuracy. Further research should explore how seasonal variations in vegetation cover and differing vegetation species affect erosion rates across salt marshes in various regions. Additionally, longer simulation periods would help validate the observed effects of vegetation on erosion control.

This study used a 2DH model to simulate the erosion of salt marsh cliffs in Wierum. However, considering the complexity of the processes involved, exploring 3D or 2DV models in future studies could further improve predictive accuracy. A 3D model would allow for a more detailed simulation of vertical hydrodynamic forces, such as stratification and undercutting, which can influence erosion, particularly in areas with high variability in wave action or sediment composition.

A 2DV model, on the other hand, maybe more appropriate in scenarios where vertical gradients in flow and sediment transport dominate. This is especially relevant in environments where cliff erosion is significant and where horizontal processes alone may not fully capture the dynamics of erosion. Testing these models in future studies could reveal whether they better represent the complex interactions between vegetation, waves, and sediment transport.

These recommendations aim to enhance the accuracy and reliability of erosion models, supporting better coastal management practices and contributing to the resilience of coastal ecosystems. By incorporating these insights and addressing identified limitations, future studies can build on the findings of this research to develop more effective and robust erosion control strategies.

Bibliography

AHN. (2023). *Actueel Hoostebestand Nederland*.

Anderson, M. E., & Smith, J. M. (2014). Wave attenuation by flexible, idealized salt marsh vegetation. *Coastal Engineering*, *83*, 82–92. https://doi.org/10.1016/j.coastaleng.2013.10.004

Asuero, A. G., Sayago, A., & González, A. G. (2006). The correlation coefficient: An overview. In *Critical Reviews in Analytical Chemistry* (Vol. 36, Issue 1, pp. 41–59). https://doi.org/10.1080/10408340500526766

Balke, T., Herman, P. M. J., & Bouma, T. J. (2014). Critical transitions in disturbance-driven ecosystems: Identifying windows of opportunity for recovery. *Journal of Ecology*, *102*(3), 700–708. https://doi.org/10.1111/1365-2745.12241

Baptist, M. J. (2005). *Modelling floodplain biogeomorphology*.

Basismonitoring Wadden. (2024). *Waddenviewer*. https://viewer.openearth.nl/wadden-viewer/

Belliard, J. P., Di Marco, N., Carniello, L., & Toffolon, M. (2016). Sediment and vegetation spatial dynamics facing sea-level rise in microtidal salt marshes: Insights from an ecogeomorphic model. *Advances in Water Resources*, *93*, 249–264. https://doi.org/10.1016/j.advwatres.2015.11.020

Bendoni, M., Francalanci, S., Cappietti, L., & Solari, L. (2014). On salt marshes retreat: Experiments and modeling toppling failures induced by wind waves. *Journal of Geophysical Research: Earth Surface*, *119*(3), 603–620. https://doi.org/10.1002/2013JF002967

Boorman, L. A. (2018). The role of freshwater flows on salt marsh growth and development. In *Coastal Wetlands: An Integrated Ecosystem Approach* (pp. 597–618). Elsevier. https://doi.org/10.1016/B978-0-444-63893-9.00017-4

Cahoon, D. R. (2006). *A Review of Major Storm Impacts on Coastal Wetland Elevations*.

Cameron, A. C., & Windmeijer, F. A. G. (1997). An R-squared measure of goodness of fit for some common nonlinear regression models. *Journal of Econometrics*, *77*(2), 329–342. https://doi.org/10.1016/S0304-4076(96)01818-0

Christiansen, T., Wiberg, P. L., & Milligan, T. G. (2000). Flow and sediment transport on a tidal salt marsh surface. *Estuarine, Coastal and Shelf Science*, *50*(3), 315–331. https://doi.org/10.1006/ecss.2000.0548

Coco, G., Zhou, Z., van Maanen, B., Olabarrieta, M., Tinoco, R., & Townend, I. (2013). Morphodynamics of tidal networks: Advances and challenges. In *Marine Geology* (Vol. 346, pp. 1–16). https://doi.org/10.1016/j.margeo.2013.08.005

Coldren, G. A., Barreto, C. R., Wykoff, D. D., Morrissey, E. M., Langley, J. A., Feller, I. C., & Chapman, S. K. (2016). Chronic warming stimulates growth of marsh grasses more than mangroves in a coastal wetland ecotone. *Ecology*, *97*(11), 3167–3175. https://doi.org/10.1002/ecy.1539

Cui, B. S., He, Q., & An, Y. (2011). Community Structure and Abiotic Determinants of Salt Marsh Plant Zonation Vary Across Topographic Gradients. *Estuaries and Coasts*, *34*(3), 459–469. https://doi.org/10.1007/s12237-010-9364-4

Darby, F. A., & Turner, R. E. (2008). Below- and aboveground biomass of Spartina alterniflora: Response to nutrient addition in a Louisiana salt marsh. *Estuaries and Coasts*, *31*(2), 326–334. https://doi.org/10.1007/s12237-008-9037-8

De Battisti, D., Fowler, M. S., Jenkins, S. R., Skov, M. W., Bouma, T. J., Neyland, P. J., & Griffin, J. N. (2020). Multiple trait dimensions mediate stress gradient effects on plant biomass allocation, with implications for coastal ecosystem services. *Journal of Ecology*, *108*(4), 1227–1240. https://doi.org/10.1111/1365-2745.13393

Deltares. (2015). *Delft3D 3D/2D modelling suite for integral water solutions User Manual*.

Deltares. (2019). *Delft3D fM Suite Simulation software for safe, sustainable and future deltas User Manual D-Flow Flexible Mesh*.

Deltares. (2022). *D-Flow FM 2D Noordzee*.

Deltares. (2023a). *SWAN-Kuststrook*. https://iplo.nl/thema/water/applicaties-

Deltares. (2024). *User Manual D-Waves*.

Dorreboom, L. (2022). *De kwelder bij Wierum* [Video recording].

Du, H., Liu, L., Su, L., Zeng, F., Wang, K., Peng, W., Zhang, H., & Song, T. (2019). Seasonal changes and vertical distribution of fine root biomass during vegetation restoration in a Karst area, southwest China. *Frontiers in Plant Science*, *9*. https://doi.org/10.3389/fpls.2018.02001

Dzimballa, S. (2023). *Biogeomorphological evolution of salt marshes under natural conditions and the influence of artificial structures* [Proposal]. University of Twente.

Esselink, P. , van D. W. , B. J. , C. J. , F. E. , F. J. , G. M. , de G. A. , H. N. , H. U. , J. K. , K. P. , P. J. , S. M. , & G. de A. (2017). *Salt marshes*. Wadden Sea World Heritage.

Evans, B. R., Brooks, H., Chirol, C., Kirkham, M. K., Möller, I., Royse, K., Spencer, K., & Spencer, T. (2022). Vegetation interactions with geotechnical properties and erodibility of salt marsh sediments. *Estuarine, Coastal and Shelf Science*, *265*. https://doi.org/10.1016/j.ecss.2021.107713

Fagherazzi, S., Carniello, L., D'alpaos, L., & Defina, A. (2006). Critical bifurcation of shallow microtidal landforms in tidal flats and salt marshes. In *PNAS* (Vol. 103). www.pnas.orgcgidoi10.1073pnas.0508379103

Fagherazzi, S., FitzGerald, D. M., Fulweiler, R. W., Hughes, Z., Wiberg, P. L., McGlathery, K. J., Morris, J. T., Tolhurst, T. J., Deegan, L. A., & Johnson, D. S. (2013). Ecogeomorphology of Tidal Flats. In *Treatise on Geomorphology: Volume 1-14* (Vols. 1–14, pp. 201–220). Elsevier. https://doi.org/10.1016/B978-0-12-374739-6.00403-6

Fagherazzi, S., FitzGerald, D. M., Fulweiler, R. W., Hughes, Z., Wiberg, P. L., McGlathery, K. J., Morris, J. T., Tolhurst, T. J., Deegan, L. A., Johnson, D. S., Lesser, J. S., & Nelson, J. A. (2013). Ecogeomorphology of

Salt Marshes. *Treatise on Geomorphology*, 445–464. https://doi.org/10.1016/B978-0-12-818234-5.00194-2

Fagherazzi, S., Mariotti, G., & Wiberg, P. L. (2013). Marsh collapse does not require sea level rise. *Oceanography*, *26*(3), 70–77. https://doi.org/10.5670/oceanog.2013.47

Feagin, R. A., Lozada-Bernard, S. M., Ravens, T. M., Möller, I., Yeager, K. M., & Baird, A. H. (2009). Does vegetation prevent wave erosion of salt marsh edges? *Proceedings of the National Academy of Sciences*, *106*(25), 10109–10113. https://doi.org/10.1073/pnas.0901297106

Finotello, A., Marani, M., Carniello, L., Pivato, M., Roner, M., Tommasini, L., & D'alpaos, A. (2020a). Control of wind-wave power on morphological shape of salt marsh margins. *Water Science and Engineering*, *13*(1), 45–56. https://doi.org/10.1016/j.wse.2020.03.006

Finotello, A., Marani, M., Carniello, L., Pivato, M., Roner, M., Tommasini, L., & D'alpaos, A. (2020b). Control of wind-wave power on morphological shape of salt marsh margins. *Water Science and Engineering*, *13*(1), 45–56. https://doi.org/10.1016/j.wse.2020.03.006

FitzGerald, D. M., & Hughes, Z. J. (2021). State of Salt Marshes. In *Salt Marshes* (pp. 1–6). Cambridge University Press. https://doi.org/10.1017/9781316888933.001

French, J. (2006). Tidal marsh sedimentation and resilience to environmental change: Exploratory modelling of tidal, sea-level and sediment supply forcing in predominantly allochthonous systems. *Marine Geology*, *235*(1-4 SPEC. ISS.), 119–136. https://doi.org/10.1016/j.margeo.2006.10.009

French, J. (2018). Tidal salt marshes: Sedimentology and geomorphology. In *Coastal Wetlands: An Integrated Ecosystem Approach* (pp. 479–517). Elsevier. https://doi.org/10.1016/B978-0-444-63893-9.00014-9

Friedrichs C. T., & Perry J. E. (2001). Tidal Salt Marsh Morphodynamics: A Synthesis. *Journal of Coastal Research*, 1–32.

Ganju, N. K., Nidzieko, N. J., & Kirwan, M. L. (2013). Inferring tidal wetland stability from channel sediment fluxes: Observations and a conceptual model. *Journal of Geophysical Research: Earth Surface*, *118*(4), 2045–2058. https://doi.org/10.1002/jgrf.20143

Gedan, K. B., Kirwan, M. L., Wolanski, E., Barbier, E. B., & Silliman, B. R. (2011). The present and future role of coastal wetland vegetation in protecting shorelines: Answering recent challenges to the paradigm. In *Climatic Change* (Vol. 106, Issue 1, pp. 7–29). https://doi.org/10.1007/s10584-010-0003-7

Gedan, K. B., Silliman, B. R., & Bertness, M. D. (2009). Centuries of human-driven change in salt marsh ecosystems. In *Annual Review of Marine Science* (Vol. 1, pp. 117–141). https://doi.org/10.1146/annurev.marine.010908.163930

Georgiou, I., Miner, M., Hemmerling, S., Bregman, M., Di Leonardo, D., Esposito, C., Jung, H., & McMann, B. (2022). *A COMMUNITY-INFORMED TRANSDISCIPLINARY APPROACH TO MAXIMIZING BENEFITS OF DREDGED SEDIMENT FOR WETLAND RESTORATION PLANNING AT PORT FOURCHON, LOUISIANA*. www.thewaterinstitute.org.

Gorakhki, M. H., & Bareither, C. A. (2015). Salinity effects on sedimentation behavior of kaolin, bentonite, and soda ash mine tailings. *Applied Clay Science*, *114*, 593–602. https://doi.org/10.1016/j.clay.2015.07.018

Haarbrink, R. (2023). *Sneak Preview AHN5*.

Houttuijn Bloemendaal, L. J., FitzGerald, D. M., Hughes, Z. J., Novak, A. B., & Georgiou, I. Y. (2023). Reevaluating the wave power-salt marsh retreat relationship. *Scientific Reports*, *13*(1). https://doi.org/10.1038/s41598-023-30042-y

Huckle, J. M., Potter, J. A., & Marrs, R. H. (2000). Influence of environmental factors on the growth and interactions between salt marsh plants: Effects of salinity, sediment and waterlogging. *Journal of Ecology*, *88*(3), 492–505. https://doi.org/10.1046/j.1365-2745.2000.00464.x

Hussey, A., & Long, S. P. (1982). Seasonal Changes in Weight of Above-and Below-Ground Vegetation and Dead Plant Material in a Salt Marsh at Colne Point. In *Source: Journal of Ecology* (Vol. 70, Issue 3).

Langlois, E., Bonis, A., & Bouzillé, J. B. (2001). The response of Puccinellia maritima to burial: A key to understanding its role in salt-marsh dynamics? . *Journal of Vegetation Science*, *12*(2), 289–297. https://doi.org/10.2307/3236613

Leonardi, N., Carnacina, I., Donatelli, C., Ganju, N. K., Plater, A. J., Schuerch, M., & Temmerman, S. (2018). Dynamic interactions between coastal storms and salt marshes: A review. In *Geomorphology* (Vol. 301, pp. 92–107). Elsevier B.V. https://doi.org/10.1016/j.geomorph.2017.11.001

Leonardi, N., & Fagherazzi, S. (2014). How waves shape salt marshes. *Geology*, *42*(10), 887–890. https://doi.org/10.1130/G35751.1

Leonardi, N., & Fagherazzi, S. (2015). Effect of local variability in erosional resistance on large-scale morphodynamic response of salt marshes to wind waves and extreme events. *Geophysical Research Letters*, *42*(14), 5872–5879. https://doi.org/10.1002/2015GL064730

Leonardi, N., Ganju, N. K., & Fagherazzi, S. (2016). A linear relationship between wave power and erosion determines salt-marsh resilience to violent storms and hurricanes. *Proceedings of the National Academy of Sciences of the United States of America*, *113*(1), 64–68. https://doi.org/10.1073/pnas.1510095112

Lo, V. B., Bouma, T. J., van Belzen, J., Van Colen, C., & Airoldi, L. (2017). Interactive effects of vegetation and sediment properties on erosion of salt marshes in the Northern Adriatic Sea. *Marine Environmental Research*, *131*, 32–42. https://doi.org/10.1016/j.marenvres.2017.09.006

Marani, M., D'Alpaos, A., Lanzoni, S., & Santalucia, M. (2011). Understanding and predicting wave erosion of marsh edges. *Geophysical Research Letters*, *38*(21). https://doi.org/10.1029/2011GL048995

Marin-Diaz, B., van der Wal, D., Kaptein, L., Martinez-Garcia, P., Lashley, C. H., de Jong, K., Nieuwenhuis, J. W., Govers, L. L., Olff, H., & Bouma, T. J. (2023). Using salt marshes for coastal protection: Effective but hard to get where needed most. *Journal of Applied Ecology*, *60*(7), 1286–1301. https://doi.org/10.1111/1365-2664.14413

Marion, C., Anthony, E. J., & Trentesaux, A. (2009). Short-term (≤2 yrs) estuarine mudflat and saltmarsh sedimentation: High-resolution data from ultrasonic altimetery, rod surface-elevation table, and filter traps. *Estuarine, Coastal and Shelf Science*, *83*(4), 475–484. https://doi.org/10.1016/j.ecss.2009.03.039

Mariotti, G., & Canestrelli, A. (2017). Long-term morphodynamics of muddy backbarrier basins: Fill in or empty out? *Water Resources Research*, *53*(8), 7029–7054. https://doi.org/10.1002/2017WR020461

Micheli, E. R., & Kirchner, J. W. (2002). Effects of wet meadow riparian vegetation on streambank erosion. 2. Measurements of vegetated bank strength and consequences for failure mechanics. *Earth Surface Processes and Landforms*, *27*(7), 687–697. https://doi.org/10.1002/esp.340

Möller, I., Kudella, M., Rupprecht, F., Spencer, T., Paul, M., Van Wesenbeeck, B. K., Wolters, G., Jensen, K., Bouma, T. J., Miranda-Lange, M., & Schimmels, S. (2014). Wave attenuation over coastal salt marshes under storm surge conditions. *Nature Geoscience*, *7*(10), 727–731. https://doi.org/10.1038/NGEO2251

Mudd, S. M., Fagherazzi, S., Morris, J. T., & Furbish, D. J. (2013). *Flow, Sedimentation, and Biomass Production on a Vegetated Salt Marsh in South Carolina: Toward a Predictive Model of Marsh Morphologic and Ecologic Evolution* (pp. 165–188). https://doi.org/10.1029/ce059p0165

Mullarney, J. C., & Henderson, S. M. (2010). Wave-forced motion of submerged single-stem vegetation. *Journal of Geophysical Research: Oceans*, *115*(12). https://doi.org/10.1029/2010JC006448

Néelz, S., & Pender, G. (2007). Sub-grid scale parameterisation of 2D hydrodynamic models of inundation in the urban area. *Acta Geophysica*, *55*(1), 65–72. https://doi.org/10.2478/s11600-006-0039-2

Neumeier, U., & Amos, C. L. (2006). The influence of vegetation on turbulence and flow velocities in European salt-marshes. *Sedimentology*, *53*(2), 259–277. https://doi.org/10.1111/j.1365-3091.2006.00772.x

Palmer, M. R., Nepf, H. M., Pettersson, T. J. R., & Ackerman, J. D. (2004). Observations of particle capture on a cylindrical collector: Implications for particle accumulation and removal in aquatic systems. *Limnology and Oceanography*, *49*(1), 76–85. https://doi.org/10.4319/lo.2004.49.1.0076

Pearey, R. W., & Ustin, S. L. (1983). *Oecologia (Berlin) (1984) 62:68-73 Effects of salinity on growth and photosynthesis of three California tidal marsh species*.

Peralta, G., Van Duren, L. A., Morris, E. P., & Bouma, T. J. (2008). Consequences of shoot density and stiffness for ecosystem engineering by benthic macrophytes in flow dominated areas: A hydrodynamic flume study. *Marine Ecology Progress Series*, *368*, 103–115. https://doi.org/10.3354/meps07574

Priestas, A. M., Mariotti, G., Leonardi, N., & Fagherazzi, S. (2015). Coupled wave energy and erosion dynamics along a salt marsh boundary, hog island bay, Virginia, USA. *Journal of Marine Science and Engineering*, *3*(3), 1041–1065. https://doi.org/10.3390/jmse3031041

Rijkswaterstaat. (2017). *Morfologie*.

Rijkswaterstaat. (2024). *Rijkswaterstaat WaterInfo*.

Rosencranz, J. A., Ganju, N. K., Ambrose, R. F., Brosnahan, S. M., Dickhudt, P. J., Guntenspergen, G. R., MacDonald, G. M., Takekawa, J. Y., & Thorne, K. M. (2016). Balanced Sediment Fluxes in Southern California's Mediterranean-Climate Zone Salt Marshes. *Estuaries and Coasts*, *39*(4), 1035–1049. https://doi.org/10.1007/s12237-015-0056-y

Siemes, R. W. A., Borsje, B. W., Daggenvoorde, R. J., & Hulscher, S. J. M. H. (2020). Artificial structures steer morphological development of salt marshes: A model study. *Journal of Marine Science and Engineering*, *8*(5). https://doi.org/10.3390/JMSE8050326

Temmerman, S., Bouma, T. J., Van de Koppel, J., Van der Wal, D., De Vries, M. B., & Herman, P. M. J. (2007). Vegetation causes channel erosion in a tidal landscape. *Geology*, *35*(7), 631–634. https://doi.org/10.1130/G23502A.1

Temmerman, S., Meire, P., Bouma, T. J., Herman, P. M. J., Ysebaert, T., & De Vriend, H. J. (2013). Ecosystem-based coastal defence in the face of global change. In *Nature* (Vol. 504, Issue 7478, pp. 79–83). https://doi.org/10.1038/nature12859

Tonelli, M., Fagherazzi, S., & Petti, M. (2010). Modeling wave impact on salt marsh boundaries. *Journal of Geophysical Research: Oceans*, *115*(9). https://doi.org/10.1029/2009JC006026

Valentine, K., & Mariotti, G. (2019). Wind-driven water level fluctuations drive marsh edge erosion variability in microtidal coastal bays. *Continental Shelf Research*, *176*, 76–89. https://doi.org/10.1016/j.csr.2019.03.002

Van der Wal, D., Wielemaker-Van den Dool, A., & Herman, P. M. J. (2008). Spatial patterns, rates and mechanisms of saltmarsh cycles (Westerschelde, The Netherlands). *Estuarine, Coastal and Shelf Science*, *76*(2), 357–368. https://doi.org/10.1016/j.ecss.2007.07.017

Van Eerdt, M. M. (1985). Salt marsh cliff stability in the oosterschelde. *Earth Surface Processes and Landforms*, *10*(2), 95–106. https://doi.org/10.1002/esp.3290100203

Vernberg, F. J. (1993). Salt-marsh processes: A Review. In *Environmental Toxicology and Chemistry* (Vol. 12, Issue 12, pp. 2167–2195). https://doi.org/10.1002/etc.5620121203

Vuik, V., Borsje, B. W., Willemsen, P. W. J. M., & Jonkman, S. N. (2019). Salt marshes for flood risk reduction: Quantifying long-term effectiveness and life-cycle costs. *Ocean and Coastal Management*, *171*, 96–110. https://doi.org/10.1016/j.ocecoaman.2019.01.010

Wamsley, T. V., Cialone, M. A., Smith, J. M., Atkinson, J. H., & Rosati, J. D. (2010). The potential of wetlands in reducing storm surge. *Ocean Engineering*, *37*(1), 59–68. https://doi.org/10.1016/j.oceaneng.2009.07.018

Wanner, A., Suchrow, S., Kiehl, K., Meyer, W., Pohlmann, N., Stock, M., & Jensen, K. (2014). Scale matters: Impact of management regime on plant species richness and vegetation type diversity in Wadden Sea salt marshes. *Agriculture, Ecosystems and Environment*, *182*, 69–79. https://doi.org/10.1016/j.agee.2013.08.014

Wetterskip Fryslân. (2019). *DINOloket*. https://www.dinoloket.nl/ondergrondgegevens

Willemsen, P. W. J. M., Smits, B. P., Borsje, B. W., Herman, P. M. J., Dijkstra, J. T., Bouma, T. J., & Hulscher, S. J. M. H. (2022). Modeling Decadal Salt Marsh Development: Variability of the Salt Marsh Edge Under Influence of Waves and Sediment Availability. *Water Resources Research*, *58*(1). https://doi.org/10.1029/2020WR028962

Willmott, C. J., & Matsuura, K. (2005). *Advantages of the mean absolute error (MAE) over the root mean quare error (RMSE) in assessing average model performance*. www.int-res.com

Windham, L. (2001). COMPARISON OF BIOMASS PRODUCTION AND DECOMPOSITION BETWEEN PHRAGMITES AUSTRALIS (COMMON REED) AND SPARTINA PATENS (SALT HAY GRASS) IN BRACKISH TIDAL MARSHES OF NEW JERSEY, USA. *The Society of Wetland Scientists*. https://doi.org/10.1672/0277

Appendix A

The correlation coefficient is a statistical metric that quantifies the strength and direction of the linear relationship between two variables. This coefficient is a dimensionless value ranging from -1 to 1. Values close to 1, indicate a strong positive correlation between the observed ($Observed_i$) and predicted ($Predicted_i$) data sets (Equation 7). A correlation close to -1, indicates a strong negative correlation. Values close to zero indicate no correlation. An increase in this coefficient indicates that the model's predictions are more closely aligned with the observed data, reducing the likelihood of large deviations. This means the model is better at predicting the general trend of erosion (Asuero et al., 2006).

$$r = \frac{n(\sum_{i=1}^{n} Observed_i * Predicted_i) - (\sum_{i=1}^{n} Observed_i) * (\sum_{i=1}^{n} Predicted_i)}{\sqrt{(n\sum_{i=1}^{n} Observed_i^2 - \left(\sum_{i=1}^{n} Observed_i\right)^2)(n\sum_{i=1}^{n} Predicted_i^2 - \left(\sum_{i=1}^{n} Predicted_i\right)^2}} \quad [7]$$

MAE provides a straightforward measure of the average absolute differences between the observed values and the corresponding model predictions. This metric is determined by calculating the average of the absolute differences between the observed and predicted values for each data point (Equation 8). A lower MAE suggests a smaller average magnitude of errors, indicating a better overall fit of the model to the observed data (Willmott & Matsuura, 2005).

$$MAE = \frac{1}{n}\sum_{i=1}^{n} |Observed_i - Predicted_i| \quad [8]$$

Similar to MAE, RMSE quantifies the average error between observed and predicted values. However, RMSE places more emphasis on larger errors as it involves taking the square root of the average squared differences between the observed and predicted values (Equation 9). This metric is particularly useful for penalizing significant discrepancies, providing a balanced assessment of model performance. A decrease in RMSE indicates that the variability in the prediction errors has decreased, leading to more consistent and reliable model predictions (Willmott & Matsuura, 2005).

$$RMSE = \sqrt{\frac{1}{n}\sum_{i=1}^{n} (Observed_i - Predicted_i)^2} \quad [9]$$

R-squared evaluates the proportion of variance in the observed data that can be explained by the model. Ranging from 0 to 1, with higher values indicating a better fit, R-squared is a crucial measure of the model's explanatory power. The formula (Equation 10) compares the sum of squared differences between observed and predicted values to the sum of squared differences between observed values and their mean ($\overline{Observed}$), providing an overall assessment of how effectively the model accounts for the variability within the data. An increase in R^2 signifies that the model is better at capturing the underlying patterns in the data, enhancing its explanatory power and ability to explain the variance in the observed data (Cameron & Windmeijer, 1997).

$$R^2 = 1 - \frac{\sum_{i=1}^{n} (Observed_i - Predicted_i)^2}{\sum_{i=1}^{n} \left(Observed_i - \overline{Observed}\right)^2} \quad [10]$$

Appendix B

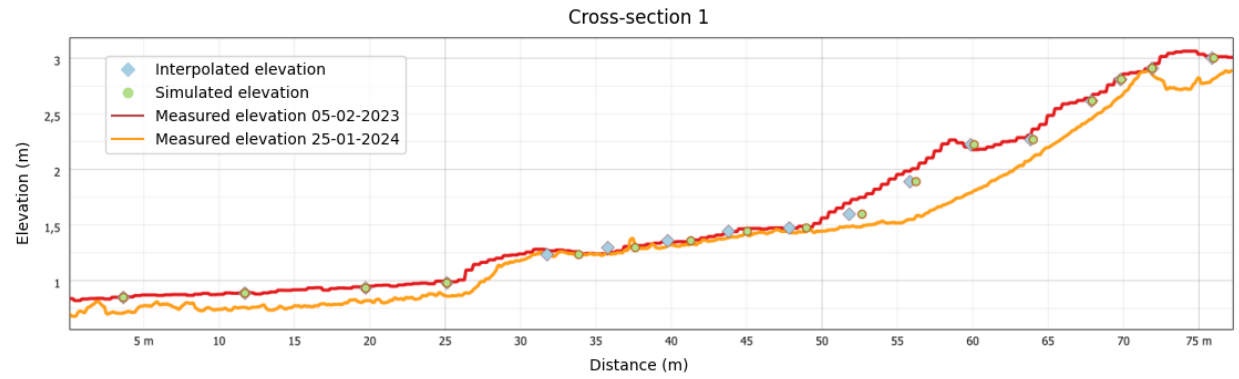
Cross-section 1
Interpolated elevation
Simulated elevation
Measured elevation 05-02-2023
Measured elevation 25-01-2024
Elevation (m)
Distance (m)

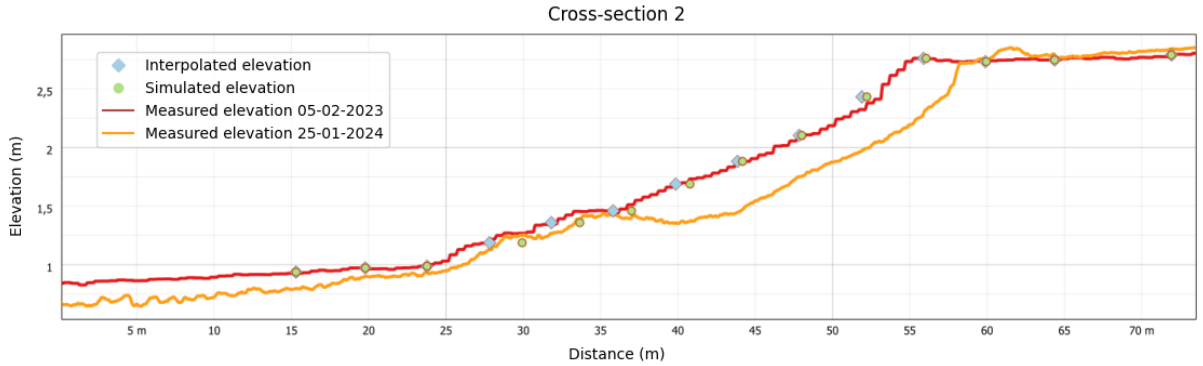
Cross-section 2
Interpolated elevation
Simulated elevation
Measured elevation 05-02-2023
Measured elevation 25-01-2024
Elevation (m)
Distance (m)

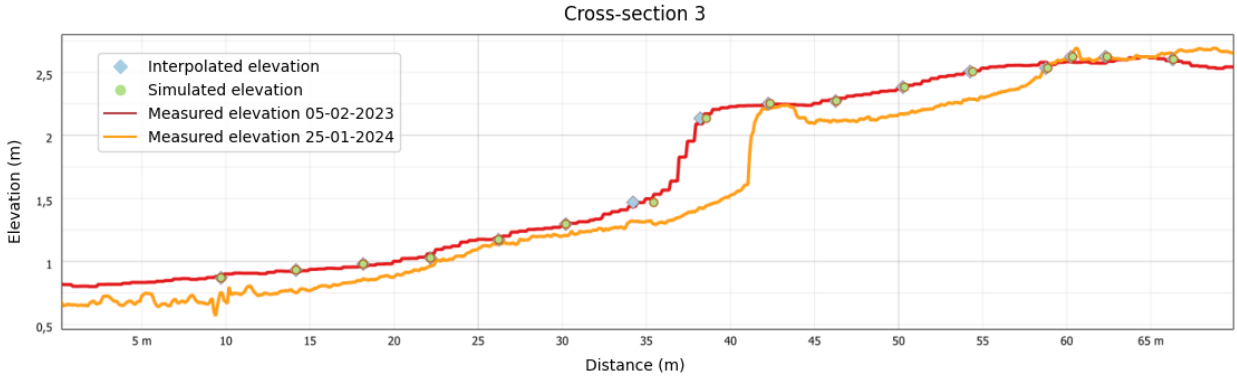
Cross-section 3
Interpolated elevation
Simulated elevation
Measured elevation 05-02-2023
Measured elevation 25-01-2024
Elevation (m)
Distance (m)

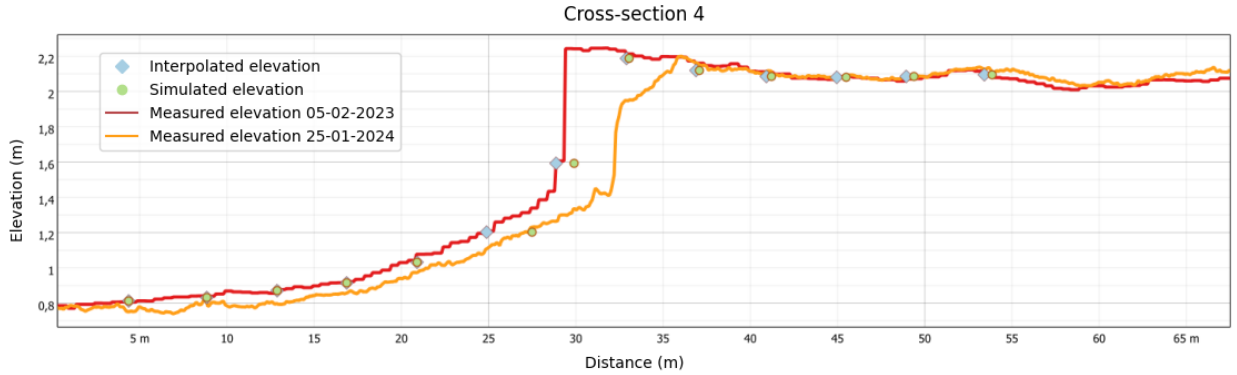
Cross-section 4
Interpolated elevation
Simulated elevation
Measured elevation 05-02-2023
Measured elevation 25-01-2024
Elevation (m)
Distance (m)

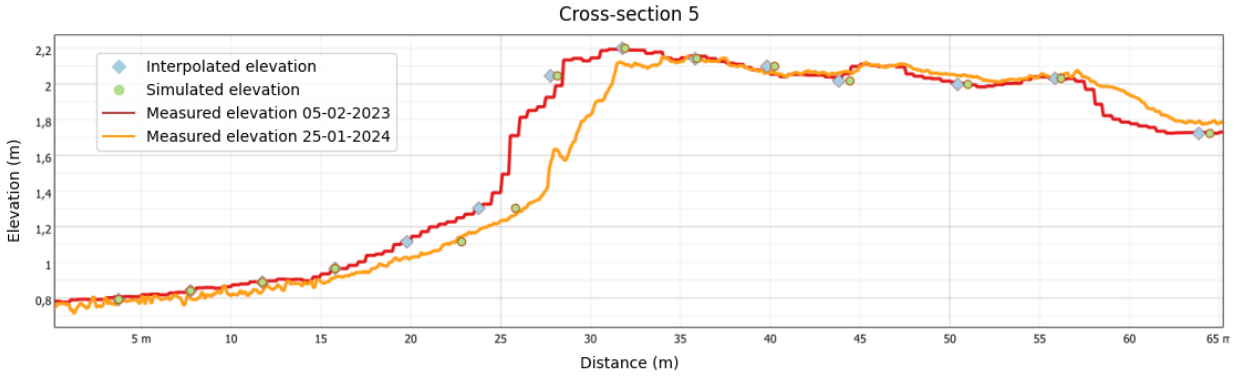
Cross-section 5
Interpolated elevation
Simulated elevation
Measured elevation 05-02-2023
Measured elevation 25-01-2024
Elevation (m)
Distance (m)

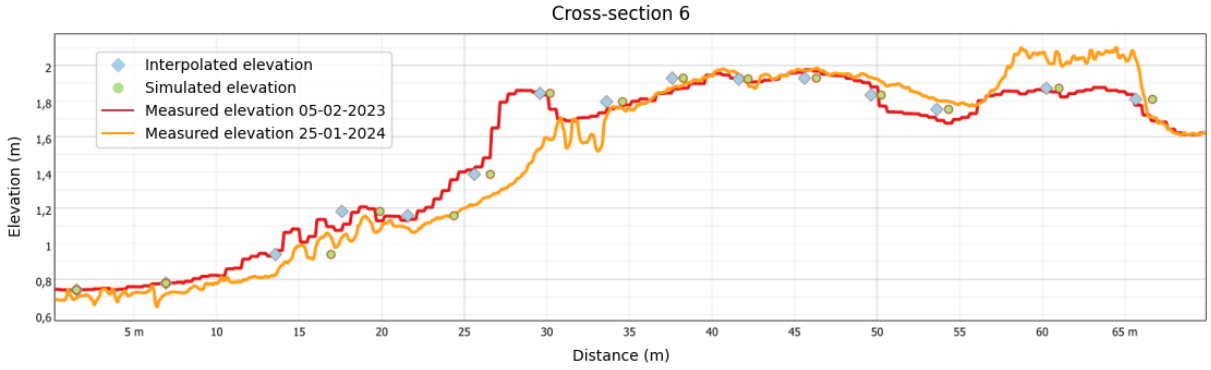
Cross-section 6
Interpolated elevation
Simulated elevation
Measured elevation 05-02-2023
Measured elevation 25-01-2024
Elevation (m)
Distance (m)

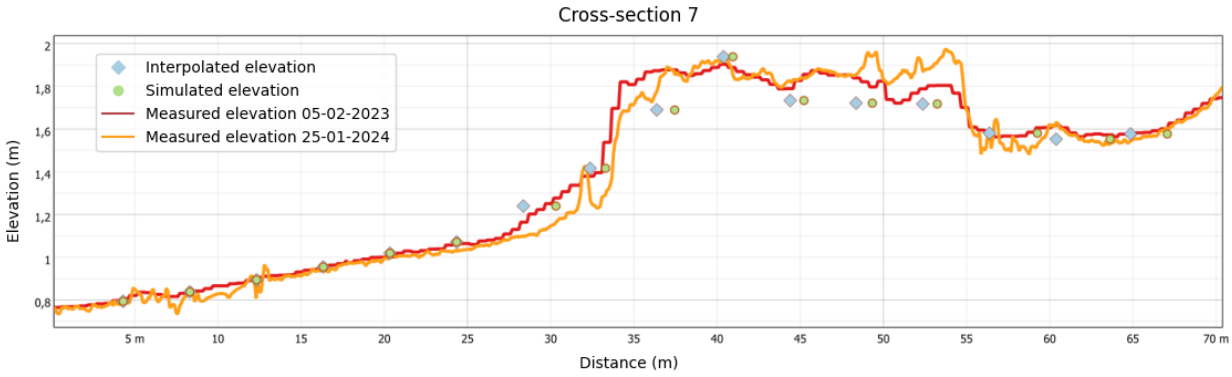
Cross-section 7
Interpolated elevation
Simulated elevation
Measured elevation 05-02-2023
Measured elevation 25-01-2024
Elevation (m)
Distance (m)

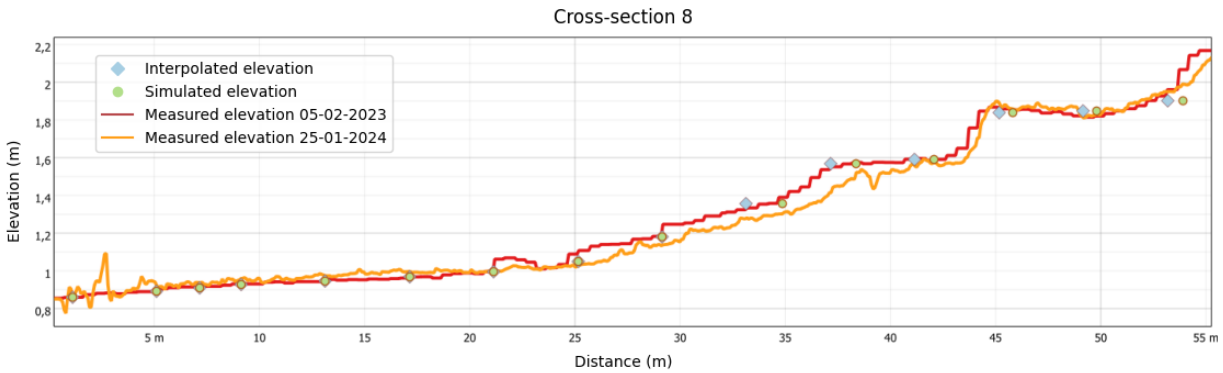
Cross-section 8
Interpolated elevation
Simulated elevation
Measured elevation 05-02-2023
Measured elevation 25-01-2024
Elevation (m)
Distance (m)

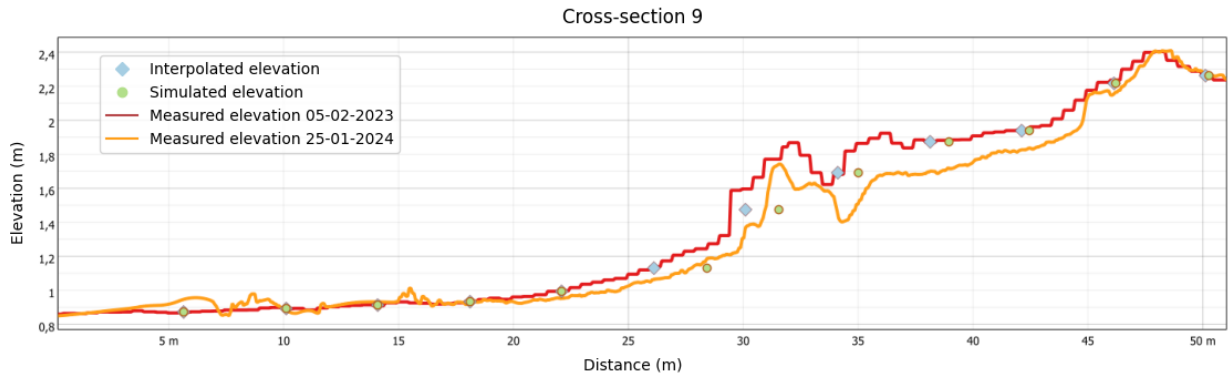
Cross-section 9
Interpolated elevation
Simulated elevation
Measured elevation 05-02-2023
Measured elevation 25-01-2024
Elevation (m)
Distance (m)

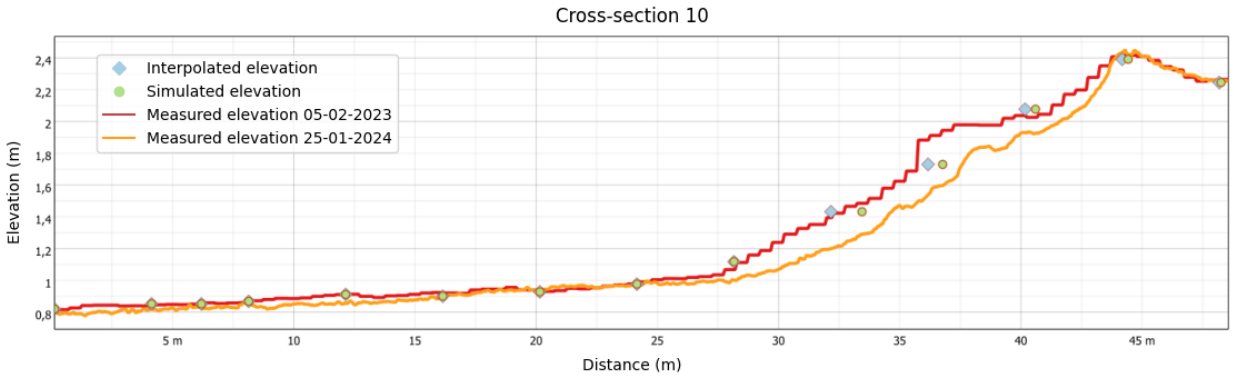
Cross-section 10
Interpolated elevation
Simulated elevation
Measured elevation 05-02-2023
Measured elevation 25-01-2024
Elevation (m)
Distance (m)

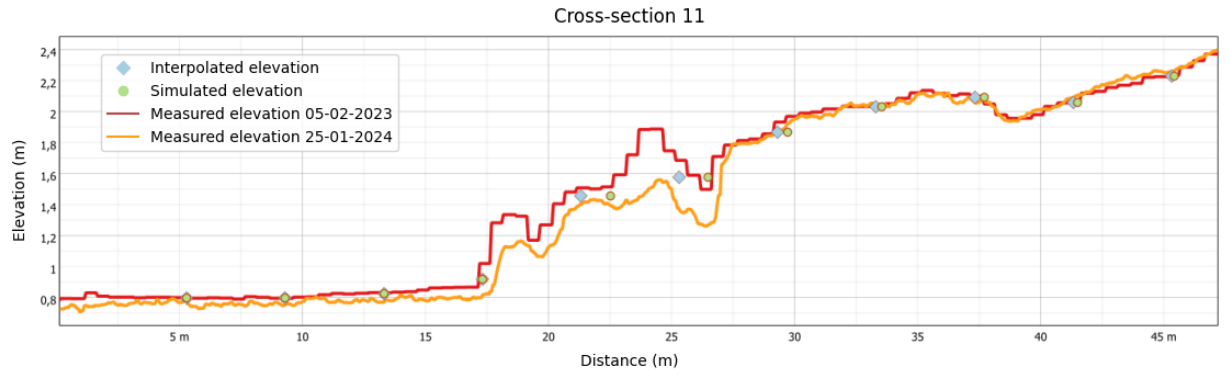
Cross-section 11
Interpolated elevation
Simulated elevation
Measured elevation 05-02-2023
Measured elevation 25-01-2024
Elevation (m)
Distance (m)

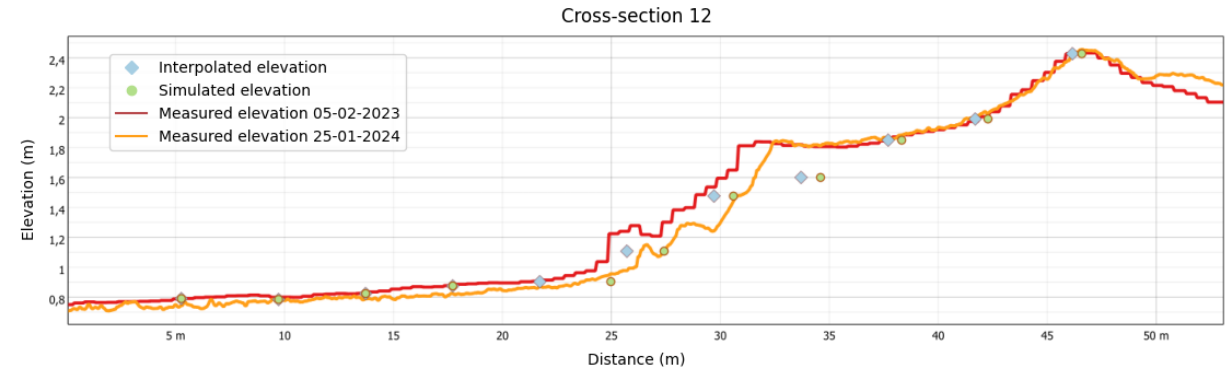
Cross-section 12
Interpolated elevation
Simulated elevation
Measured elevation 05-02-2023
Measured elevation 25-01-2024
Elevation (m)
Distance (m)

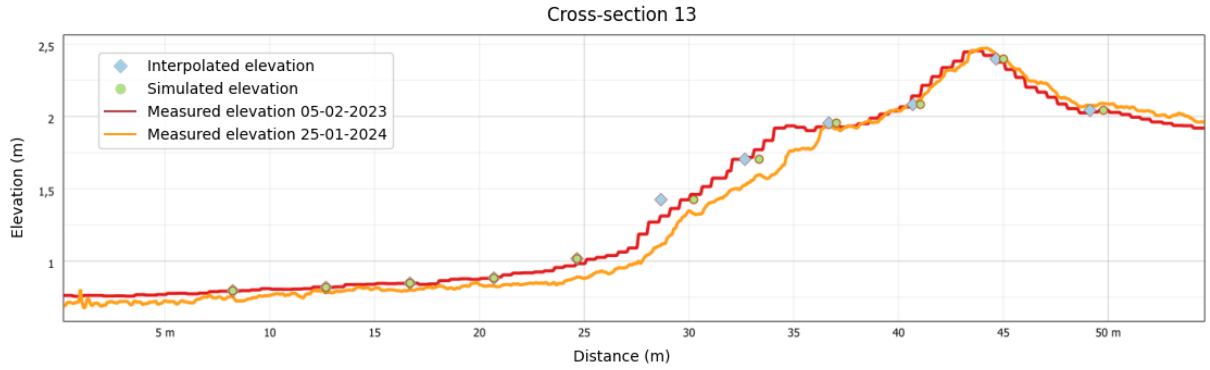
Cross-section 13
Interpolated elevation
Simulated elevation
Measured elevation 05-02-2023
Measured elevation 25-01-2024
Elevation (m)
Distance (m)

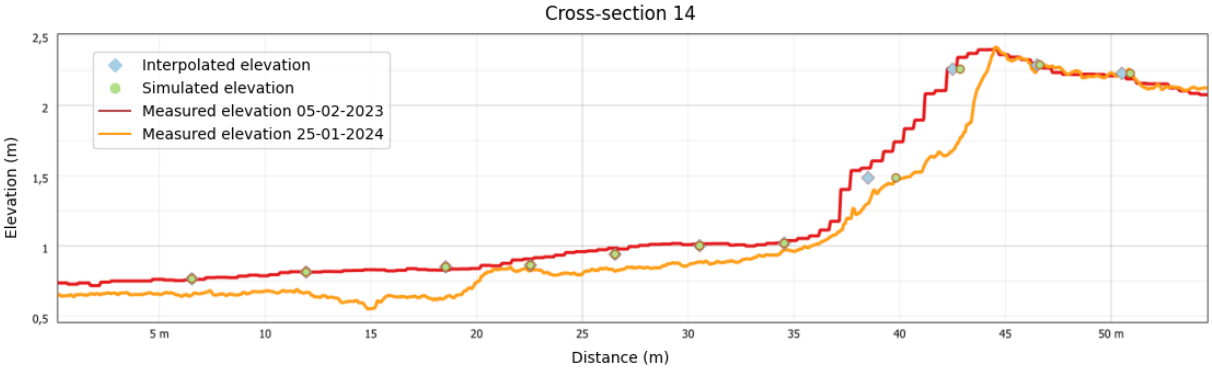
Cross-section 14
Interpolated elevation
Simulated elevation
Measured elevation 05-02-2023
Measured elevation 25-01-2024
Elevation (m)
Distance (m)

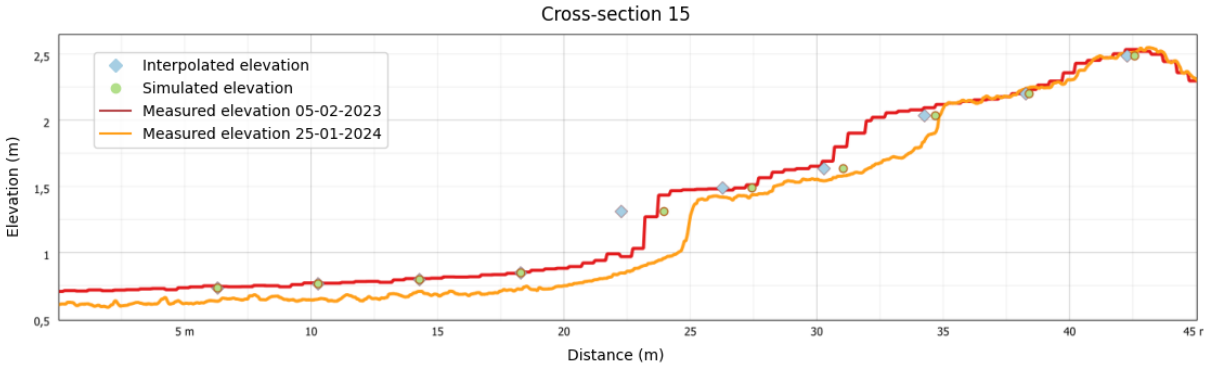
Cross-section 15
Interpolated elevation
Simulated elevation
Measured elevation 05-02-2023
Measured elevation 25-01-2024
Elevation (m)
Distance (m)

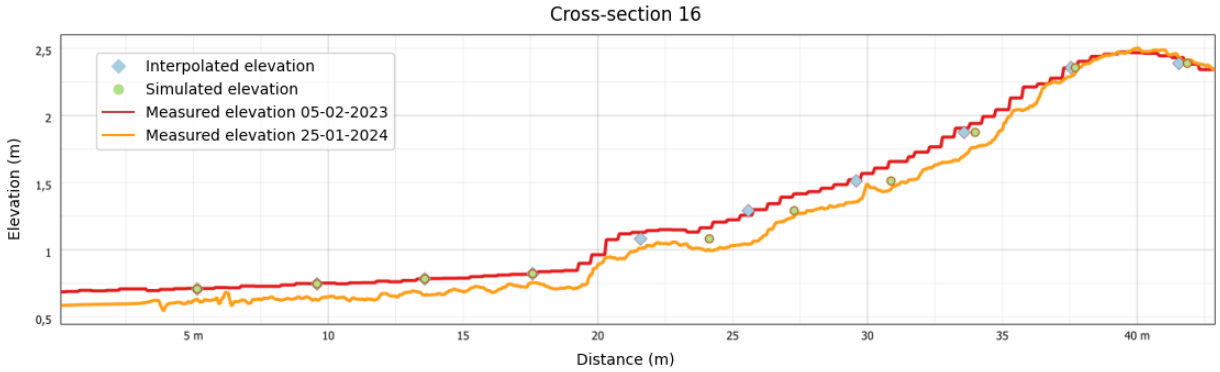
Cross-section 16
Interpolated elevation
Simulated elevation
Measured elevation 05-02-2023
Measured elevation 25-01-2024
Elevation (m)
Distance (m)

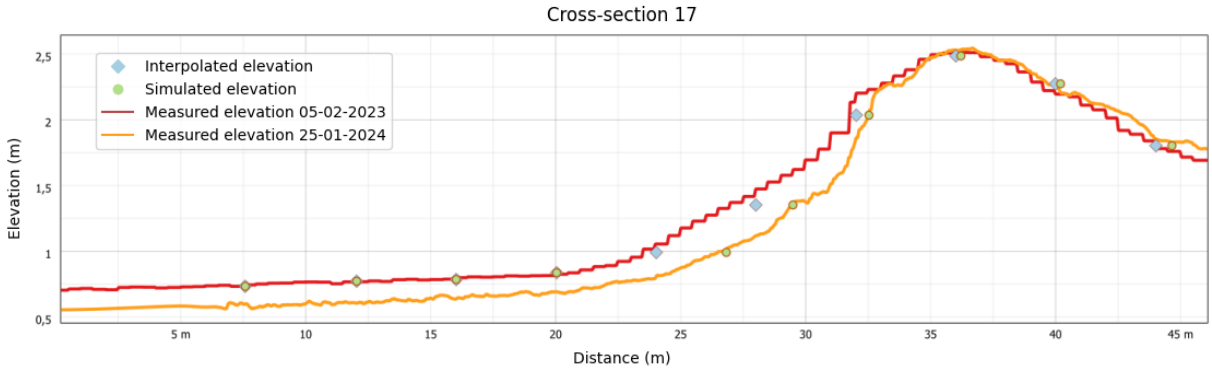
Cross-section 17
Interpolated elevation
Simulated elevation
Measured elevation 05-02-2023
Measured elevation 25-01-2024
Elevation (m)
Distance (m)

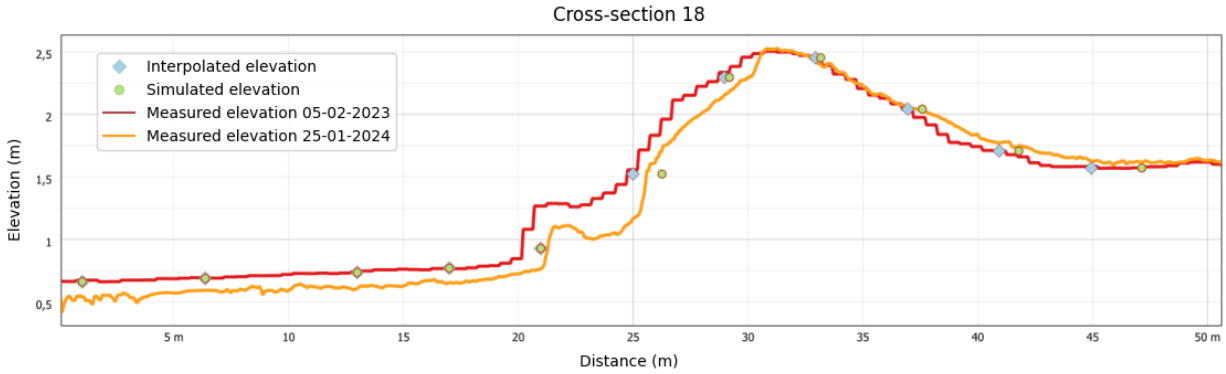
Cross-section 18
Interpolated elevation
Simulated elevation
Measured elevation 05-02-2023
Measured elevation 25-01-2024
Elevation (m)
Distance (m)

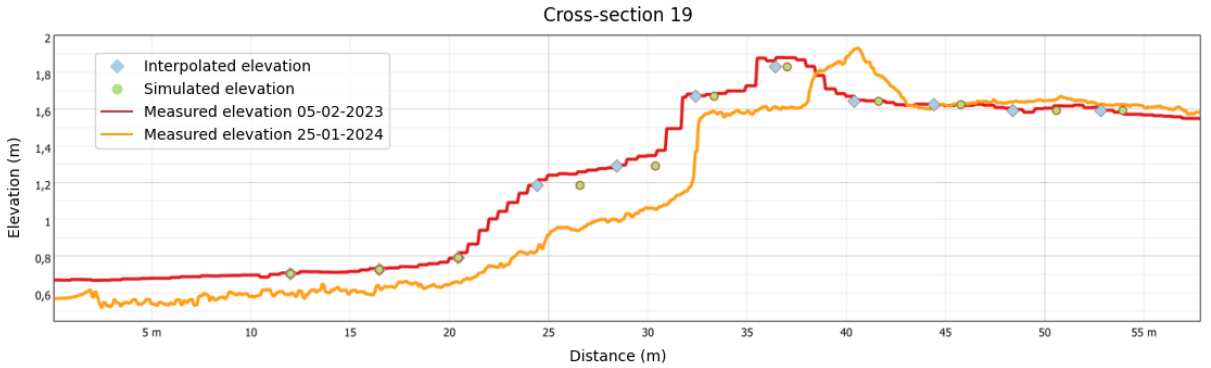
Cross-section 19
Interpolated elevation
Simulated elevation
Measured elevation 05-02-2023
Measured elevation 25-01-2024
Elevation (m)
Distance (m)

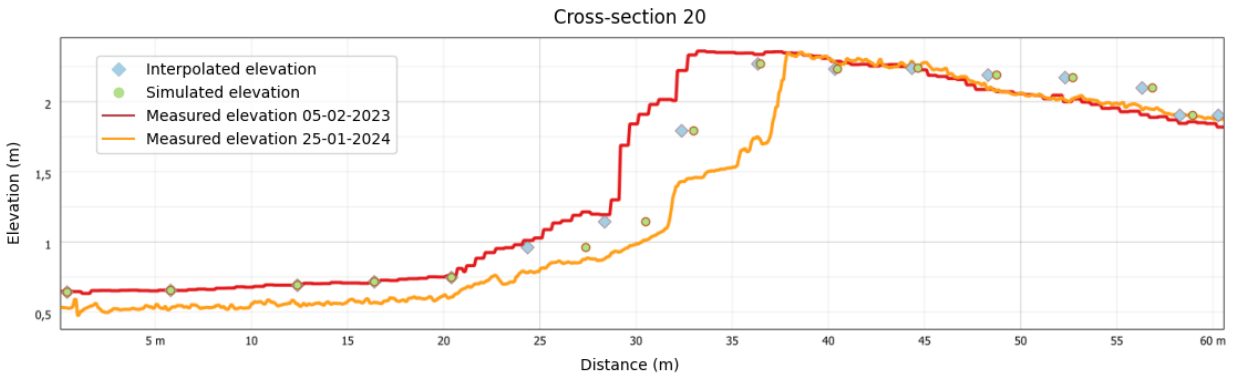
Cross-section 20
Interpolated elevation
Simulated elevation
Measured elevation 05-02-2023
Measured elevation 25-01-2024
Elevation (m)
Distance (m)

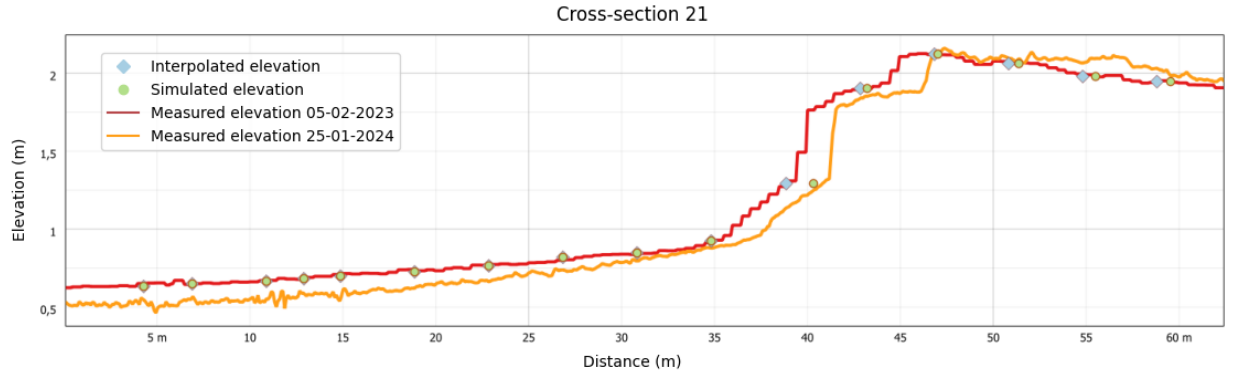
Cross-section 21
Interpolated elevation
Simulated elevation
Measured elevation 05-02-2023
Measured elevation 25-01-2024
Elevation (m)
Distance (m)

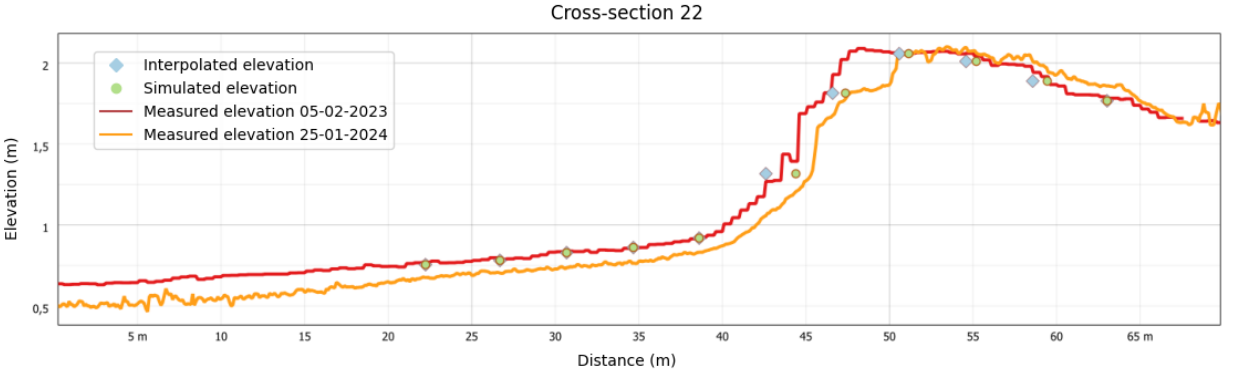
Cross-section 22
Interpolated elevation
Simulated elevation
Measured elevation 05-02-2023
Measured elevation 25-01-2024
Elevation (m)
Distance (m)

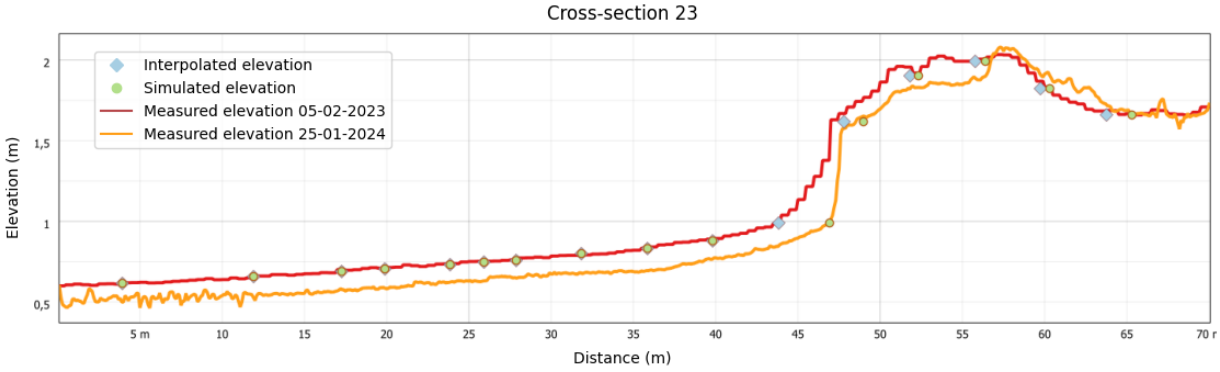
Cross-section 23
Interpolated elevation
Simulated elevation
Measured elevation 05-02-2023
Measured elevation 25-01-2024
Elevation (m)
Distance (m)

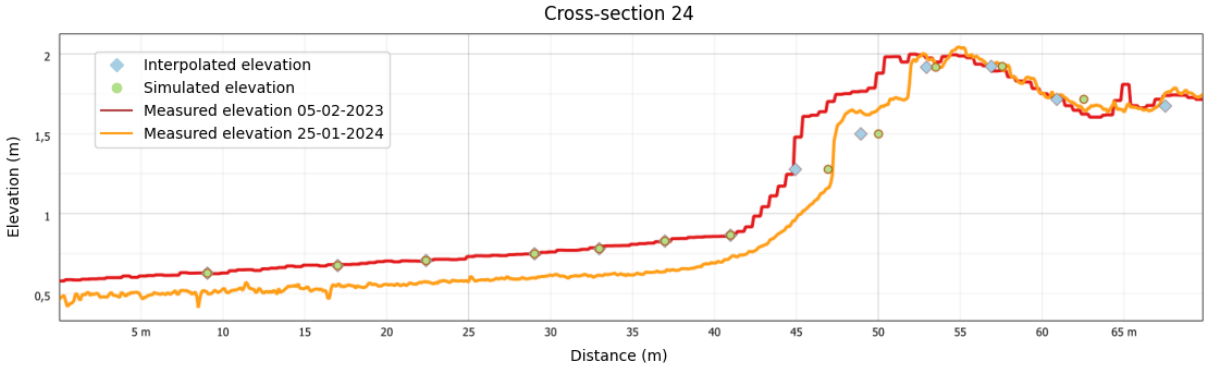
Cross-section 24
Interpolated elevation
Simulated elevation
Measured elevation 05-02-2023
Measured elevation 25-01-2024
Elevation (m)
Distance (m)

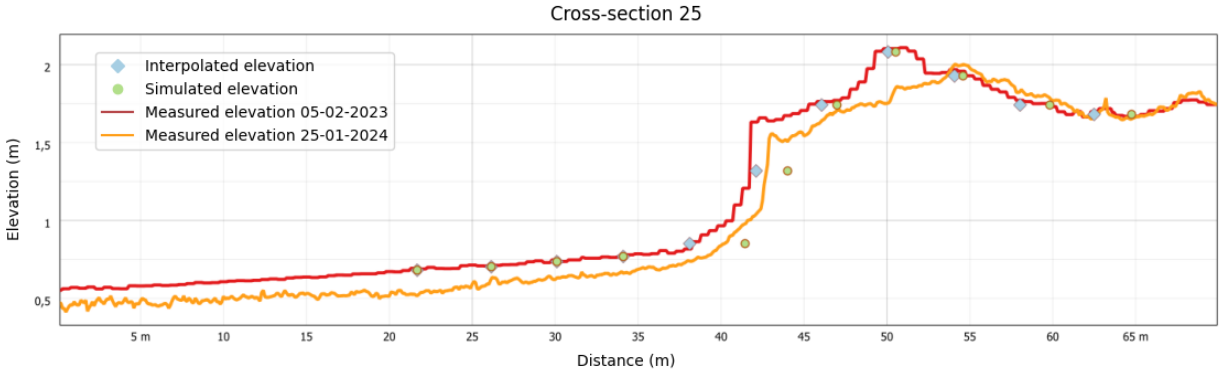
Cross-section 25
Interpolated elevation
Simulated elevation
Measured elevation 05-02-2023
Measured elevation 25-01-2024
Elevation (m)
2
1,5
1
0,5
5 m
10
15
20
25
30
35
40
45
50
55
60
65 m
Distance (m)

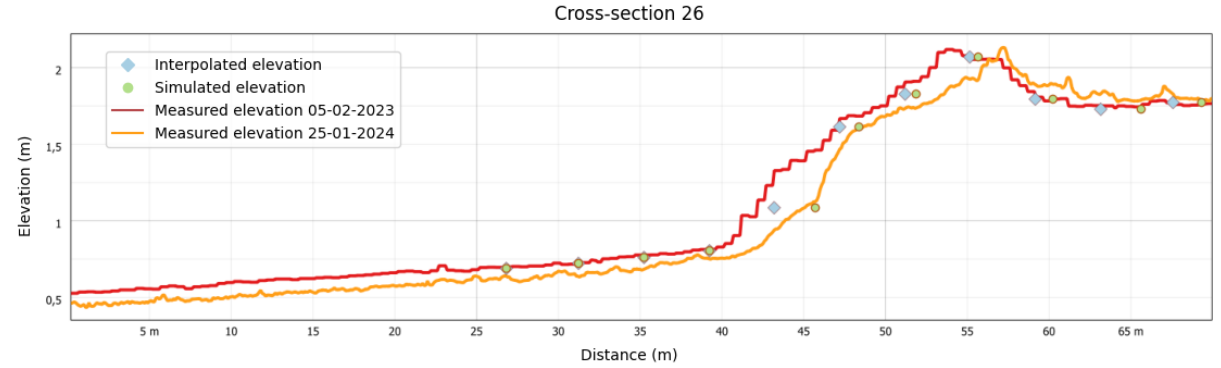
Cross-section 26
Interpolated elevation
Simulated elevation
Measured elevation 05-02-2023
Measured elevation 25-01-2024
Elevation (m)
2
1,5
1
0,5
5 m
10
15
20
25
30
35
40
45
50
55
60
65 m
Distance (m)

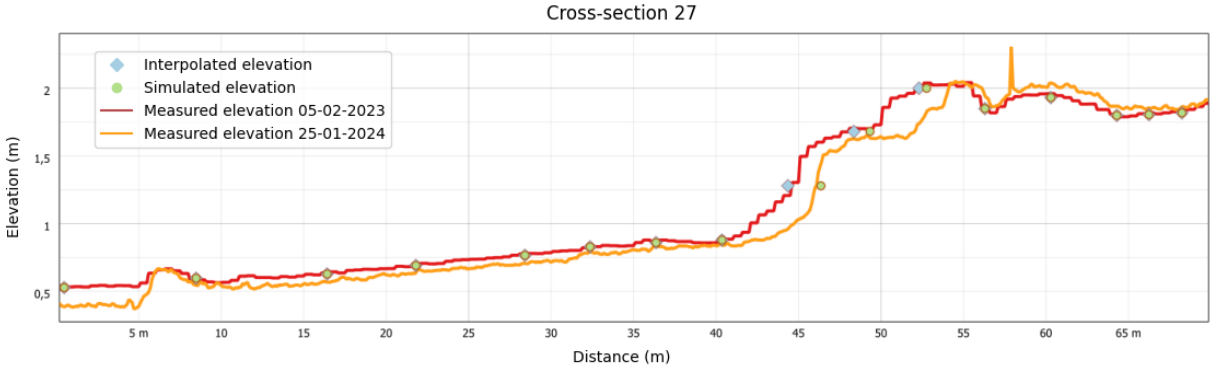
Cross-section 27
Interpolated elevation
Simulated elevation
Measured elevation 05-02-2023
Measured elevation 25-01-2024
Elevation (m)
2
1,5
1
0,5
5 m
10
15
20
25
30
35
40
45
50
55
60
65 m
Distance (m)